Stresses in Soil Beneath Triangular Shell Foundations

Alireza Ansari

A Thesis

in

The Department

of

Building, Civil and Environmental Engineering

Presented in Partial Fulfillment of the Requirements

for the Degree of Master of Applied Science (Civil Engineering)

at

Concordia University

Montreal, Quebec, Canada

April 2022

CONCORDIA UNIVERSITY

School of Graduate Studies

This is to certify that the thesis prepared

By: Alireza Ansari

Entitled: Stresses in Soil Beneath Triangular Shell Foundations

and submitted in partial fulfillment of the requirements for the degree of

Master of Applied Science (Civil Engineering)

complies with the regulations of the University and meets the accepted standards with respect to originality and quality.

Signed by the final Examining Committee:

_____Chair

Dr. E. Erkmen

_____Examiner

Dr. R. Ganesan

_____Examiner

Dr. E. Erkmen

_____Supervisor

Dr. A. M. Hanna

Approved by _____

Dr. A. Bagchi Chair, Department of Building, Civil, and Environmental Engineering

_____

Dr. M. Debbabi Dean, Faculty of Engineering and Computer Science

ABSTRACT

Stresses in Soil Beneath Triangular Shell Foundations

Alireza Ansari

Foundations perform a crucial role in structures to transmit the loads from the superstructure to the soil beneath. The first utilization of shells as foundations was about six decades ago in Mexico. Shells are structures that transmit loads based on their form rather than mass, allowing to preserve more material. Investigations illustrated that the shell foundations provide higher bearing capacity and better settlement characteristics relative to traditional flat footings. In order to improve the geotechnical behavior of shell foundations, researchers attempt to obtain the optimum shape of shell footings by achieving more uniform stress distributions beneath the soil.

This thesis scrutinizes the stress distributions below embedded triangular shell strip footings resting on loose, medium, and dense sands by examining the effect of the edge angle. A series of two-dimensional numerical models are developed and calibrated with conducted experimental results in the literature. Mohr-Coulomb failure yield criteria are employed to simulate the soils with elastic-perfectly plastic behavior. Also, plane strain conditions are assumed to model the soils. The results indicate an increase in average stress distributions below the shell foundations by reducing the edge angle under a particular applied load. Triangular shell foundations demonstrate higher load-carrying capacity and more uniform stress distributions beneath the soil than flat foundations. Contact pressure at the soil-foundation interface and stress distributions at different depths are attained and presented. This study reveals that the optimum edge angle for triangular strip shell foundations in loose, medium, and dense sand states is 55 degrees.

ACKNOWLEDGMENTS

I would like to express my sincere gratitude to my supervisor, professor Adel M. Hanna, for his important guidance, patience, financial support, and encouragement throughout the process of developing this research. I am honored to carry out the present investigation under his supervision.

I would like to give special thanks to my mother because of her encouragement and belief in me. I appreciate my father's support, and I am thankful for his pride in me. I am deeply thankful to my sister and brother for their life-long friendship and unconditional support.

Table of Contents

List of Figures

Chapter 1

Chapter 2

Chapter 3

Chapter 4

List of Tables

Chapter 3

List of Symbols

$\theta = Edge\ angle\ of\ shell\ foundations$

$B = Width\ of\ foundations$

$Z = Depth$

$q_u = ultimate\ bearing\ capacity$

$C = Soil\ cohesion$

$q_0 = surcharge\ load$

$\gamma = soil\ unit\ weight$

$N_{ct}, N_{qt}, N_{\gamma t} = Shell\ foundations\ bearing\ capacity\ coefficients$

$N_c, N_q, N_\gamma = Bearing\ capacity\ coefficients$

$F_c, F_q = Shell\ factors\ for\ changing\ bearing\ capacity\ coefficients$

$\Phi = angle\ of\ shearing\ resistance\ of\ soil$

$\nu = Poisson's\ ratio$

$E = modulus\ of\ elasticity$

$\sigma_{xx} = horizontal\ stress$

$\sigma_{yy} = vertical\ stress$

$\tau_{xy} = shear\ stress$

$\varepsilon_{xx} = horizontal\ strain$

$\varepsilon_{yy} = vertical\ strain$

$\varepsilon_{xy} = shear\ strain$

$D = embedded\ depth\ of\ footings$

$\rho = mass\ density\ of\ soil$

$\psi = dilation\ angle$

$\mu, \lambda = Lame's\ parameters$

CHAPTER 1

INTRODUCTION

1.1 General

As the world's population continues to grow and densify, the demand for high-rise buildings increases as well. Eventually, appropriate lands for structures are being absorbed. Due to the limited suitable areas, seeking effective and practical methods to design structures is challenging for civil engineers.

Foundations perform a crucial role in structures to transmit the loads from the superstructure to the soil beneath. The primary goals for any foundation design and implementation are safety, quality, and cost. Recently, by improving the technology and appearing modern science, foundation engineers have been attempting to explore the best approaches to minimize and optimize the material used and the shape of the foundations to be more economical and efficient.

The ultimate bearing capacity and tolerable settlement are the essential components of designing shallow foundations. To examine a precise bearing capacity and foundation designing, foundation designers employ stress distribution below the foundations due to the imposed load on the foundation. Bowles (1996) reported the stress distribution below shallow flat foundations on cohesionless soils, cohesive soils, and soil with assumed conditions in figure 1.1. Due to the presented parabolic contact pressure distribution below the flat foundations, it can be perceived that flat footings do not utilize the ultimate capacity of soil beneath. Conclusively, investigating a uniform stress distribution below foundations is prominent in foundation engineering.

Recent studies have been devoted to new types of foundations that illustrate more improvements in geotechnical characteristics such as uniform stress distribution in the soil, higher bearing capacity, and lesser settlement relative to conventional flat foundations. Shell foundations are the title given to these modern models.

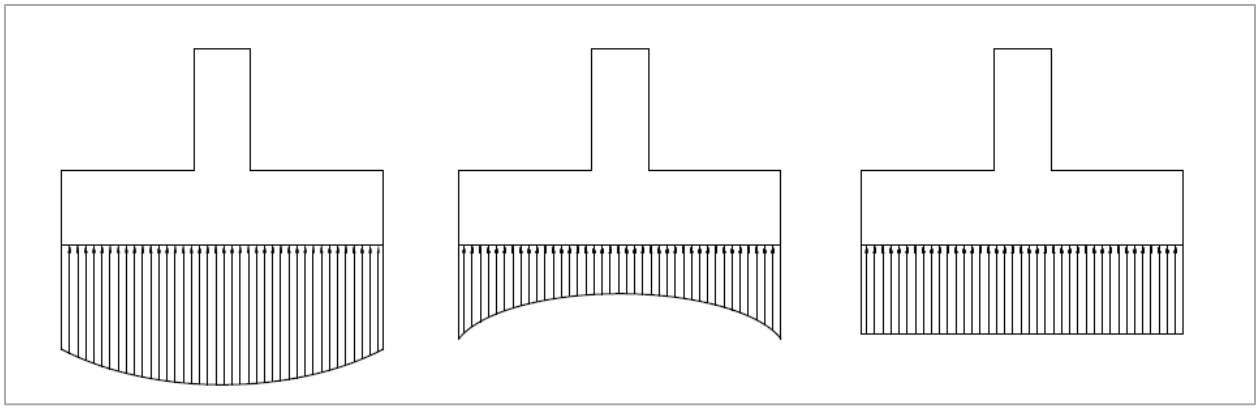

Figure 1.1 Stress distribution below rigid foundations. (a) On a cohesionless soil (b) cohesive soil (c) assumed conditions (Bowels 1996)

1.2 Shell foundations

Shells are structures that transmit loads based on their form rather than mass, resulting in substantial material savings. In developing countries around the world, where construction materials are scarce and expensive but the workforce is comparatively cheap and widely available, the ensuing economics is significant.

Shells in foundations appeared around sixty years ago when Mexican architect, Felix Candela, first applied this method. Since then, the application of shells in foundation engineering has prompted widespread attention across many areas worldwide. It is believed that when intense superstructural loads are to be transmitted to weaker soils, large areas and more materials are consumed for flat footings. Accordingly, shell foundations are more cost-effective than alternative shallow foundations since they demand less ground and construction supplies.

Shell foundations are structural elements with various geometrical shapes. To achieve optimum structural performance, shell foundations are frequently constructed in arched, circular, triangular, conical, cylindrical, spherical, pyramidal, square, and strip shapes.

Foundation design is categorized into structural performance and geotechnical behavior. The first phase, which is structural design, is focused on acquiring the structural parameters, such

as stress, strain, shear, flexure, and ultimate strength of the structural elements of the foundation like concrete and steel reinforcements. As mentioned above, the geotechnical design aims to satisfy the design requirements of foundations, which are the ultimate bearing capacity and settlement.

Stress distribution below foundations features a profound significance in deriving the indicated requirements. Uniform contact pressure in the soil prevents differential settlement and provides suitable geotechnical characteristics. This study concentrates on the geotechnical behavior of shell foundations by determining the contact pressure and stresses in the soil below the triangular shell foundations and examining multiple angles (shown in figure 1.2) to obtain a better uniformity of stress distribution beneath the foundations and explore the optimum geometry of triangular strip shell footings.

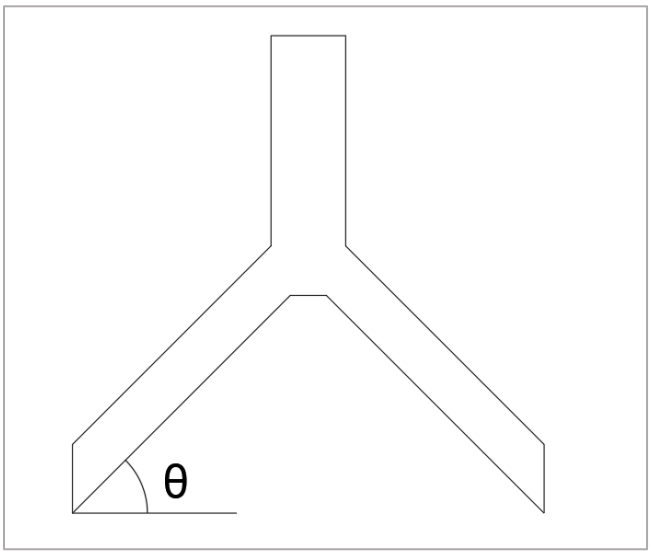

Figure 1.2 Triangular shell foundation model

CHAPTER 2

LITERATURE REVIEW

2.1 General Overview

In the literature, numerous studies have investigated the geotechnical behavior of shell foundations. Due to modernity, the number of these studies is few and far between in comparison to the amount of research conducted on conventional flat foundations.

Available reports have developed the behavior of the shell foundations primarily based on the results of experimental modeling and numerical modeling analysis. Moreover, limited cases of analytical modeling are obtainable.

Due to the diversity of the shell types and geometries, analytical models are incredibly complex to be proposed. On the other hand, numerical modeling based on finite element modeling is a powerful tool to expand and analyze any model.

2.2 Historical Review

Hanna and Hadid (1983) established a mathematical model to compare the stress distribution below different shell foundations with flat foundations. They utilized a computer program to develop the model and discover the stresses at the points of the specified mesh in figure 2.1. Two-dimensional analysis was employed to simulate the models. The soil part was considered to behave isotropically and homogeneous, and the linear stress-strain relationship was governed. Furthermore, Winkler's model was applied to simulate the soil. Eventually, the stress distributions up to a depth of about 2.5 of the foundation width were extracted and shown in figures. More uniform stress distributions and slighter vertical stresses than conventional flat foundations were their concluding remarks. They also reported that shell foundations possess a higher bearing capacity and lower settlements compared to alternative flat foundations.

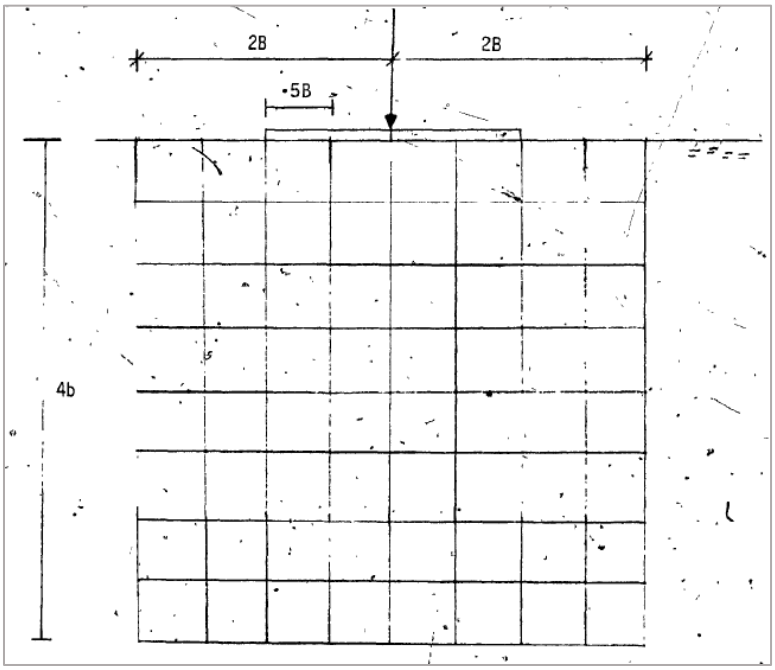

Figure 2.1 Stresses were calculated at the located points in this mesh (Hanna and Hadid, 1983)

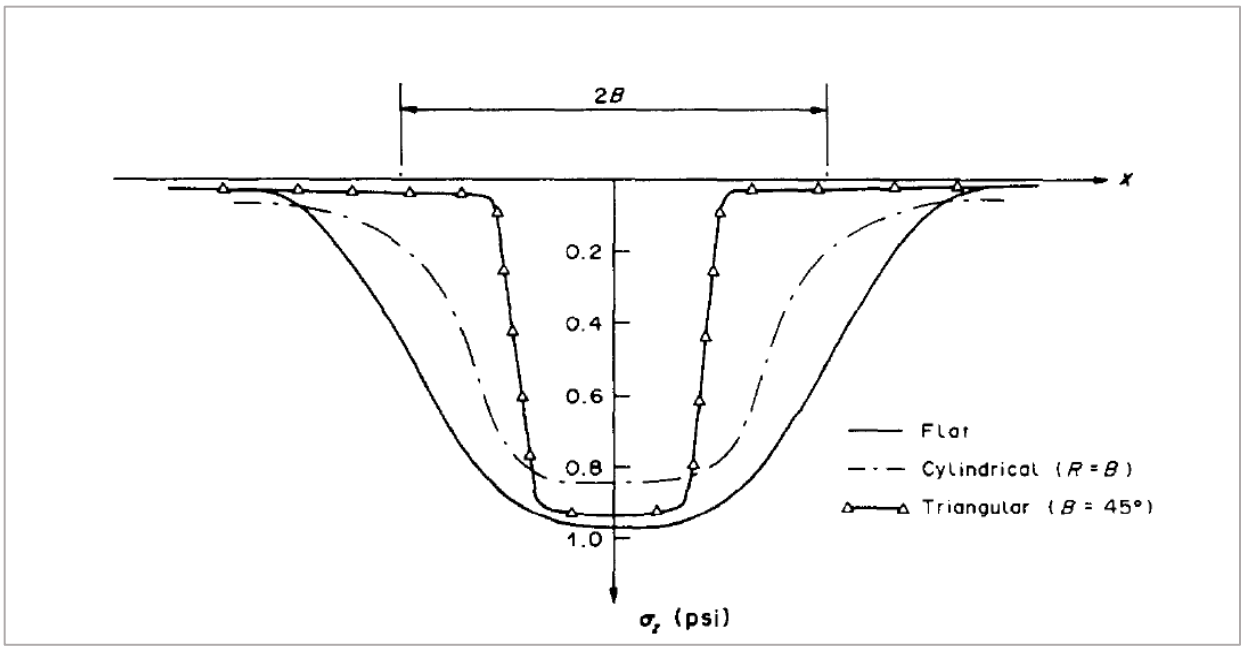

Figure 2.2 The comparison of stresses below flat, cylindrical, and triangular shell footings at depth Z = 0.5B (Hanna and Hadid, 1983)

Hanna and Abdel-Rahman (1987) limited their studies on the experimental and theoretical modeling of the triangular strip shell footings on sand. They applied the theory of plasticity in order to investigate the effects of peak angles on the bearing capacity and validate it with the experimental models. Experimental specimens were organized with five peak angles from 180 degrees (flat foundation) to 60 degrees, examined at the surface, and embedded in the soil. As a result, it was proved that the shell foundations experienced 36% higher bearing capacity and better settlement characteristics than the alternative flat foundations. They also presented a bearing capacity formula for triangle shell foundations on sand using the superposition principle and Hansen expression.

$$q_u = cN_{ct} + q_0 N_{qt} + \frac{1}{2}\gamma B N_{\gamma t} \tag{2.1}$$

Where,

$$N_{ct} = \cot \Phi \, (F_q N_q - 1) F_c \tag{2.2}$$

$$N_{qt} = N_q F_q \tag{2.3}$$

$$N_{\gamma t} = 1.80 \left(F_q N_q - 1\right) tan\Phi \tag{2.4}$$

All factors were generated from a computer program as a function of peak angle of the shell footings and angle of friction of sand and are obtainable in presented figures.

Hanna and Abdel-Rahman (1996) extended their studies to examine the contact pressure below shells, stress distribution beneath the soil, settlements, and the bearing capacity of several shell types on loose, medium, and dense sands experimentally, numerically, and theoretically. Laboratory tests were performed on strip flat, triangular, circular flat, conical, square flat, and pyramidal footings in embedded and on-surface conditions. Finite element modeling using Mohr-Coulomb's yield criteria to simulate the soils was employed to develop numerical modeling of shell foundations. For the theoretical modeling, they used the classical theory of ultimate bearing capacity and introduced a Shell Ratio (SR) to represent the effect of peak angle in triangular strip shell foundations. They concluded that by keeping all plain dimensions the same, the ultimate bearing capacity of the shell foundations is significantly larger than the flat counterparts. They

reported that in the cases of surface and embedded triangular shell foundations, the maximum contact pressure appears at 2/3B of the center. However, this trend reaches the maximum for square flat footings at the center.

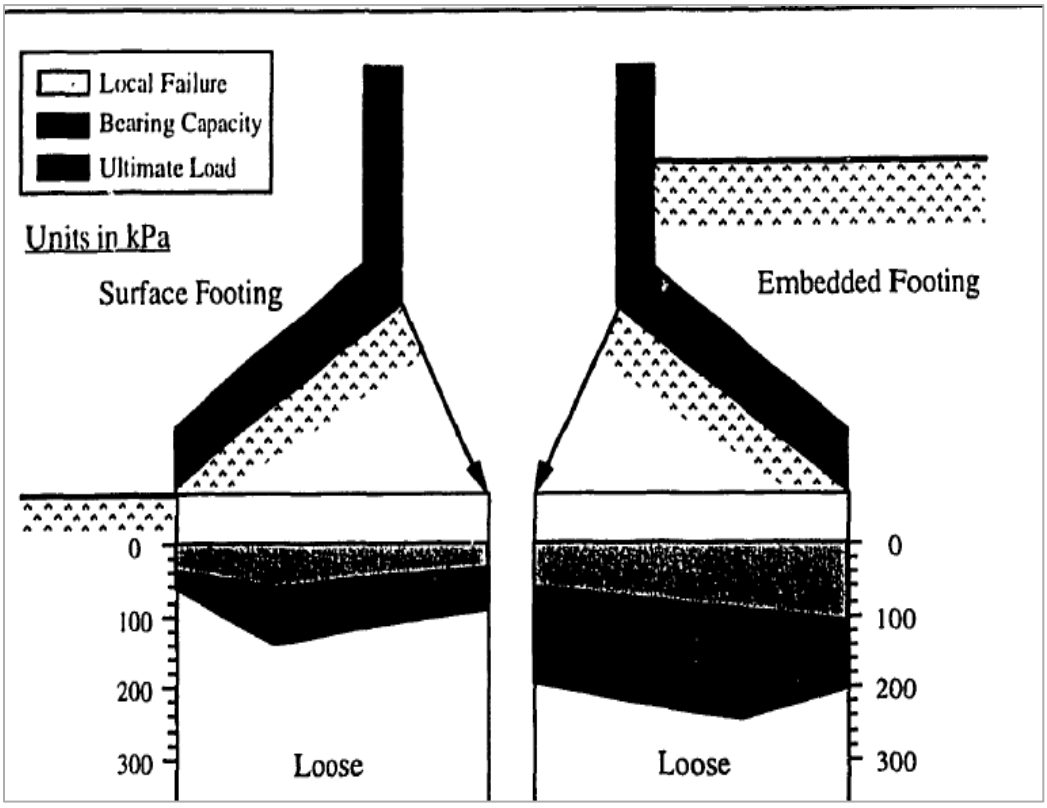

Figure 2.3 The contact pressure below the triangular shell foundation on loose sand (Abdel-Rahman 1996)

Kurian (2005) carried out numerical modeling to analyze conical, spherical, and hyper shell foundations and compared with the flat counterparts on dry sand by considering the exact plan dimensions. The authors used Numerically Integrated Elements for Systems Analysis package to develop the numerical modeling by finite element methods. Furthermore, they examined the models subjected to various loading conditions with vertical with and without eccentricity and horizontal forces and their combinations (inclined loads). The results showed that when a conical shell is subjected to an inclined load, bearing capacity experienced a 70% decrease, compared with the same footing under the vertical load only. Nonetheless, the shell illustrated 23% more bearing

capacity. Additionally, they reported higher bearing capacities for all other shell models in upright and inverted positions under different loading conditions.

Huat et al. (2006 and 2007) conducted field tests and numerical modeling using the non-linear finite element method to study the geotechnical behavior of upright and inverted shell foundations. They also considered the effect of thickness on the ultimate bearing capacity of shell footings. They developed the numerical modeling by using Plaxis and LUSAS computer software. Besides, Mohr-Coulomb yield criteria were implemented to simulate the soil behavior. The results showed a good agreement between the finite element results and the field results with experimental test results by Abdel-Rahman (1996). The better contact stress distribution for inverted triangular shells with higher vertical load-carrying capacity compared with upright triangular and flat strip footings was reported. The contact pressure was concentrated in the edge parts of the upright triangular shells. They also found that the bearing capacity was raised by attaching edge beams to the base and increasing the embedding ratio of shell foundations.

Figure 2.4 The upright and inverted triangular shell foundations (Huat 2007)

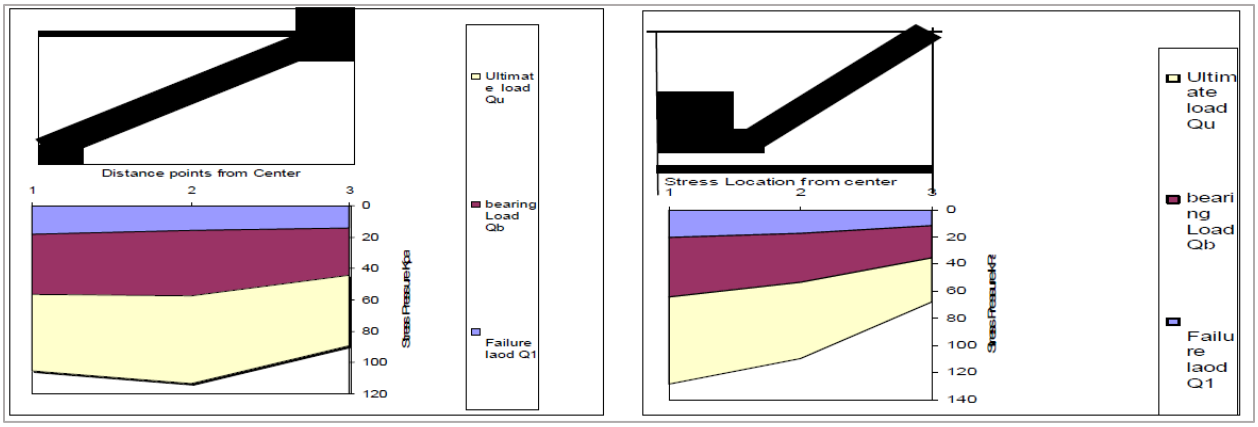

Figure 2.5 The contact pressure below the upright and inverted triangular shell footings (Huat 2007)

Esmaili and Hataf (2008 and 2013) studied the ultimate load capacity of shell foundations by performing some laboratory tests, numerical analysis, and dimensional analysis. They used conical and pyramidal shell types resting on reinforced and unreinforced sands. The dimensional analysis was based on the Buckingham-Pi theorem by defining a set with the following parameters: ultimate load capacity of shell foundations, dry unit weight of sand, angle of shearing resistance of sand, the relative density of sand, height and dimension of soil core, and thickness of shell models. By applying the Buckingham-Pi theorem and generating a formula containing mentioned parameters with constants, they formulated the ultimate load capacity by employing the laboratory test results for pyramidal and conical shell foundations. Moreover, the numerical and empirical results showed a good agreement and certified that shell foundations' ultimate load capacities on reinforced sands are higher than those rested on unreinforced sands and greater than flat counterparts.

Rinaldi (2012) presented the bearing capacity and contact pressure by encapsulating their studies on inverted and upright shell foundations and implementing numerical and laboratory tests. One of the major concerns in this study was optimizing the shells by achieving the vertical pressure at the shell-soil interface to a uniform distribution. Ultra–high-performance iShell Mix concrete using fiber–reinforced polymeric (FRP) microfibers were used for their shell prototypes. The influence of different peak angles of triangular shapes was examined in experimental and finite element modeling using Plaxis, which concluded that increasing the thickness and the peak angle increases the load-carrying capacity. By interpreting the results, they agreed that inverted triangular shell foundations experiences more uniform contact pressure than the upright ones. The experimental investigations demonstrated that applying Mohr–Coulomb's failure criterion on an elastic perfectly plastic soil model produces a satisfactory depiction of the behavior of soil-structure interaction in cohesionless soil.

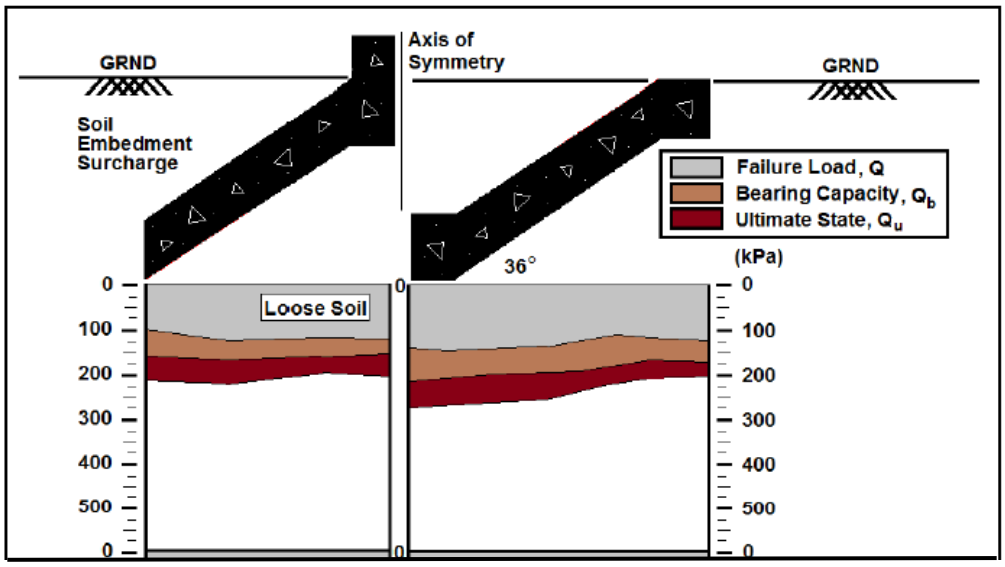

Figure 2.6 Contact pressure below upright and inverted shell foundations on loose sand (Rinaldi 2012)

Ebrahimi and Hamidi (2013) developed numerical modeling to obtain the optimum form of shell footings by considering bearing capacity, settlement, foundation area, and material consumption volume. They simulated 3D models of pyramidal and conical forms of shells by ABAQUS. Regarding the small thickness of shells, the difference between the volumes of the pyramid and the conic shapes is negligible. Setting the mentioned parameter aside, the pyramid shell foundation provides more appropriate geotechnical behavior and can be a superior option.

Colmeranes et al. (2013) extended the classic solution for the bearing capacity of circular flat foundations to obtain a theoretical formula for conical shell foundations on mixed soils. Also, they validated their work experimentally and ascertained the failure mechanism by examining four different models with specified peak angles. Bearing capacity coefficients were proposed in design charts as a function of the friction angle of the soil and the peak angle acquirable from the geometry of the conical shell footings.

Azzam and Nasr (2015) focused on investigating the bearing capacity of shell strip footings on sand with and without a layer of reinforcement and compared it with flat counterparts experimentally. They also examined the influence of the embedment depth ratio of the footings on the load carrying capacity. A significant increase in ultimate load and decrease in the settlement were found in the cases of footings rested on reinforced sand, particularly in the existence of the low-density subgrade. Shell efficiency factor was introduced to represent the difference in the ultimate load between a shell footing and an alternative flat one. The results showed that the increase in the shear angle and embedment depth increases shell efficiency. In addition, the wedge of the rupture surface occurs in the lower depths in the presence of a reinforced layer.

El-kady and Badrawi (2017) aimed to reduce steel reinforcements in order to economize the shell foundation materials by applying experimental and numerical models. They created several folded footing prototypes with angles 10, 20, 30, and 40 degrees with the horizon. They presented a diagram for the peak angle versus the load capacity of folded foundations and induced that the folded foundation with 30 degrees angle has saved 46% of reinforcing steel compared with the flat footings. It was concluded that the efficient folding angle for foundations is 30 degrees.

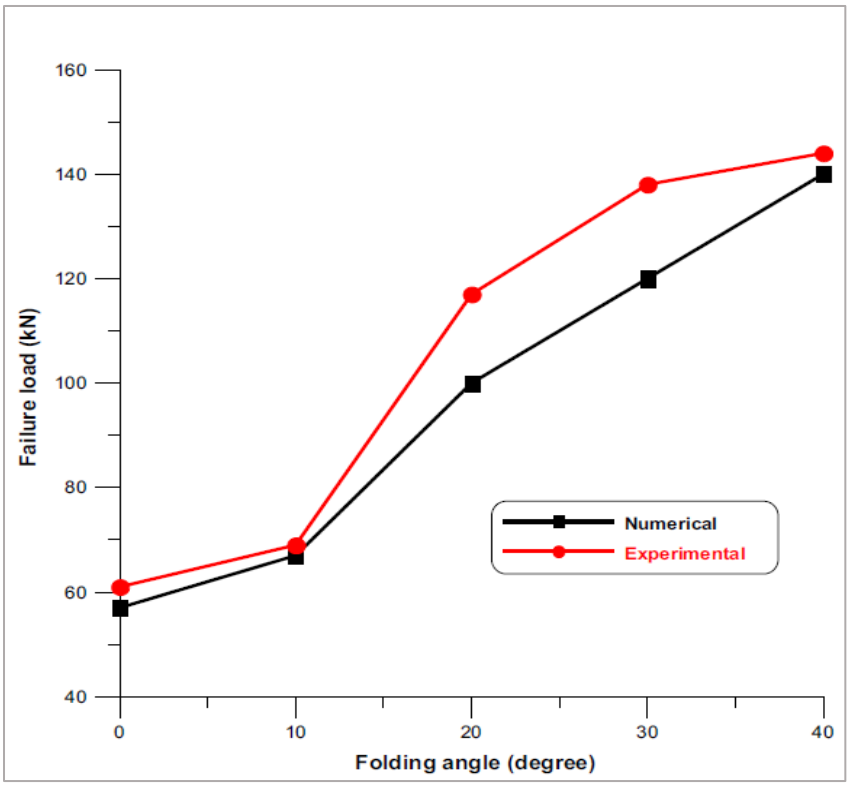

Figure 2.7 Ultimate load capacity versus folding angle (El-kady and Badrawi 2017)

Shoukath and Rajesh (2017) employed numerical modeling to investigate the seismic performance of hyperbolic paraboloid and inverted spherical shell foundations on sandy and clayey soils using ANSYS finite element software by conducting transient dynamic analysis. They defined a parameter as f/a, representing the ratio of the depth to the radius for spherical shell footings and the depth to the base. After interpreting the results, they recommended using the hyper shells with f/a ratio between 0.5 to 0.6.

Bolouri et al. (2018) conducted experimental and numerical tests on four different forms of shells and compared them with the same plain dimension flat counterpart. The models are named A, B, C, D, and E in their research, as shown in figure 2.8. They investigated the geotechnical behavior of the models by appraising the embedment depth and the type of sand. They found that shell geometry plays a vital role in the bearing capacity of these types of foundations. It was not recommended to use shell B as a replacement for flat ones. The reason is that by the same embedment depth, the flat footing exhibited higher bearing capacity in both loose and dense sand

cases. The bearing capacity of shell foundations significantly increased by improving mechanical parameters and compaction of the soil. The highest discrepancy in bearing capacity was observed in shell D on the surface of loose sand. In this condition, the bearing capacity of shell D is 72% higher than shell B. As a consequence, shell D was approved as the ideal shape.

Sajedi et al. (2018) applied numerical modeling on inverted folded shell foundations adapted by Rinaldi's study. Rinaldi's models and soil characteristics were employed in their investigation to implement an elastic-plastic analysis by PLAXIS. The isotropic hardening model provided a 30% higher bearing capacity relative to Rinaldi's results. However, elastic perfectly plastic simulations demonstrated that the outcomes approached Rinaldi's solution. Besides, the results evidence no remarkable influences of shell thickness on the bearing capacity.

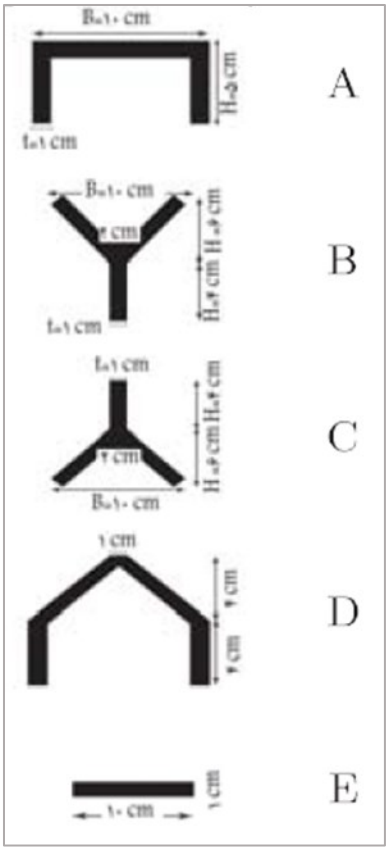

Figure 2.8 Shell foundation models (Bolouri et al. 2018)

Ebrahimi and Khazaei (2019) focused on the bearing capacity and failure pattern of triangular shell foundations employing the finite element limit analysis method. They investigate the effects of changing peak angles, embedded depth, and foundation roughness. The failure surface tends to the assumed wedge in load-bearing capacity theories and increases the ultimate bearing capacity as the foundation roughness rises. Exploring failure surfaces in this study illustrated that shell foundations provide a lower bearing capacity than flat foundations in some situations. They proposed using the shell foundations in the case of existing surface footings on strong soil with the minimum soil and foundation interface friction angle, leading to higher bearing capacity.

Pronozin et al. (2019) took an actual 17-story residential building as their case study. The ground base of the structure is composed of highly compressible overlying by robust layers. In this practical example, strip shell foundations function cost-effectively due to the excessive load transmitted by the structure. The use of driven piles is eliminated, owing to high expenses and demand for large diameters and lengths. Flat foundations produce excessive settlements and are not functional under high pressure. Actual deformations were monitored during the construction and compared with calculated results by the SCAD program. The measured settlements in the construction process reach a reasonable agreement of about 10-15% discrepancy with the calculations.

Figure 2.9 Formation of the ground for shell foundations (Pronozin et al. 2019)

Figure 2.10 The construction process to concrete the site (Pronozin et al. 2019)

Sawsan et al. (2019) tested four types of rigid aluminum foundations containing a flat plate and three pyramidal shell footings on unreinforced and reinforced soil by geogrids. Furthermore, they conducted 3-D numerical modeling employing the finite element methods with ABAQUS software. The results were investigated by considering bearing capacity ratio (BCR) and settlement reduction factor (SRF). A comparison showed a 19% improvement in bearing capacity and a 33% reduction in the ultimate settlement by placing a pyramidal shell with 45 degrees of peak angle instead of the flat footing. They also concluded that by reinforcing the soil with one and two layers of geogrids, the bearing capacity significantly increased, and settlement reduced.

Abdel-Rahman (2020) presented an analytical analysis on the lateral loading resisting for shell foundations. To simplify the calculations, the total resistance was divided into the resistance due to the base and the passive earth pressure. Three numerical examples were solved by implementing the attained formula in two embedment conditions, and sliding and overturning load resistance were acquired. It was understood that in the case of h > D (h would be the depth of the soil above the surface of flat footings, and D is the depth of the foundations), the shell foundation sliding and overturning capacities are remarkably higher than flat footings. However, this percentage increase has a lower amount in the case of h < D.

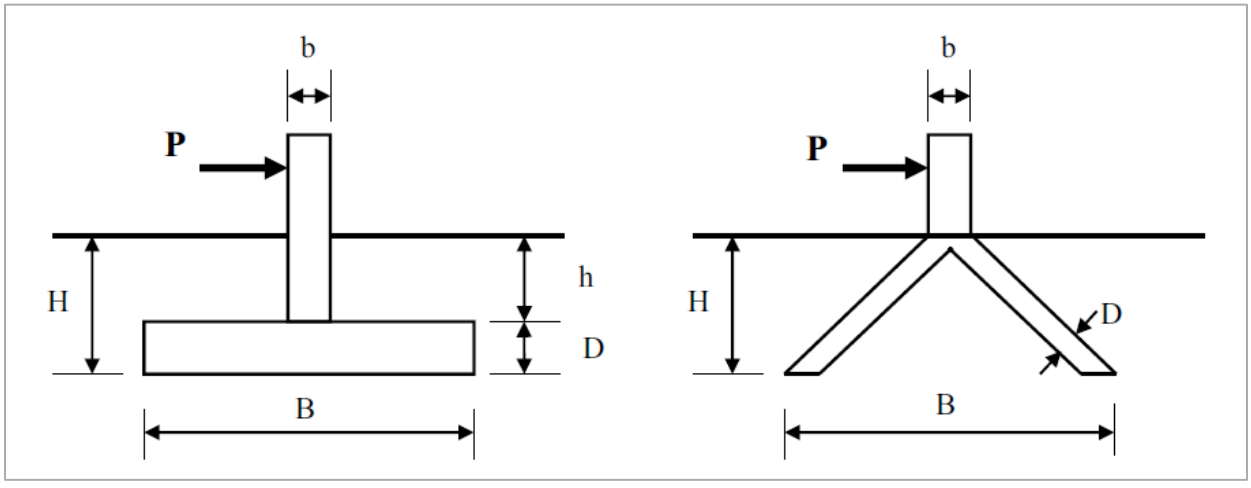

Figure 2.11 The flat and shell models for the analytical analysis (Abdel-Rahman 2020)

Sidqi and Mahmood (2020) developed numerical modeling on upright and inverted reinforced concrete pyramidal shell foundations and investigated the effects of different edge angles on load carrying capacity, settlement, and contact pressure. They also presented the influence of increasing the thickness of the footings on the geotechnical characteristics of shells and compared them with conventional footings. They came to a conclusion that the increase in the edge angles triggers reducing contact pressure at the center of both types of footings; accordingly, the center experienced lower settlements. By evaluating the bearing capacities and settlements, it was believed that the inverted shell foundations have more efficiency than upright counterparts. In addition, the ultimate load-carrying of upright shell foundations increased with increasing the thickness. The tension zones of the foundations' structure and the stress in steel reinforcement were explored. The yielding occurred at the center of the inverted foundation, while this phenomenon was observed at the outer edges of upright shells.

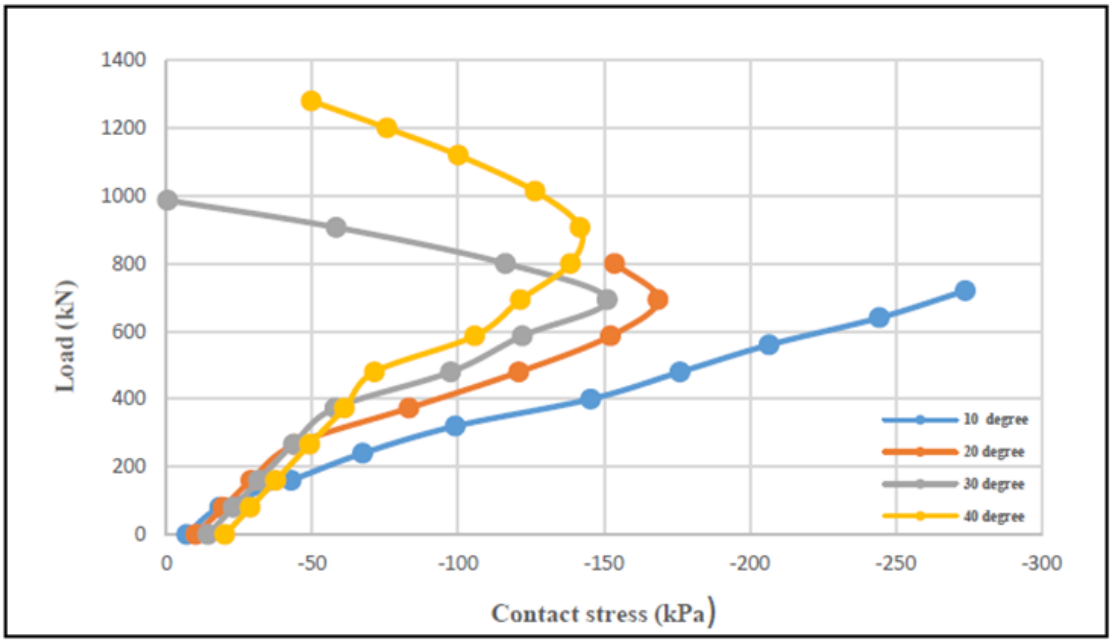

Figure 2.12 Load vs. contact pressure at the center of the inverted shell footing (Sidqi and Mahmood 2020)

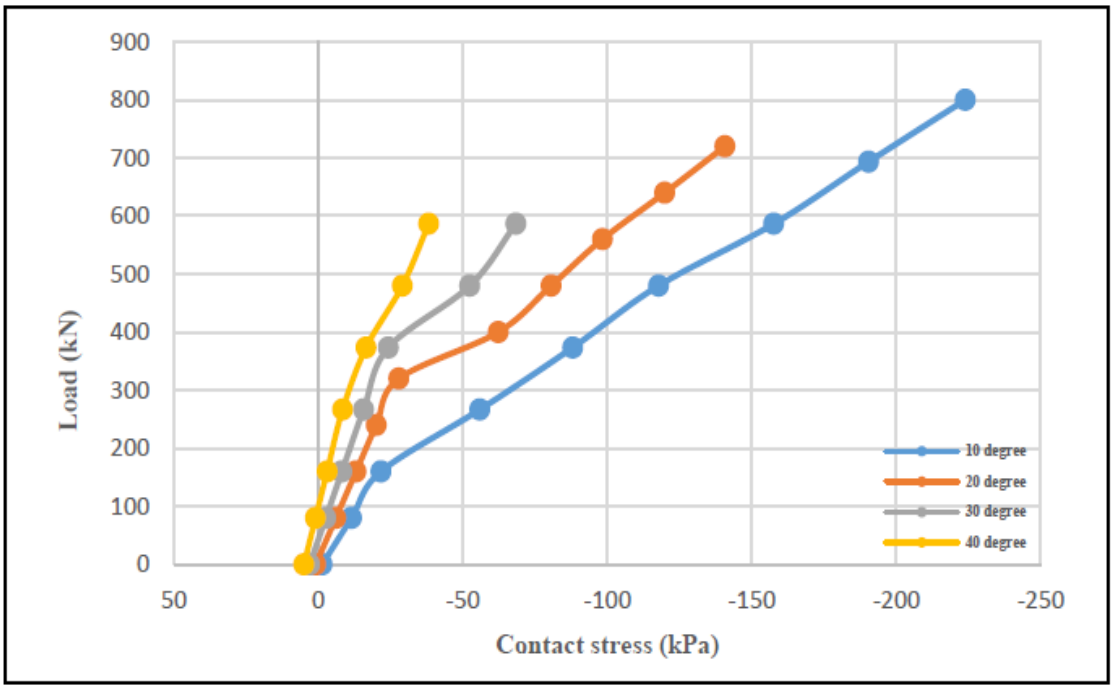

Figure 2.13 Load vs. contact pressure at the center of the upright shell footing (Sidqi and Mahmood 2020)

2.3 Discussions

By initiating employing shells in soils as foundations in the 1950s, researchers have been attracted to develop numerical, analytical, and experimental analyses to investigate the geotechnical and structural behaviors of these types of footings. Studies have proved that shell foundations provide higher bearing capacity and lower settlements than traditional flat foundations.

Due to the various shapes of shells, several studies investigated the influence of geometry on the geotechnical behavior of shell footings. They developed a wide variety of shell models to discover the most efficient types of shells in soils. One of the common types of shell foundations is upright triangular shell foundations. In the literature, Hanna and Abdel-Rahman, Rinaldi and Hanna, Huat et al., and Sidqi and Mahmood conducted field and laboratory tests and developed numerical and analytical models to examine the effect of embedded depth, thickness, and the peak angle of triangular and pyramidal shell footings. Subsequently, they concluded that the embedded triangular shell footings have a higher bearing capacity and more confined stress distributions than alternative flat ones. Additionally, changing the peak angle remarkably influences the geotechnical characteristics of triangular shell foundations. In order to examine the stress distributions, the experimental studies measured stresses at a few points experimentally to obtain an approximate contact pressure below the shell footings. Also, there is no investigation on the effect of changing geometry on stress distributions beneath the triangular shell foundations to obtain the optimum shape of these footings.

Stress distribution below foundations is a principal parameter for geotechnical designers. Uniform stress distribution and contact pressure below foundations avoid differential settlements and contribute to improving the geotechnical behaviors of foundations.

This thesis scrutinizes the stress distributions below triangular shell foundations and comparing with their flat counterparts. Also, it aims to find the optimum shape of triangular shell footings by examining the edge angle and obtaining the most uniform stress distribution beneath the loose, medium, and dense sands at specified depths numerically. Furthermore, the effects of soil densification on stress distributions will be reported. The bearing capacity of the optimum shape of triangular shell foundation will be compared with the alternative flat foundation as well.

CHAPTER 3

NUMERICAL MODEL

3.1 General

In the case of shell foundations embedded in soil, the soil-foundation interaction and the particular form of shells lead to complexity in the analyzing process. Experimental tests provide satisfactory results contingent on appropriate laboratory or field conditions, equipment, and test procedures. Despite that, they consume time and expenses. On the other hand, numerical modeling is a credible and efficient alternative leading to approximate results close to experimental tests based on previous research. Finite element method is a powerful tool to develop and analyze complex geotechnical models numerically.

3.2 Numerical Model

In this chapter, a series of numerical models are conducted on shell foundations using the commercial finite element software ABAQUS 2017. The models are established in two-dimensional space in order to simulate the strip shell footings. This study has been validated and calibrated with the conducted experimental tests results by Abdel-Rahman (1996).

The model developed employs 4-node bilinear plain-strain quadrilateral, reduced integration, hourglass control elements to precise the results. Elements would be plane strain designed for simulating the soil behavior, which is a 2D elastic-perfectly plastic continuous medium, attaining the settlement of soil beneath the foundation and avoiding movements along the thickness of the foundation. In other words, longitudinal strains are neglected. ABAQUS offers different 2D planar elements to define soil and foundation parts (i.e., deformable, discrete rigid, analytical rigid). Deformable elements have been selected for this investigation.

Furthermore, 4-node bilinear quadrilateral elements are chosen in the program. Bilinear quadrilateral elements can be utilized for plane-stress or plane-strain problems in elasticity. Each bilinear quadrilateral element has four nodes with two in-plane degrees of freedom at each node (eight degrees-of-freedom in total). In comparison to fully integrated elements, reduced-integration elements choose one fewer integration point in each direction. Linear elements with reduced integration have a single integration point at the element's centroid.

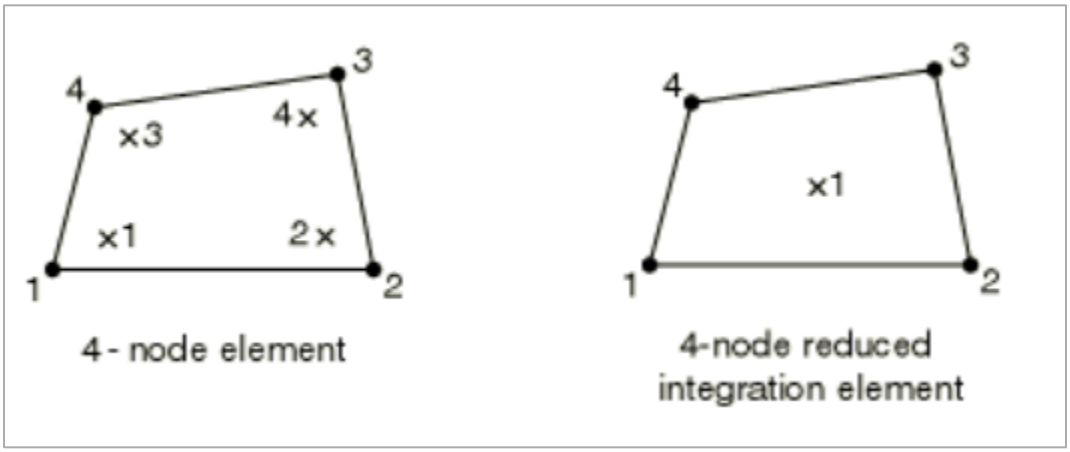

Figure 3.1 4-node element versus 4-node reduced integration element (ABAQUS Manual 2017)

3.3 Model Geometry

The model in this study simulates shell foundations with a consistent width and embedded depth by examining the edge angle from zero (plain condition) to 60 degrees. Thicknesses and the base dimension are adopted from Abdel-Rahman's research (1996). The total height of the foundation is assumed to be 200 mm in order to have a top surface above the soil surface. The embedded depth is assumed to be equal to the width of the foundations. To avoid or minimize boundary effects, soil cross-section dimensions should be assumed at a sufficient distance from the footing. Soil model dimensions are considered 20B and 5B, as shown in figure 3.2. These dimensions are large enough to prevent the boundary conditions of the sides and the base of the soil part from affecting the settlement around the foundation zone.

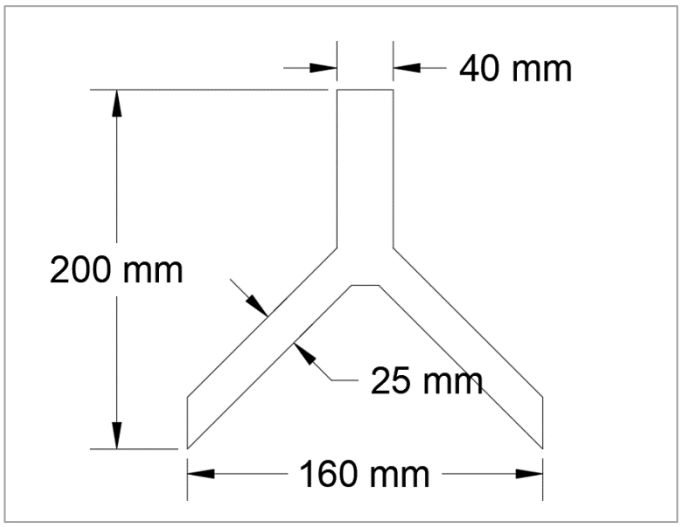

Figure 3.2 Foundation dimensions

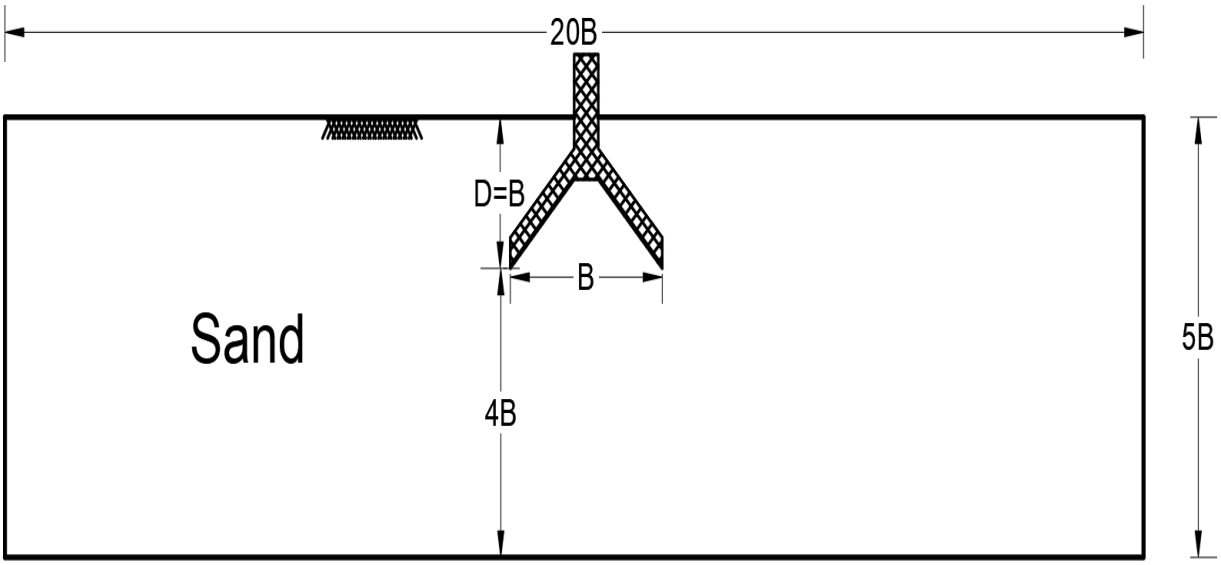

Figure 3.3 Model dimensions

3.4 Boundary Conditions

In this model, the base of the soil model is restricted in both x and y directions. The right and left sides of the soil are prevented from translation horizontally and released in the vertical direction. All models are subjected to a constant uniform pressure load at the top. In order to investigate bearing capacity, a prescribed displacement is applied to the foundations during the second step of calculations as the boundary condition.

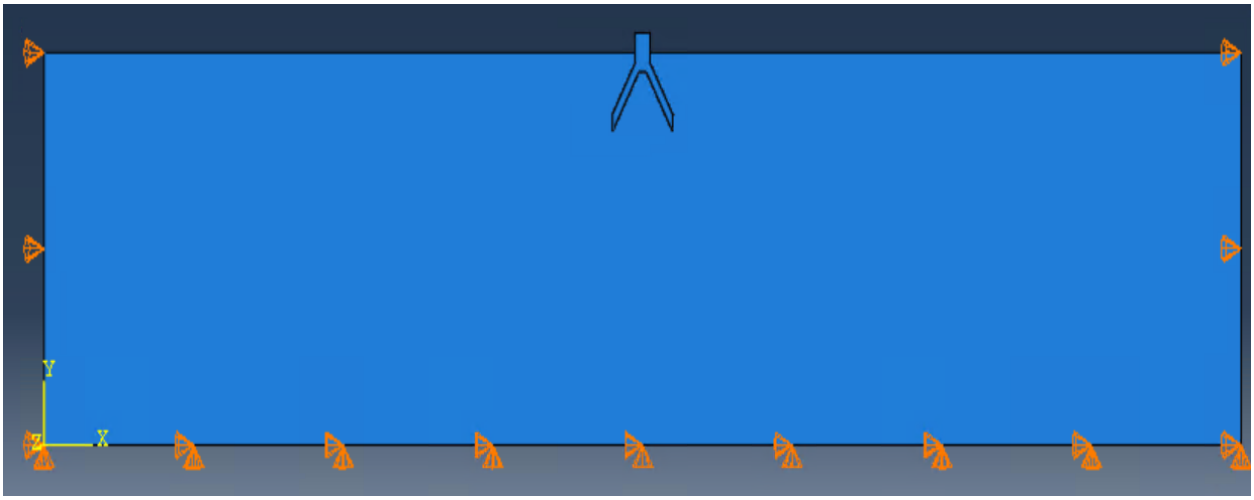

Figure 3.4 Sides and bottom boundary conditions

3.5 Constitutive Model

The foundation material is characterized as an isotropic linear elastic material that is governed by Hooke's law. The stress state in two-dimensional space on an element is demonstrated in figure 3.5.

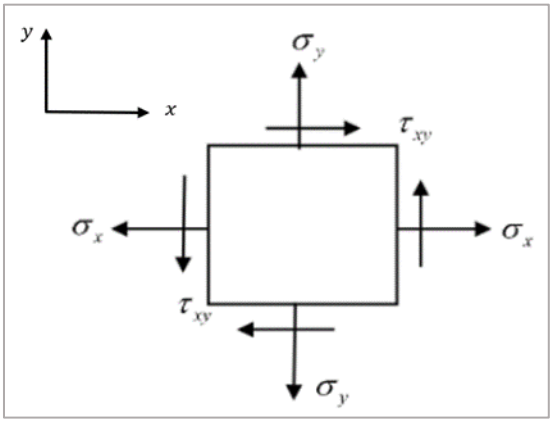

Figure 3.5 Two-dimensional stress state on an element

The stress-strain relation for plane strain conditions in 2D can be written as:

$$\begin{Bmatrix} \sigma_x \\ \sigma_y \\ \tau_{xy} \end{Bmatrix} = \frac{E}{(1+\nu)(1-2\nu)} \begin{bmatrix} 1-\nu & \nu & 0 \\ \nu & 1-\nu & 0 \\ 0 & 0 & \frac{(1-2\nu)}{2} \end{bmatrix} \begin{Bmatrix} \varepsilon_x \\ \varepsilon_y \\ \gamma_{xy} \end{Bmatrix} \quad (3.1)$$

Based on equation 3.1, the required parameters for the elastic constitutive model are the Poisson's Ratio (**ν**) and the modulus of elasticity (E).

In this research, the soil is assumed to behave elastic-perfectly plastic. Accordingly, the Mohr-Coulomb failure yield criteria are used to model soil material behavior. The following parameters are required in this constitutive model: Young's modulus (E), Poisson's ratio (**ν**), friction angle (***Φ***), dilation angle (ψ), and cohesion (C). Although the soil is granular and the cohesion value should be zero, this parameter is considered to be a small value (0.1 Pa) to avoid error in ABAQUS. The dilation angle is considered constant during plastic yielding, controlling

the amount of plastic volumetric strain developed during shearing. The dilation angle can be approximated as $\psi = \boldsymbol{\Phi}$-30 for non-cohesive soils with an internal angle greater than 30 degrees, represented by Bolton (1986). The other soil material properties are extracted from Abdel-Rahman's research (1996) and shown in table 3.1.

Table 3.1 Soil properties (Abdel-Rahman 1996)

Sand state	Unit Weight γ $(\frac{kN}{m^3})$	Angle of Shearing Resistance $\boldsymbol{\Phi}$ (°)	Dilation Angle ψ (°)	Poisson's Ratio $\boldsymbol{\nu}$	Modulus of Elasticity E (MPa)	Cohesion (Pa)
Loose	16.41	33.56	3.56	0.25	25	0.1
Medium	17.55	37.37	7.37	0.2	35	0.1
Dense	18.43	40.31	10.31	0.15	50	0.1

Concrete is assigned to shell foundation material which is necessary for ABAQUS. Shell material properties are elastic. The required shell material properties are stated in table 3.2.

Table 3.2 Shell material properties

Parameter	Value	Unit
Mass Density	2400	kg/m^3
Young's Modulus	60	GPa
Poisson's ratio	0.2	_

3.6 Soil-Foundation Interaction

Two types of interactions between the soil and the foundation in ABAQUS are eligible, general contact and surface to surface contact. General contact interactions automatically identify all contact surfaces, which consumes more time. However, the surface-to-surface interactions would be defined between deformable and rigid surfaces manually to reduce the analysis time.

To define surface to surface interactions in ABAQUS, the surface with higher rigidity should be assumed as the master surface, and the weaker material is the slave surface. Subsequently, the soil surfaces in contact with the foundation are selected as the slave surfaces, and corresponding shell sides are considered master surfaces.

Foundation and soil interaction simulates tangential behavior with isotropic directionality. Moreover, penalty friction formulation is chosen in this model. According to Naval Facilities Engineering Systems Command (NAVFAC standards), the friction factor (tan(δ)) at the soil-foundations interface when a mass concrete rested on coarse sand, clean fine to medium sand, and clean fine sand can be considered in the following ranges:

Table 3.3 Soil-foundation friction factors (NAVFAC standards)

Interface Material	Friction Factor (tan(δ))
Clean gravel, gravel-sand mixtures, coarse sand	0.55 - 0.6
Clean fine to medium sand, silty medium to coarse sand, silty or clayey gravel	0.45 - 0.55
Clean fine sand, silty or clayey fine to medium sand	0.35 – 0.45

Due to the high rigidity of the footings, hard contact is defined as pressure-overclosure for the normal behavior property at the soil-foundation interface.

3.7 Calculation steps

In addition to the initial step, which is predefined by the program, two more steps are established. The first step is the geostatic step. This step is required for all gravity loads and stresses such as weights and geostatic stresses at different elevations to reach equilibrium conditions and settle. The step time for this stage is assumed to be 0.001 seconds which is a sufficient time.

To define the last step, loading, two approaches can be followed in ABAQUS. The first is displacement control loading, and the second is force control loading. The footing load can be applied to the soil by a prescribed displacement. The foundation settles in the soil for a long time due to the applied load. This time could be several months or years; accordingly, the calculation time increases remarkably. The prescribed displacement is assigned to the foundation in ABAQUS to reduce the processing time in the second phase. This displacement is defined as a boundary condition in this program by the user. The software divides the total prescribed displacement into several steps and subjects a part of the total amount in each computational step from zero to the final value. As a result, in foundation engineering, this is an appropriate method to evaluate the bearing capacity of the foundations by plotting the stress-strain diagram and investigating the failure modes. The minimum step time can be determined by using Lame's parameters.

$$\mu = \frac{E}{2(1+\nu)} \tag{3.2}$$

$$\lambda = \frac{E\nu}{(1+\nu)(1-2\nu)} \tag{3.3}$$

where $\boldsymbol{\lambda}$ and $\boldsymbol{\mu}$ are Lame's parameters.

also, V (average velocity of the foundation) < 0.01 Cd

where, $Cd = \sqrt{\frac{\lambda+2\mu}{\rho}}$ (3.4)

In this study, the assigned load pressure is consistent for all models, and the goal is to inspect the stress distributions. Consequently, the force control loading approach is efficient and optimum for this purpose. ABAQUS splits the entire duration of this phase into certain increments, identical to the displacement control approach, and attempts to accomplish all the steps. Each portion of the total load is applied in each time increment. Finally, the total calculation time decreases remarkably compared with the prescribed displacement method.

3.8 Mesh Generation

Numerical analysis by finite element technique generally encounters errors compared to the exact analytical solutions. The discrepancy between the exact and FEM results can be rooted in mesh generation, selecting appropriate shape functions, element types, etc. Appropriate mesh refinement technique is a sophisticated instrument in the precision of the results.

The aim of this study is to interpret the stress distribution below the shell foundations. The accuracy of stress distribution diagrams is dependent on the number of the mesh elements, particularly in the local area underneath the footing. Hence, the mesh sizes in the vicinity of the footing include smaller dimensions to have more elements. Intending to reduce the computation time, the meshes gradually become coarser by receding from the footings and approaching the sides and bottom of the soil part. In this modeling, the foundation part is considered to be rigid approximately. Thus, the mesh sizes on the foundation are not necessitated to be thin and do not affect the results.

ABAQUS automatic mesh generator produces irregular types of mesh around the foundations due to the complex geometry of models. Accordingly, manually generating the meshes would be necessary for the shell and soil parts. In order to control mesh distortions, the foundation and soil parts are partitioned into several regular shapes.

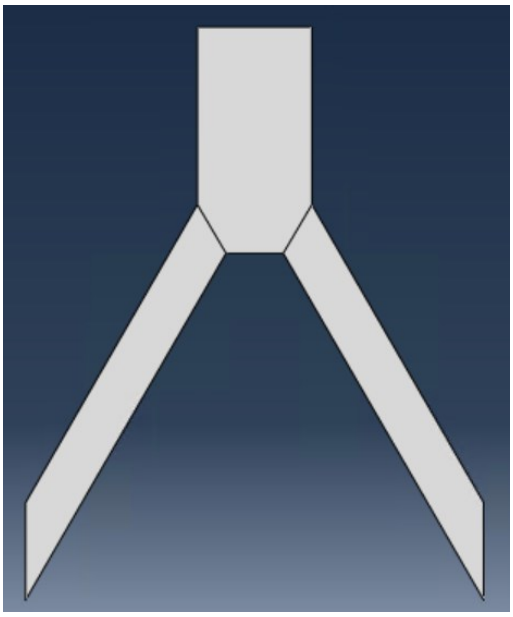

Figure 3.6 Footing partitions for the foundation with the edge angle of 60 degrees

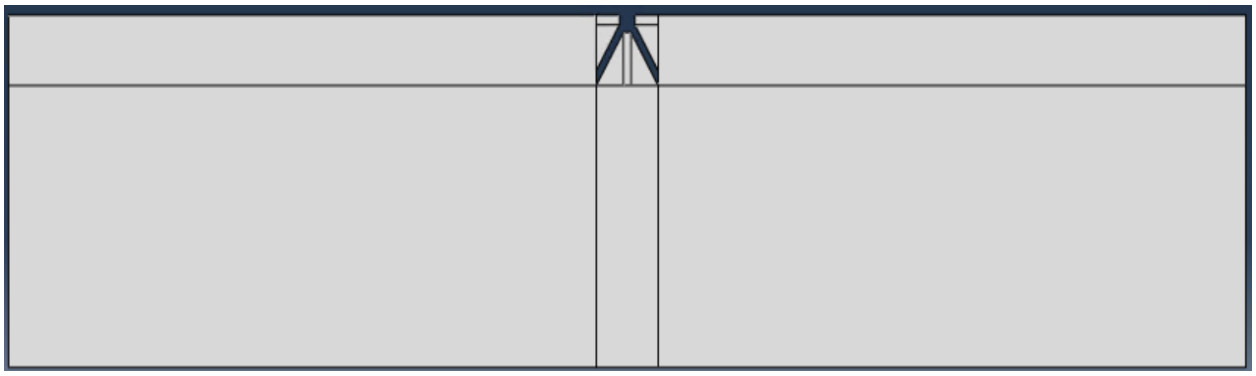

Figure 3.7 Soil part partitions

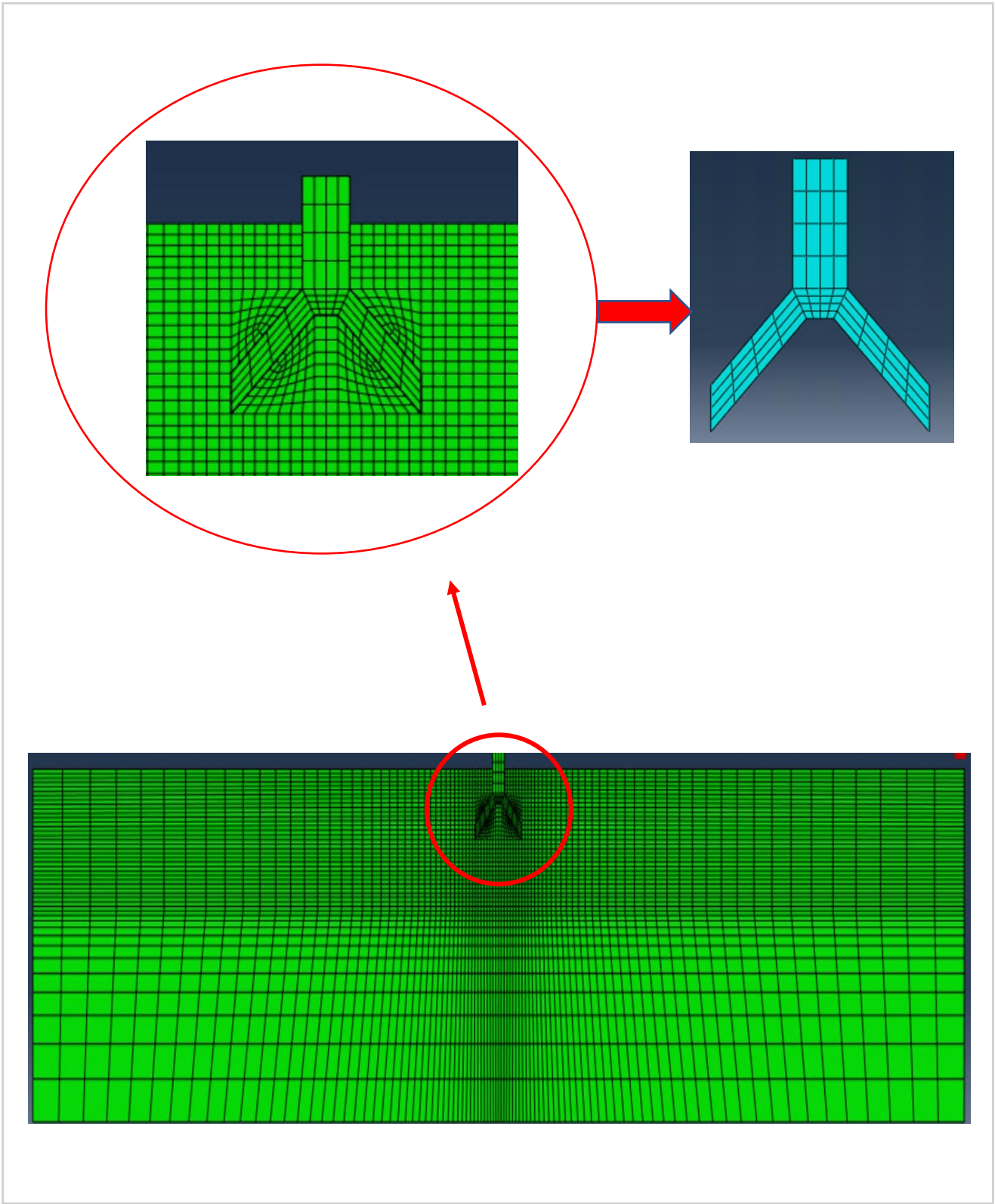

Figure 3.8 Mesh generation of the model

3.9 Validation

To calibrate the numerical model, experimental tests conducted by Abdel-Rahman (1996) have been simulated by ABAQUS to examine contact pressures. They implemented laboratory tests on two geometries of triangular strip shell footings resting on loose, medium, and dense sands shown in the following figures. They measured the contact pressure at specified points in three particular loads (Q_l) during the loading process for each case. In order to evaluate the contact pressure, three pressure transducers were installed at the locations shown in the following figures. The embedment ratio of samples was 0.75. In this section, six models have been analyzed and compared with experimental results.

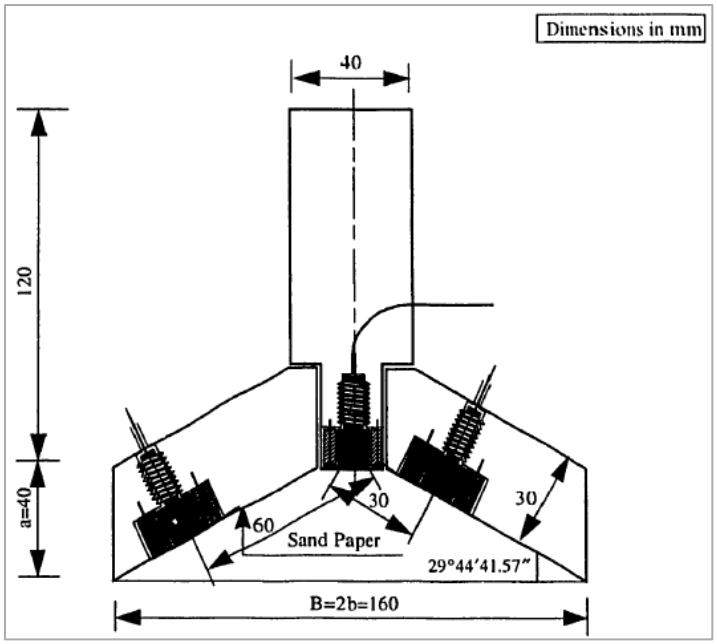

Figure 3.9 Triangular (1) strip shell footing cross-section (Abdel-Rahman 1996)

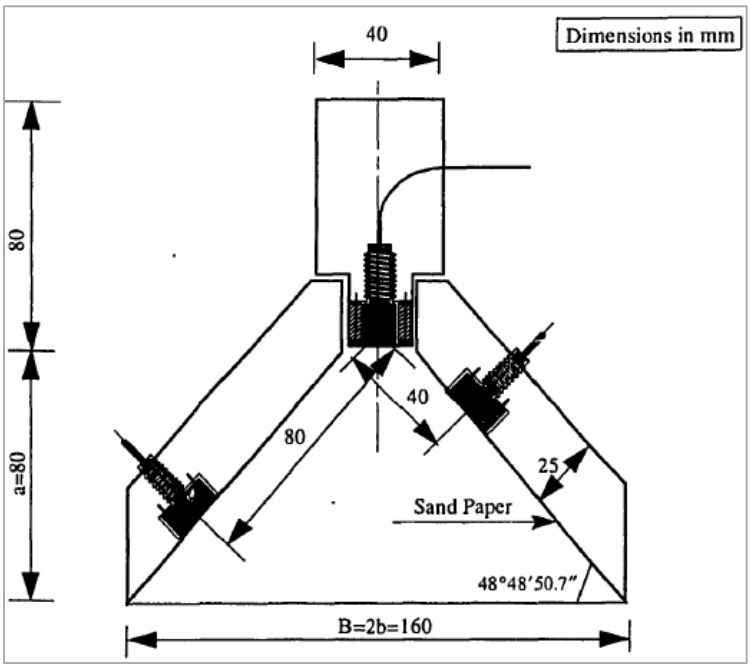

Figure 3.10 Triangular (2) strip shell footing cross-section (Abdel-Rahman 1996)

(a) (b)

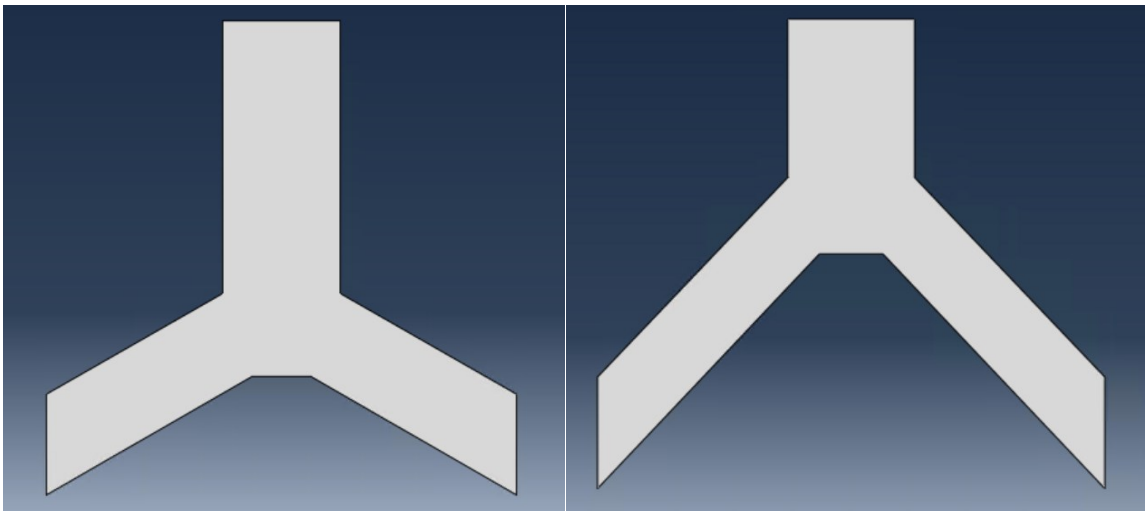
Figure 3.11 (a) Triangular (1) and (b) Triangular (2) shell footings models in ABAQUS

Tests were carried on loose, medium, and dense sands with the soil characteristics shown in table 3.1. To simulate the exerted load in ABAQUS properly, an equivalent pressure has been calculated and applied as a uniformly distributed load on the surface of the footings. The loads and equivalent pressures for each case are illustrated in table 3.3.

Table 3.4 Loads and equivalent pressures on models (Abdel-Rahman 1996)

Footing	Sand state	$Q_l\ (N)$	Equivalent pressure $(\frac{N}{m^2})$
Triangular (1) shell footing	Loose	2107	329218
	Medium	4370	682812
	Dense	6718	1049687
Triangular (2) shell footing	Loose	2192	342500
	Medium	4205	657031
	Dense	7589	1185781

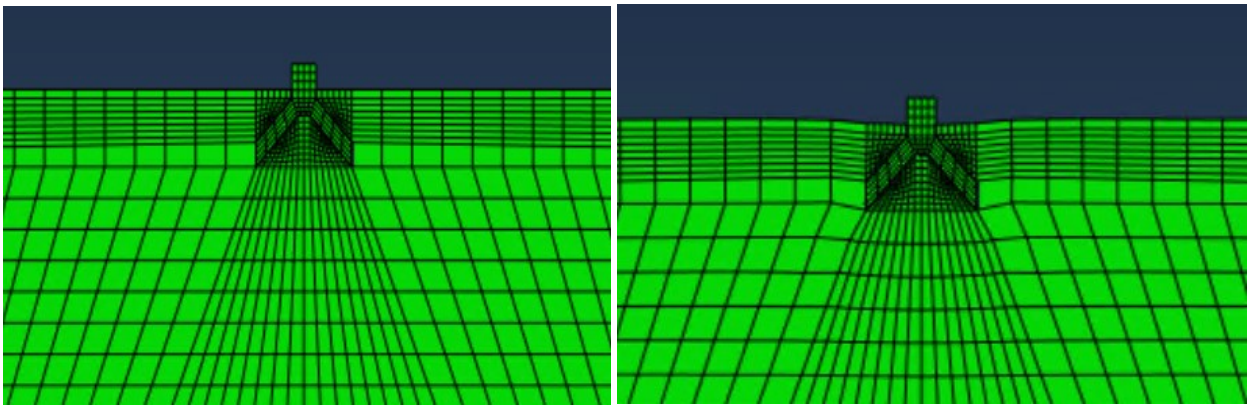

(a) (b)

Figure 3.12 (a) Undeformed and (b) deformed meshes

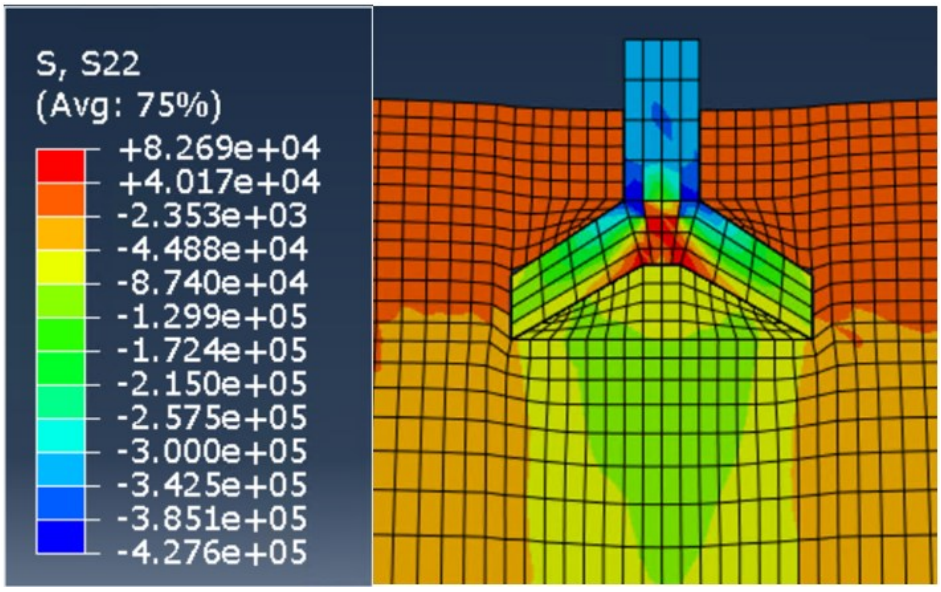

Figure 3.13 Vertical stress contours below the footing

Points (1) and (2) have distances 30 mm and 60 mm from the center of the triangular (1) shell footing. These locations are 40 mm and 80 mm from the center of the triangular (2) shell. Figure 3.14 through 3.19 compares the vertical stresses at specified points of Abdel-Rahman's (1996) experimental work and the developed numerical modeling in this study.

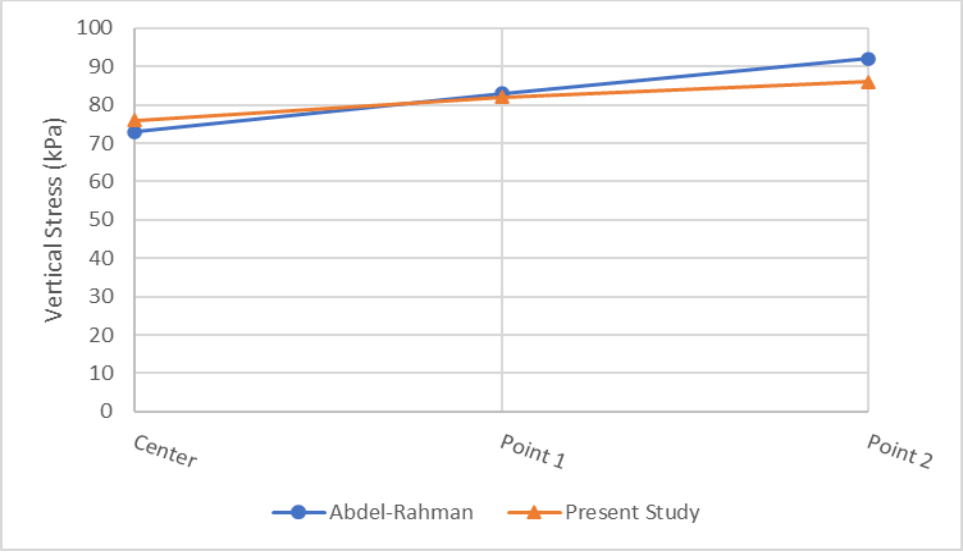

Figure 3.14 Vertical stresses at specified points for triangular (1) shell foundation on loose sand

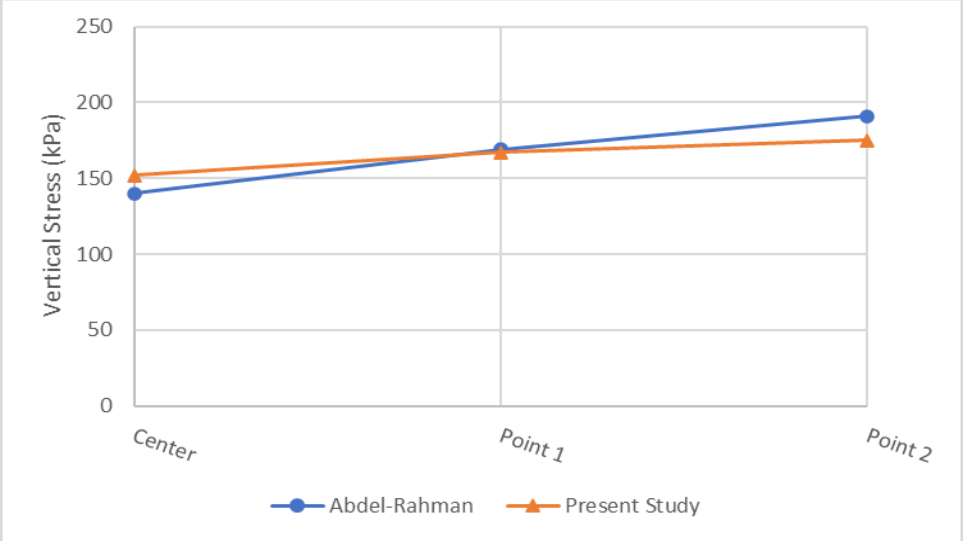

Figure 3.15 Vertical stresses at specified points for triangular (1) shell foundation on medium sand

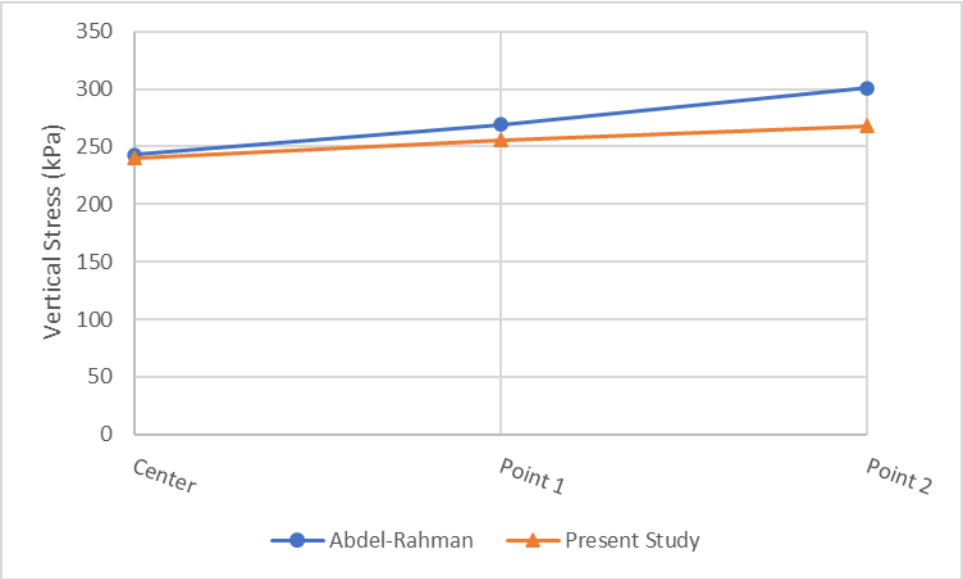

Figure 3.16 Vertical stresses at specified points for triangular (1) shell foundation on dense sand

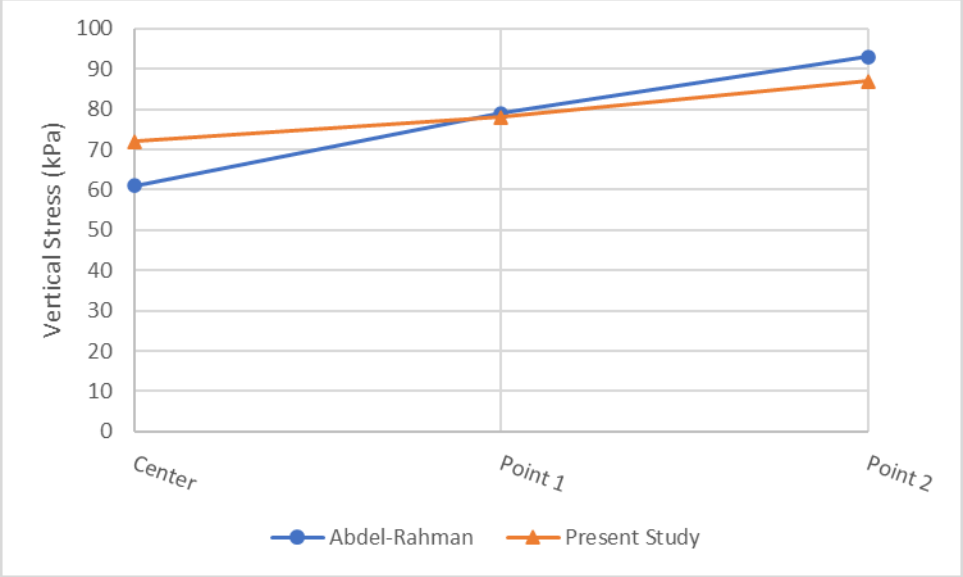

Figure 3.17 Vertical stresses at specified points for triangular (2) shell foundation on loose sand

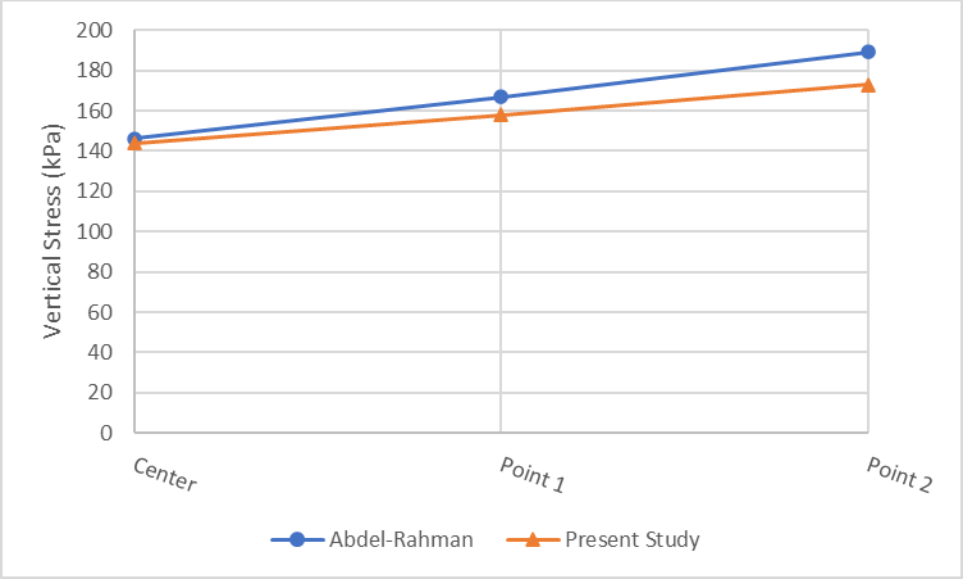

Figure 3.18 Vertical stresses at specified points for triangular (2) shell foundation on medium sand

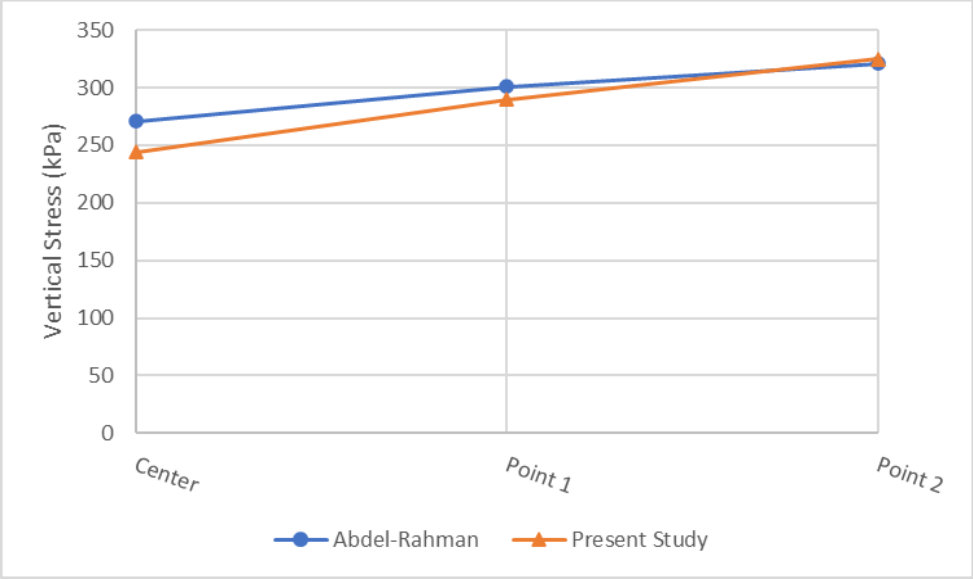

Figure 3.19 Vertical stresses at specified points for triangular (2) shell foundation on dense sand

Table 3.5 Comparison of results in the present study vs. Abdel-Rahman (1996)

Footing	Sand state	Pressure (kPa)					
		Center		Point (1)		Point (2)	
		Abdel-Rahman (1996)	This Study	Abdel-Rahman (1996)	This Study	Abdel-Rahman (1996)	This Study
Trig. (1)	Loose	73	76	83	82	92	86
	Medium	140	152	169	167	191	175
	Dense	243	240	269	256	301	268
Trig. (2)	Loose	61	72	79	78	93	87
	Medium	146	144	167	158	189	173
	Dense	271	244	301	290	321	325

Based on the comparison tables and figures, numerical results are in good agreement with experimental results. Errors can be rooted in reading mistakes in experimental tests, estimating soil and foundation material properties in numerical modeling, the rigidity assumption of footings, number and type of elements, etc.

CHAPTER 4

RESULTS AND ANALYSIS

4.1 General

In this chapter, numerical models are developed, and contact pressures and stress distributions at different depths below the triangular shell foundations are presented in graphs and tables. Stress distributions are investigated by examining the effect of edge angles, and the optimum shapes of shell foundations are recommended and compared with their flat counterparts on loose, medium, and dense sands separately. Also, the bearing capacities of the optimum shape of triangular shell foundations are evaluated and compared with the alternative flat ones on different sand states.

4.2 Test Results

In this section, a series of figures are demonstrated to reveal the stress distribution at the soil-footing interface, D = 0, D = 0.5B, and D = B below the base of the shell foundations and compared with alternative flat ones. The edge angle (θ) varies from 60 degrees to the flat configuration (i.e., θ = 0 degrees) by the increments of 5 degrees. In order to facilitate the comparison of different geometries, the vertical stresses along the slopes of the shell footings are plotted on a horizontal axis. Furthermore, the distances are normalized within the range of 0 to 1 to distinguish the sloped parts and the central plain region of the shell footings. As shown in figure 4.1, the normalized distance for the left inclined part would be from 0 to 0.45, the central horizontal zone is from 0.45 to 0.55, and the right-side inclined part ranges from 0.55 to 1. It should be noted that in each figure, the stress distributions are presented for loose, medium, and dense sand for a specific edge angle of footings in an effort to differentiate the soil densification influence on the stress distributions.

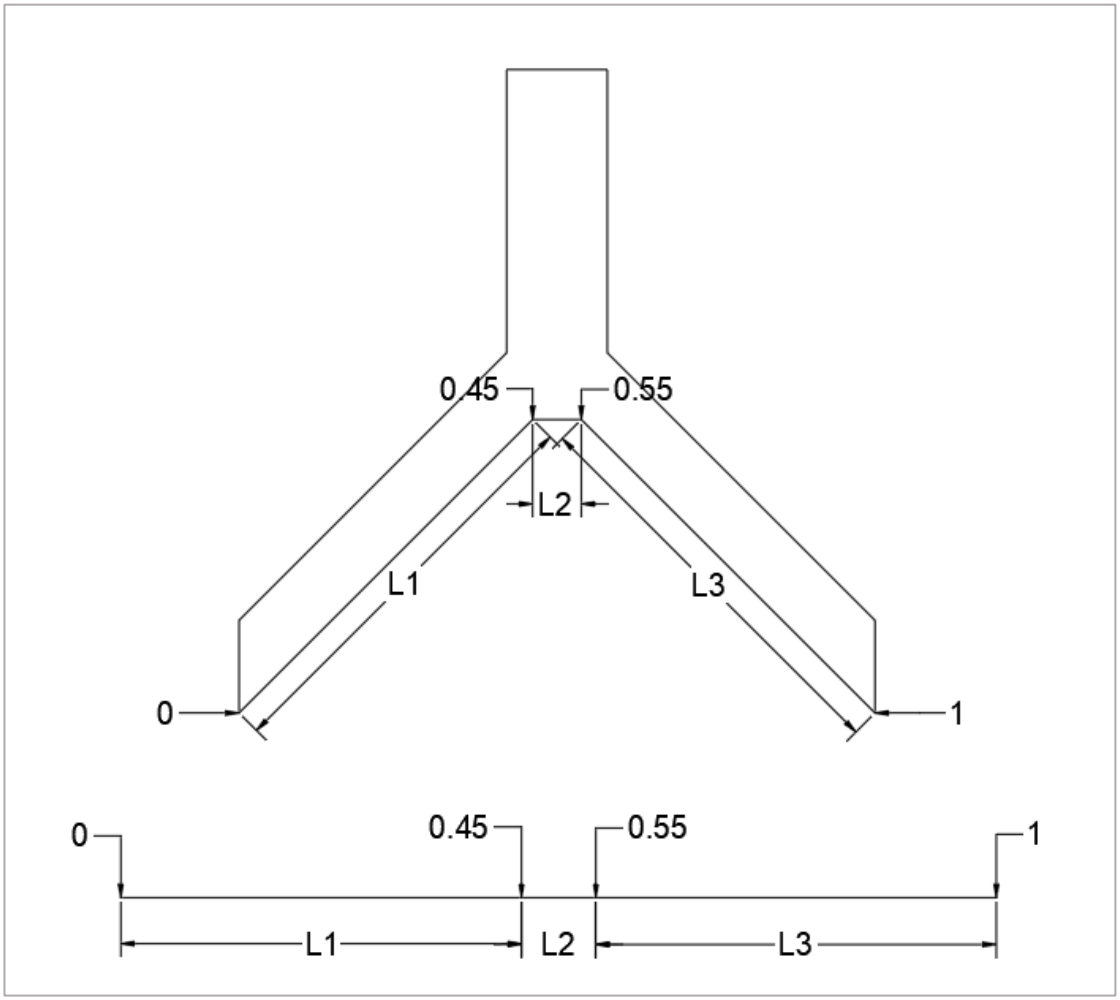

Figure 4.1 Normalized horizontal axis and zones of the shell footings for contact pressure results

4.2.1 Contact pressure below foundations

A glance at figures 4.2 to 4.14 illustrates contact pressure distributions of the shell and the flat foundations resting on loose, medium, and dense sand states. Contact pressure distributions below the shell footings divulge a similar trend for loose and medium sands. Stresses increase from the edges of the footings and reach the maximum value around 0.1 – 0.3 of inclined part lengths (L1 and L3), then experience a decrease at the center for the triangular shell foundations with the edge angle of 60 to about 20 degrees. By reducing the edge angle of shell foundations, the concave in the stress distribution at the center transforms to a peak gradually. The contact pressure diagrams confirm that the stress curves below the foundations with an edge angle lesser than 15 degrees can express a parabolic curve approximately. The maximum magnitude of stresses is located at the center in these configurations, and the minimum values happen at the peripheries.

In the case of dense sand, the contact pressure values increase from the edges and arrive at the highest amount, around 0.2 to 0.3 of the sloped parts, afterward, exhibit a concave at the center in the shells with the edge angles between 60 and 50 degrees. When edge angles vary from 50 to 10 degrees, the maximum stresses occur at the edges, and the minimum values of stresses materialize at the center zones. The contact pressure distributions below the flat footings rested on dense sand show a similar fashion as loose and dense sand states.

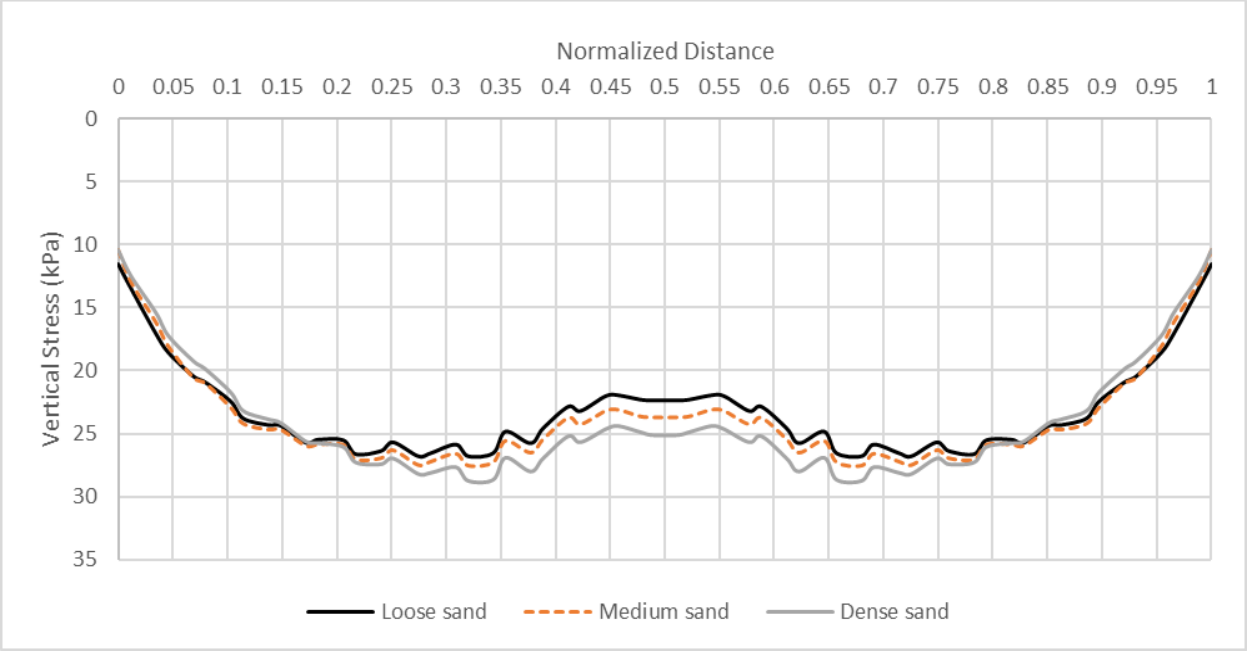

Figure 4.2 Contact pressure below the triangular shell footings with θ = 60 degrees

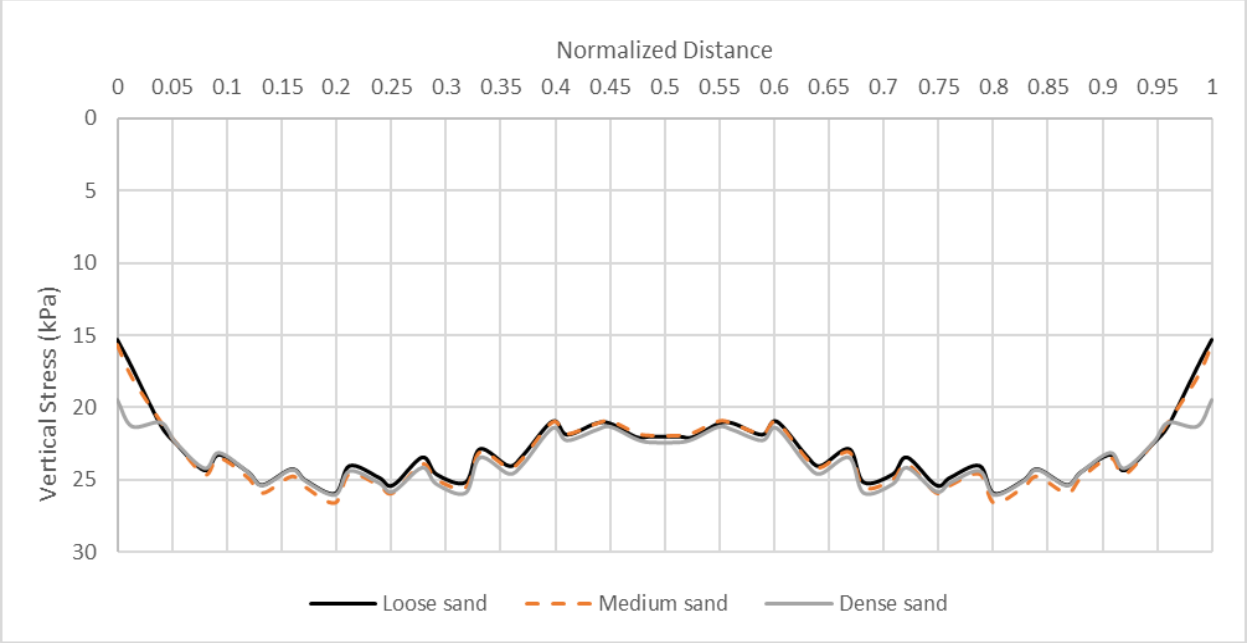

Figure 4.3 Contact pressure below the triangular shell footings with θ = 55 degrees

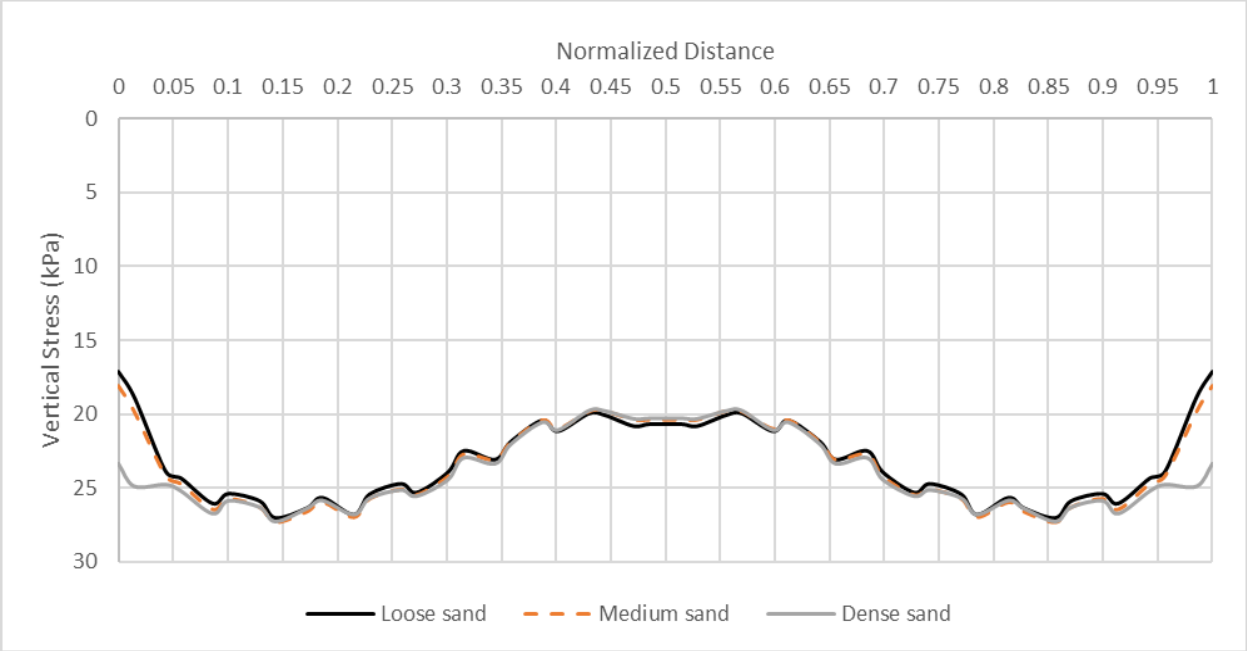

Figure 4.4 Contact pressure below the triangular shell footings with θ = 50 degrees

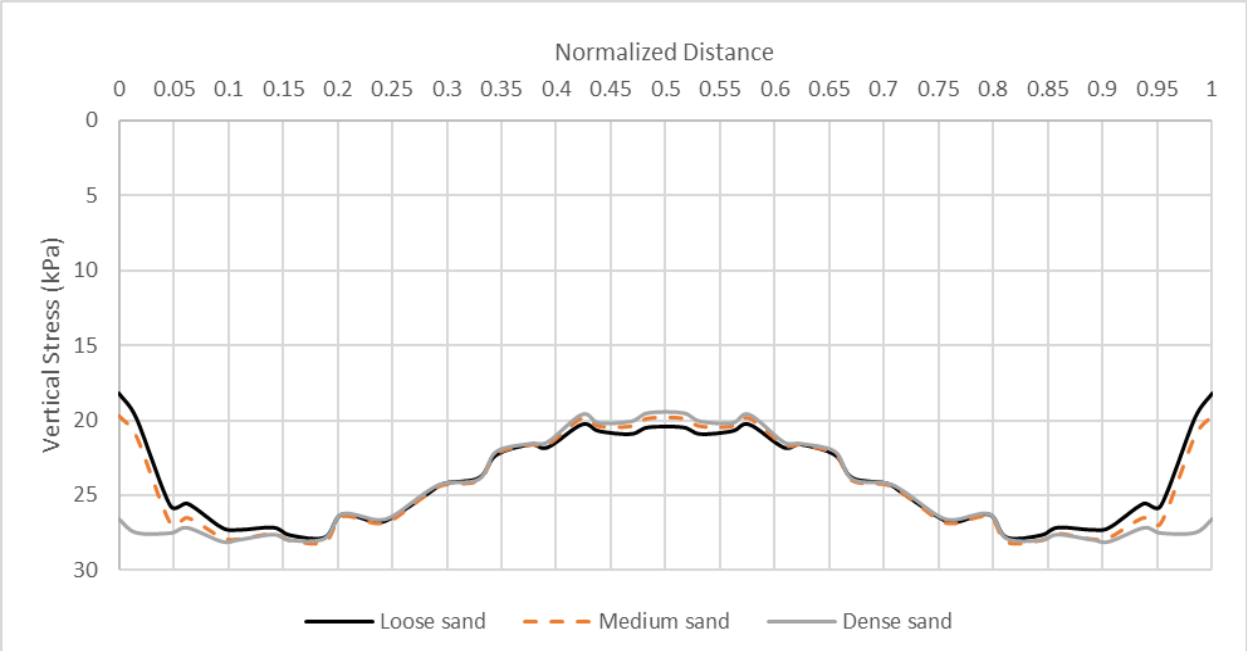

Figure 4.5 Contact pressure below the triangular shell footings with θ = 45 degrees

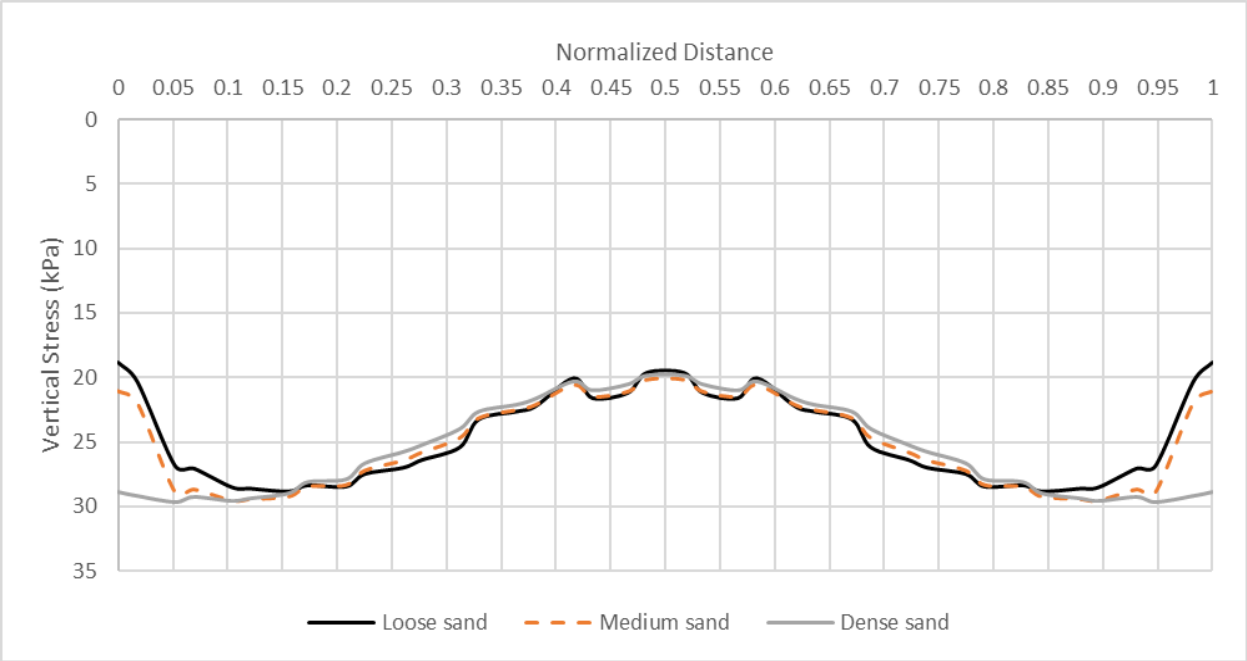

Figure 4.6 Contact pressure below the triangular shell footings with θ = 40 degrees

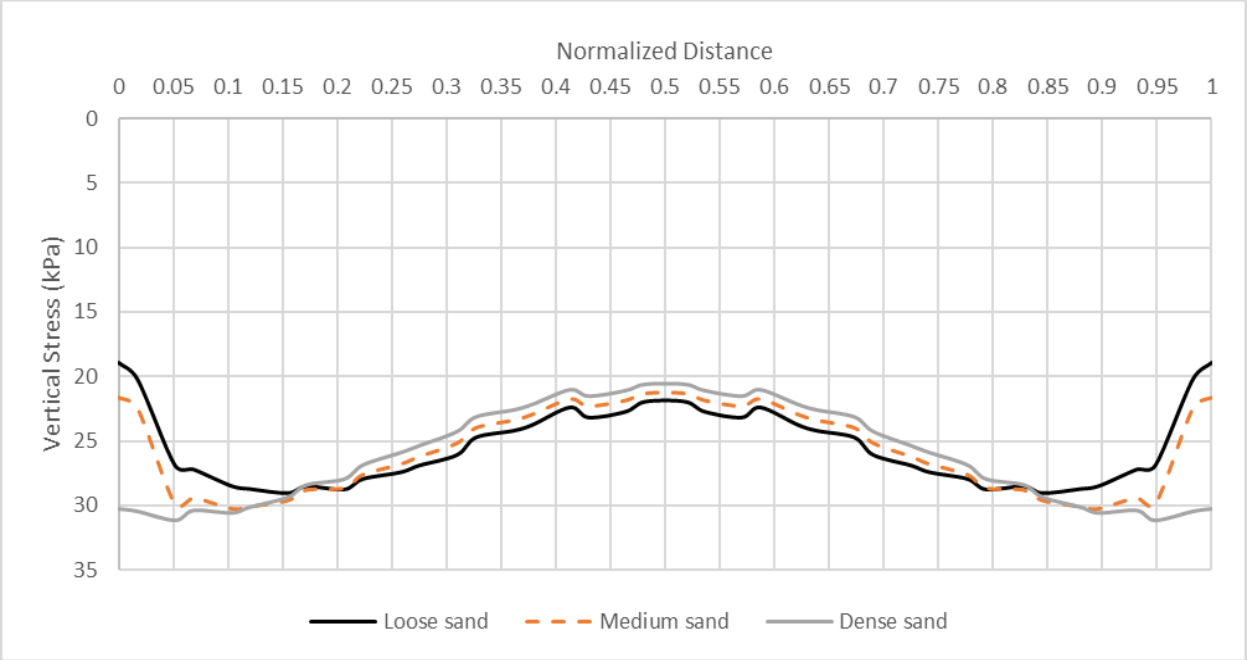

Figure 4.7 Contact pressure below the triangular shell footings with θ = 35 degrees

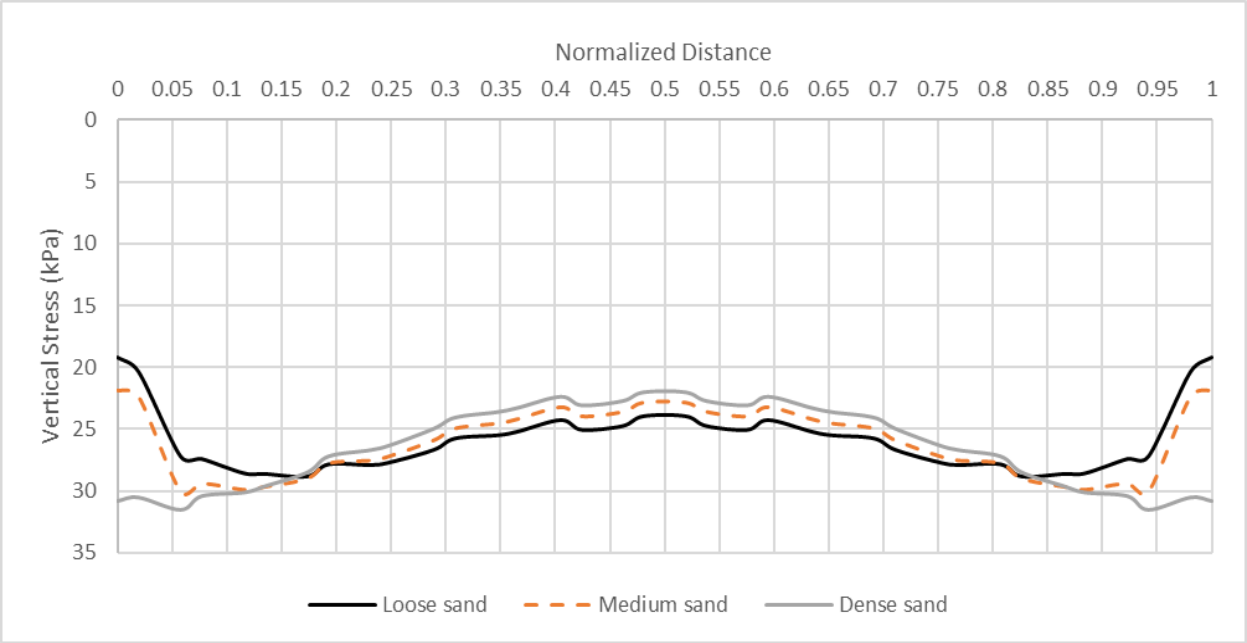

Figure 4.8 Contact pressure below the triangular shell footings with θ = 30 degrees

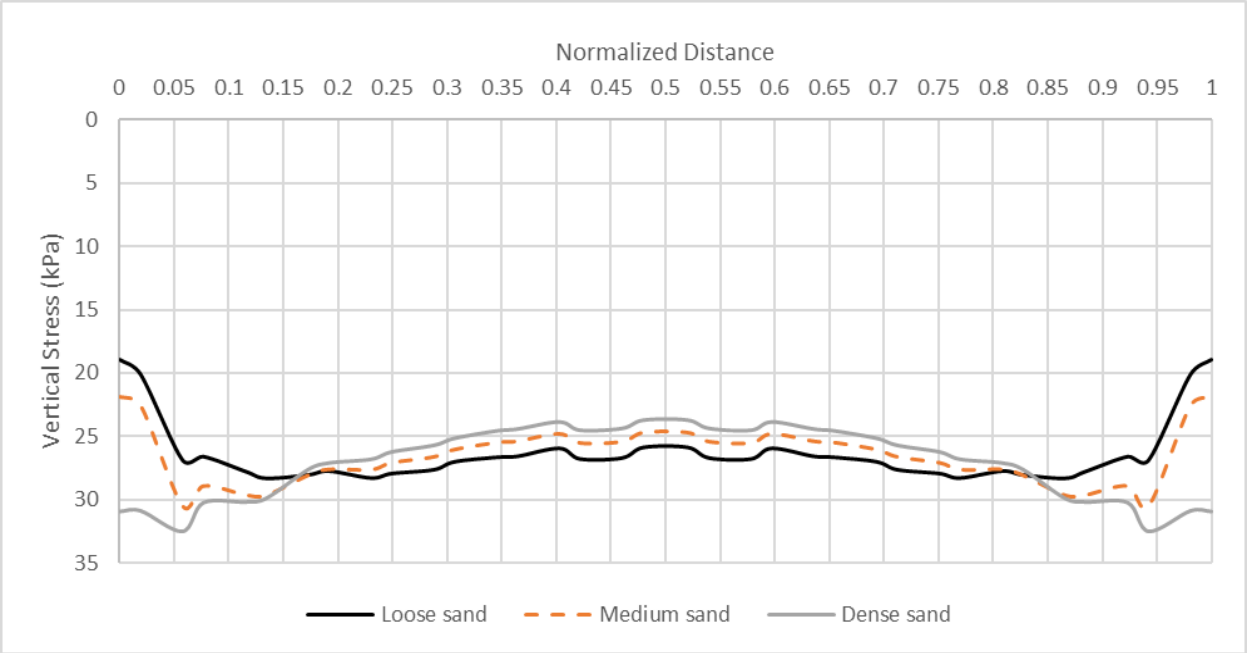

Figure 4.9 Contact pressure below the triangular shell footings with θ = 25 degrees

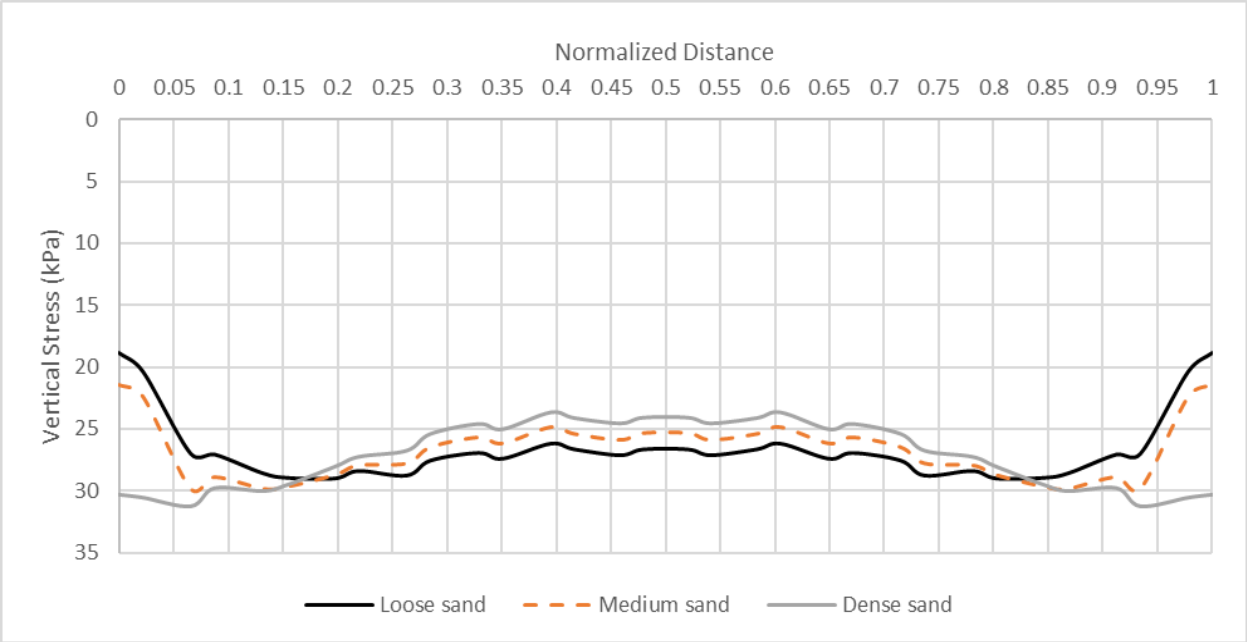

Figure 4.10 Contact pressure below the triangular shell footings with θ = 20 degrees

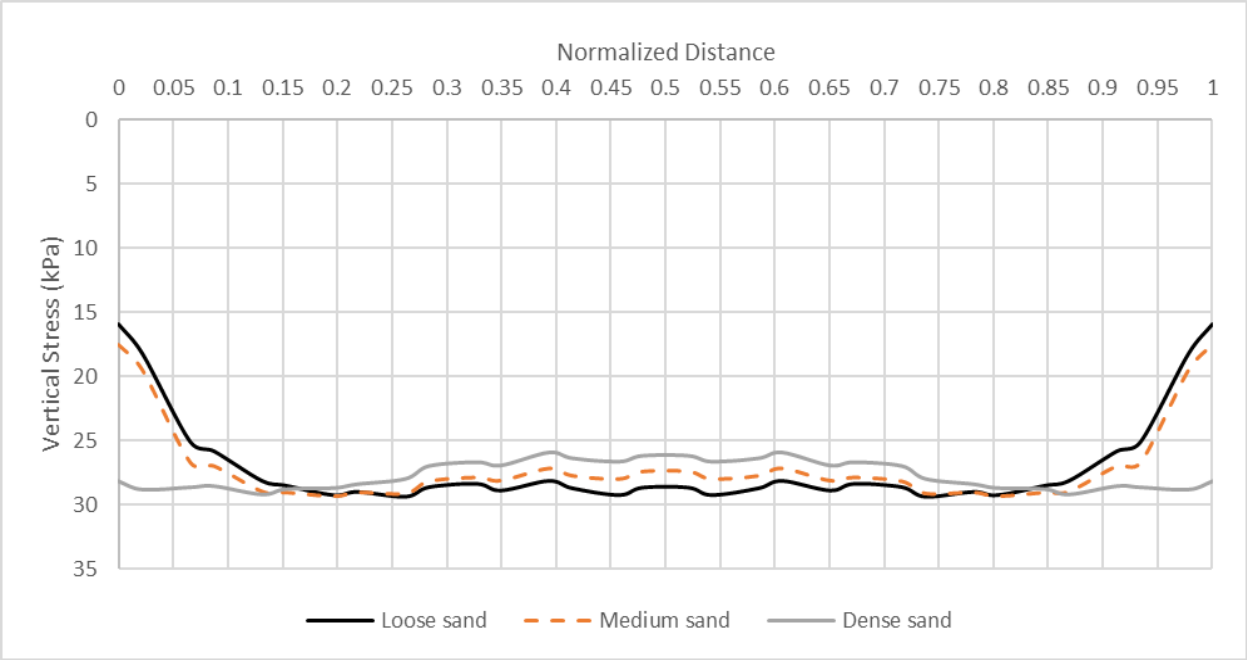

Figure 4.11 Contact pressure below the triangular shell footings with θ = 15 degrees

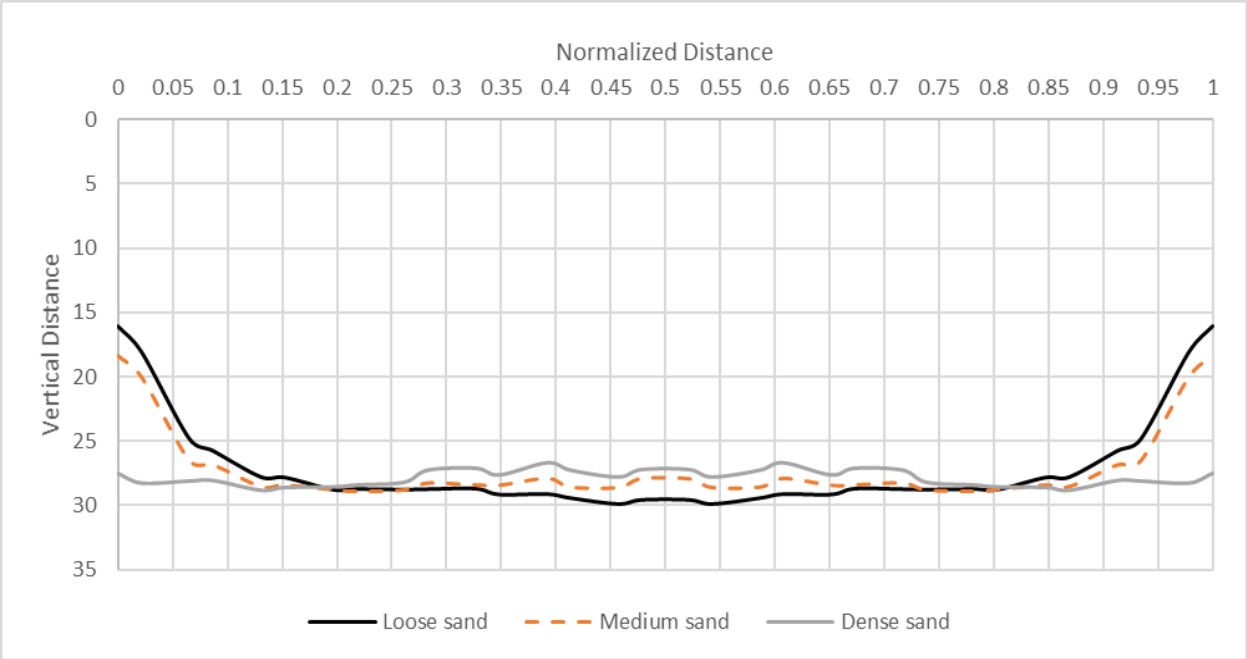

Figure 4.12 Contact pressure below the triangular shell footings with θ = 10 degrees

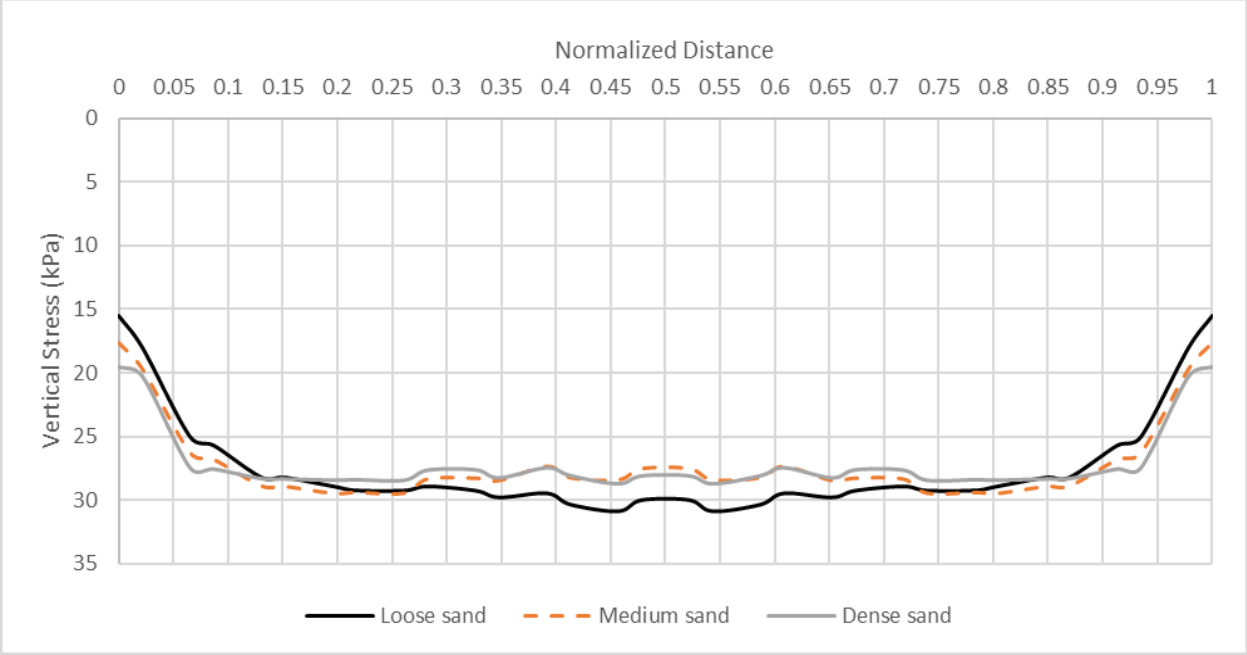

Figure 4.13 Contact pressure below the triangular shell footings with θ = 5 degrees

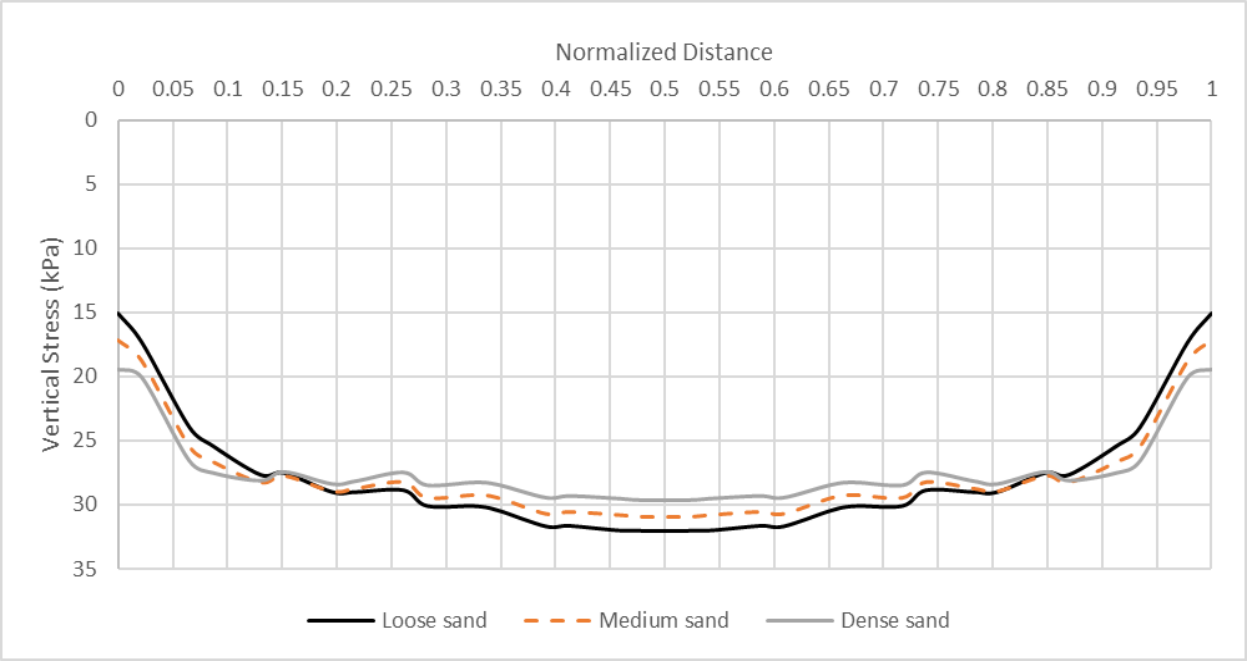

Figure 4.14 Contact pressure below the flat footings

4.2.2 Stress distribution at D = 0, 0.5B, and B below the foundations

In the following figures, the stress distributions at D = 0 below the base of the shell footings with θ = 60 to 20 degrees are presented. The stress path at D = 0 (base of the foundations) with the edge angle from 15 degrees to the flat state is approximately duplicate with the contact pressure and has the same characteristics. Afterward, this trend has been illustrated for the depths D = 0.5B and D = B for all shells foundations.

According to figures 4.16 through 4.24, the stress distributions at the base of the footings (D = 0) increase linearly from the edge of the shells to 0.1 – 0.15 times of the sloped lengths, then experience a diminution around the center in the cases of θ = 20 to 50 degrees shells resting on loose and medium sands. The reason is that for the footing with lower edge angles, the distance of the soil-footing interface and the horizontal path (D = 0) at the base of the foundations decrease. As a result, the stress distributions tend to the contact pressures at the interface that experience a reduction at the center in shell foundations. Moreover, the vertical stresses at the center of the

horizontal path at D = 0 below the shell's bases report a slight increase in the case of loose sand than medium and dense sands. This fashion exhibits a different tendency around the edges of the shells in the dense sand condition. Decreasing the edge angle confirms increases at the edges on dense sand. Shell foundations on dense sand contribute to lower stresses at the center relative to the edges. The stresses remain constant to 0.05 -0.1 of the length of the sloped parts (L1 and L3) from the edges, then reduce slightly until the center.

Figures 4.25 to 4.37 corroborate the influence of soil densification on the stress distribution under a specified load. The range of the stress variations at D = 0.5B below the base of the footings shows the greater values in loose, medium, and dense sands, respectively. It confirms that the loose sand is more sensitive to the applied load. These trends are independent of the edge angle of the footings. For all foundations geometries, as expected, the stresses have minimum values at outside zones, and maximum stresses are at the center. The maximum and minimum ranges illustrate the greater interval in loose sand, medium, and dense sand, respectively. It signifies better stress uniformity in dense sand at D = 0.5B.

Shell and load effects on the stress dispersion diminish at lower depths based on figures 4.38 to 4.50. The stress diagrams demonstrated conformity in the investigation of the stress distributions beneath the flat footings for all sands at D = B below the base of the footings. The vertical pressures show a slight variance below the shell footings by examining the soil states at D = B. In the case of the flat foundation, all stress diagrams are approximately coincident at D = B.

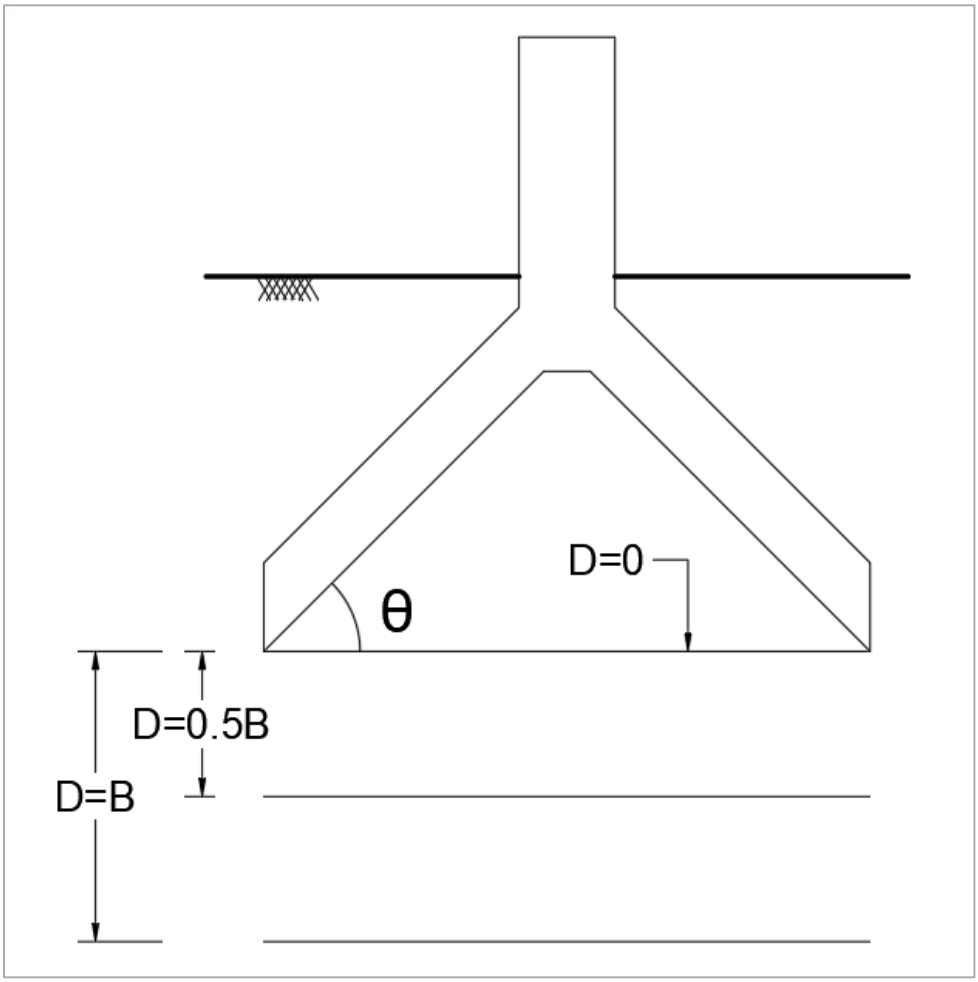

Figure 4.15 Specified depths under the base of the shell foundations

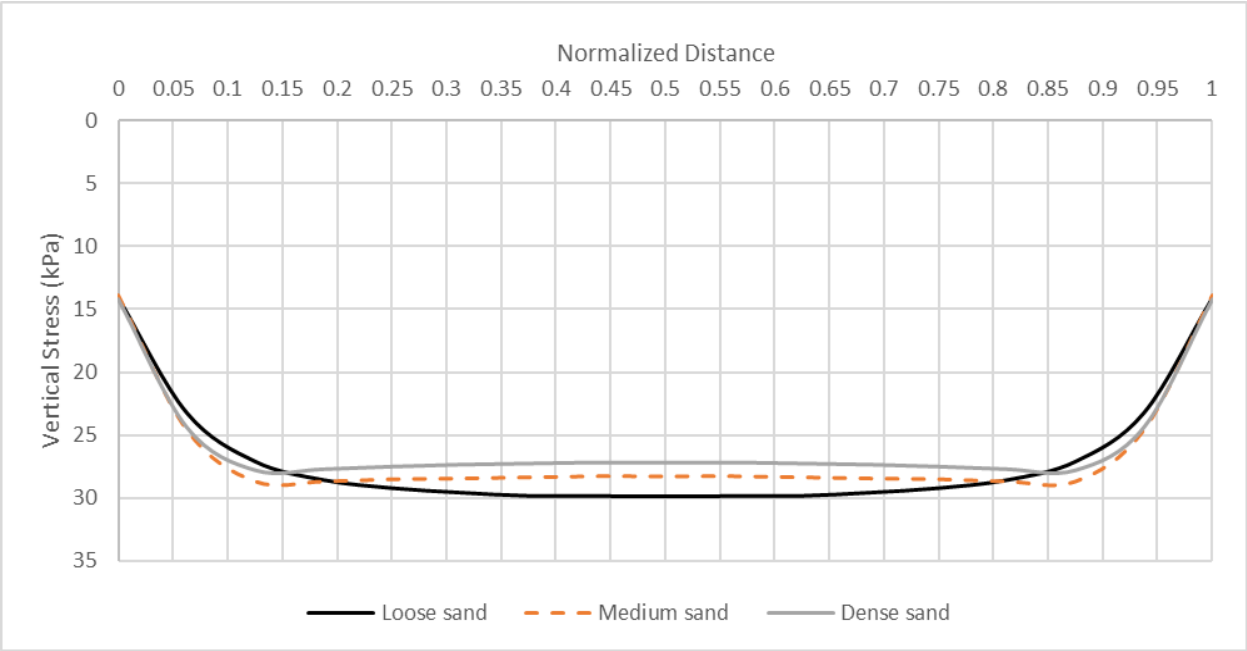

Figure 4.16 Stress distribution at D = 0 below the triangular shell footing with θ = 60 degrees

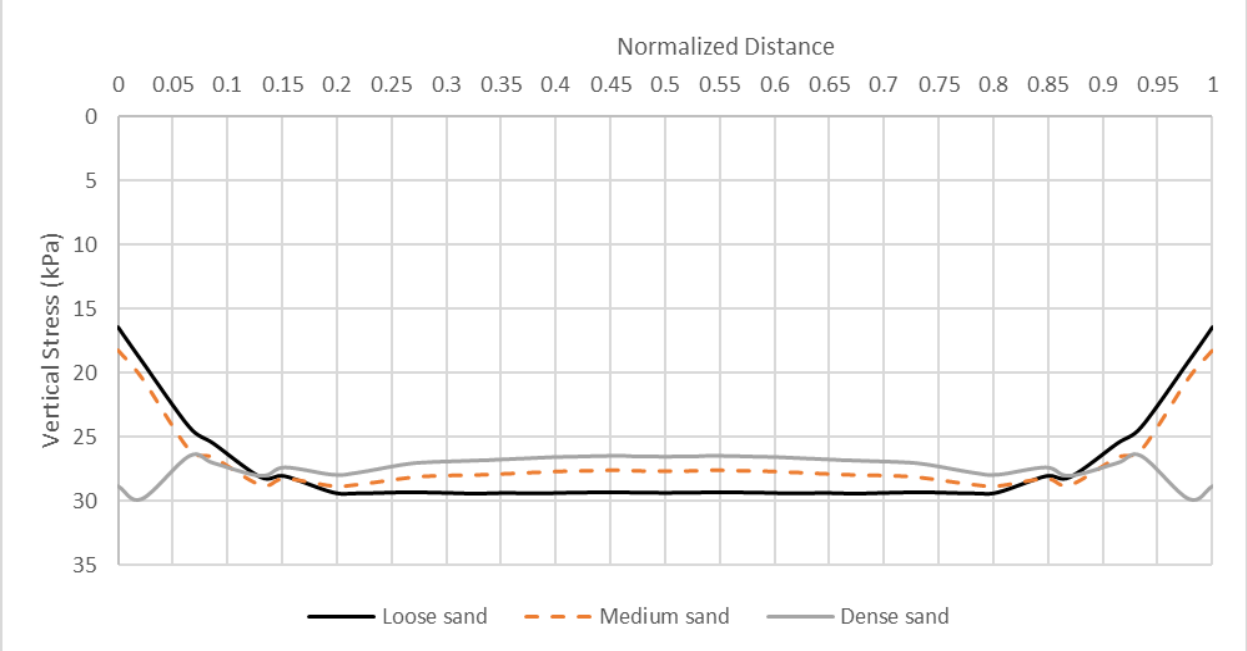

Figure 4.17 Stress distribution at D = 0 below the triangular shell footing with θ = 55 degrees

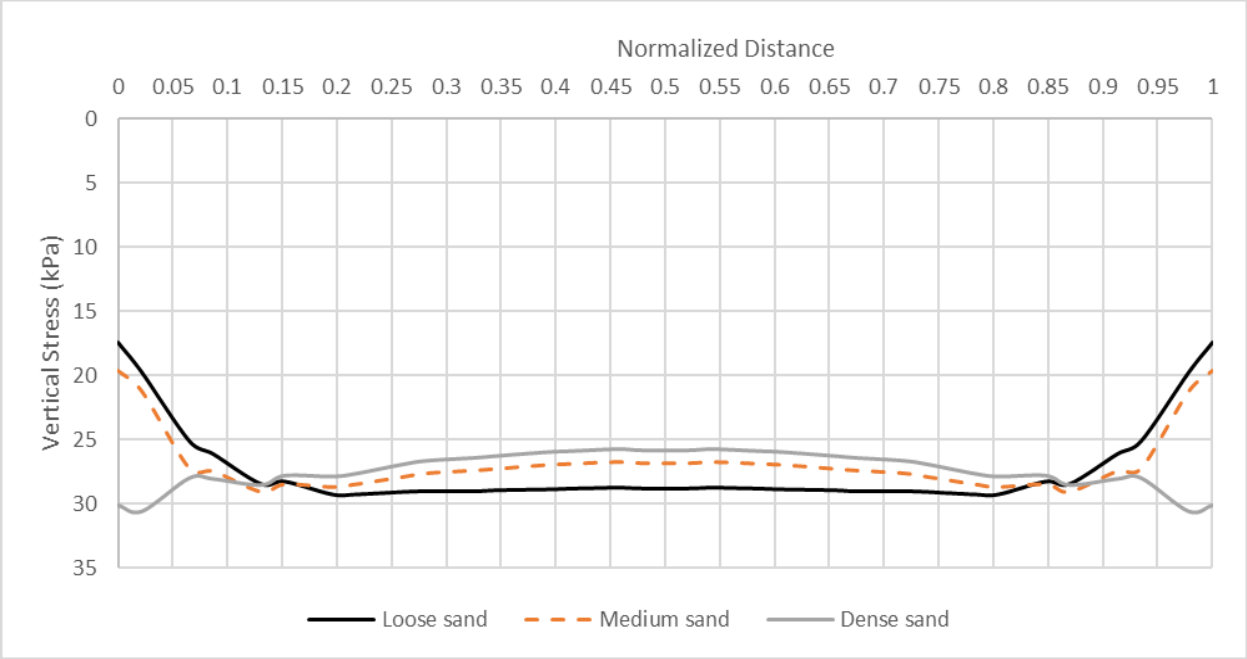

Figure 4.18 Stress distribution at D = 0 below the triangular shell footing with θ = 50 degrees

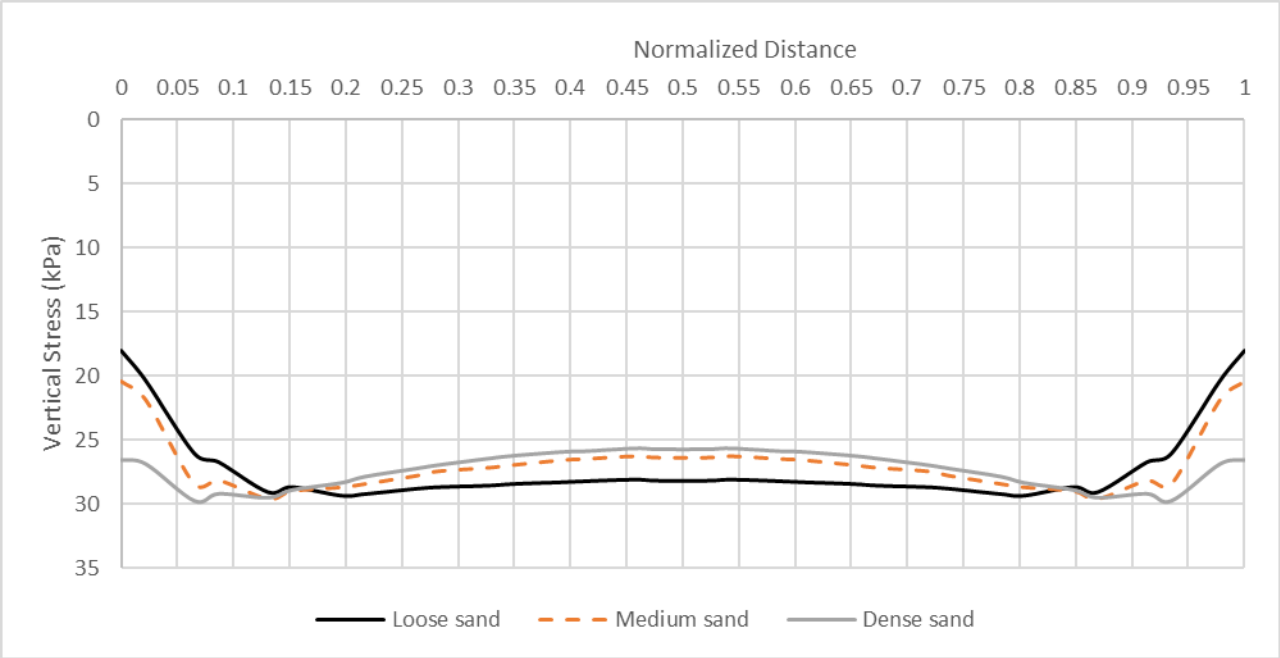

Figure 4.19 Stress distribution at D = 0 below the triangular shell footing with θ = 45 degrees

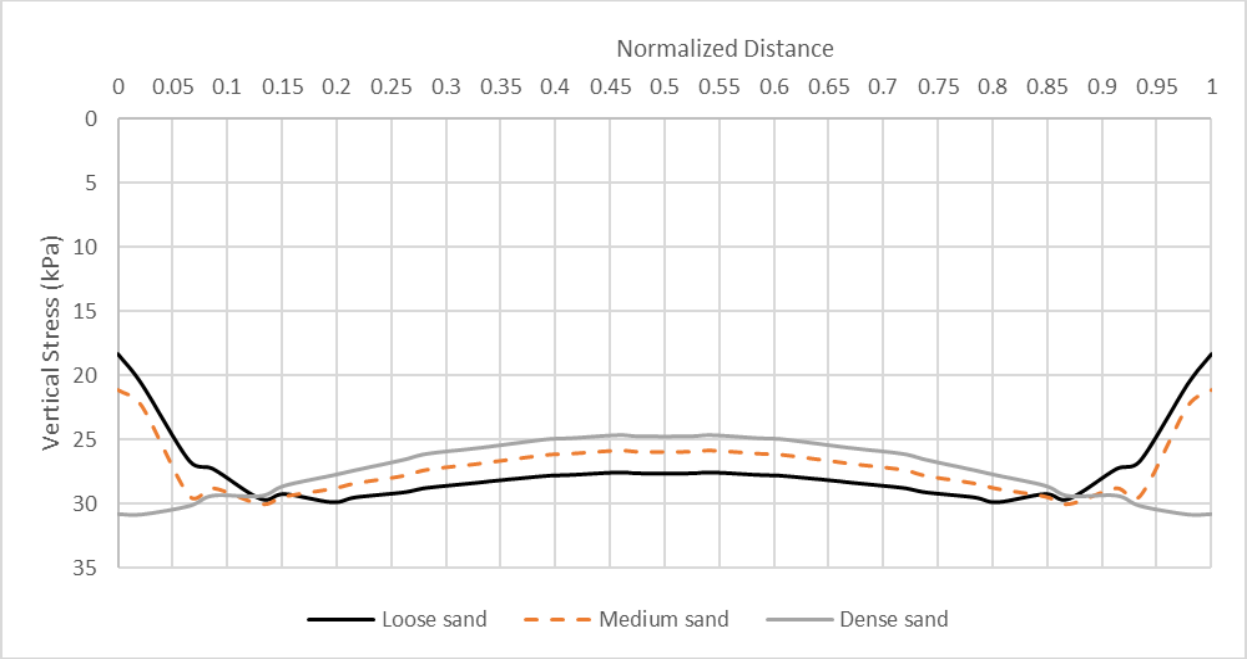

Figure 4.20 Stress distribution at D = 0 below the triangular shell footing with θ = 40 degrees

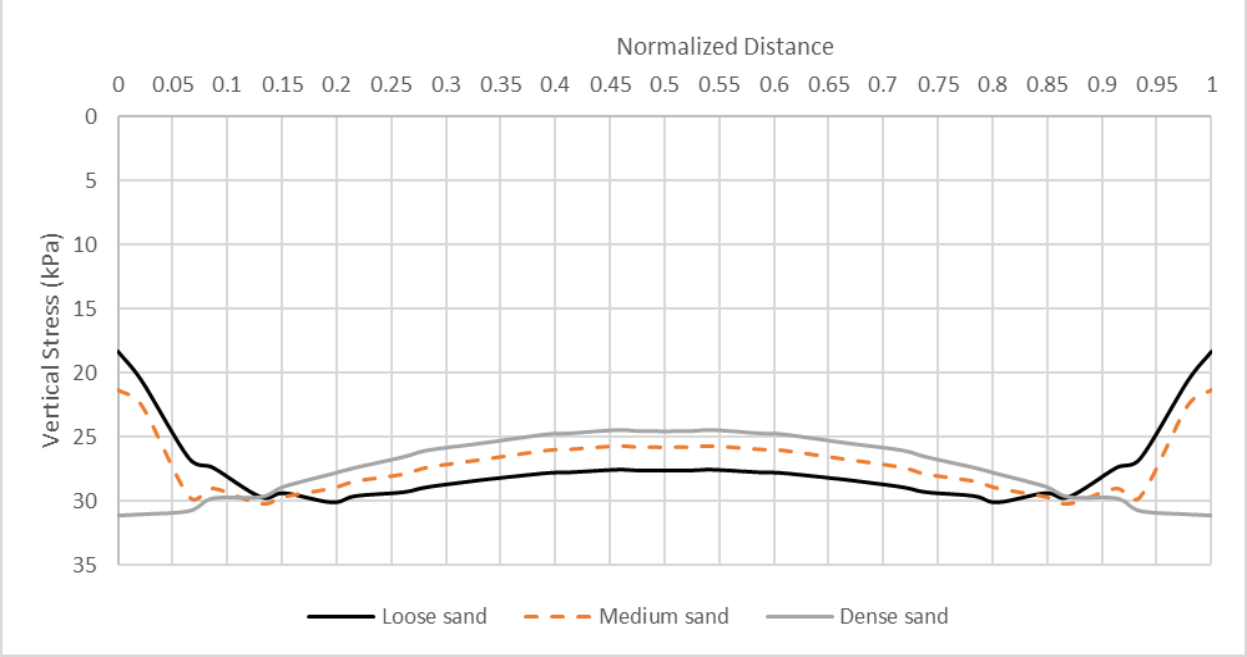

Figure 4.21 Stress distribution at D = 0 below the triangular shell footing with θ = 35 degrees

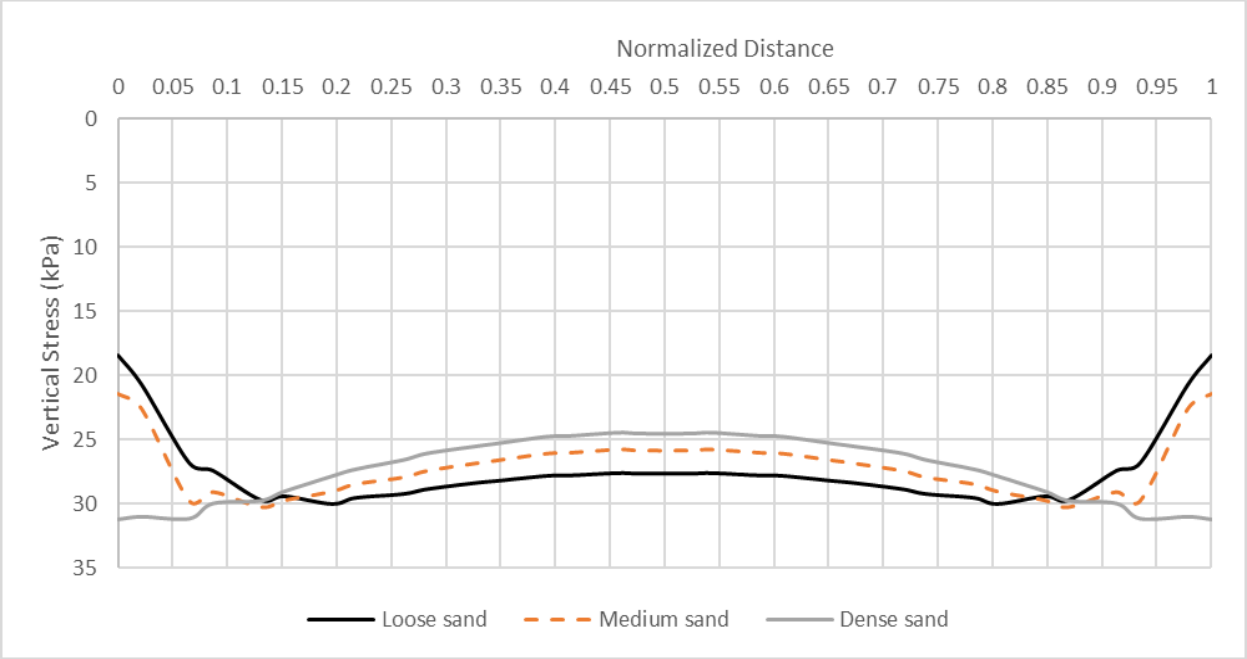

Figure 4.22 Stress distribution at D = 0 below the triangular shell footing with θ = 30 degrees

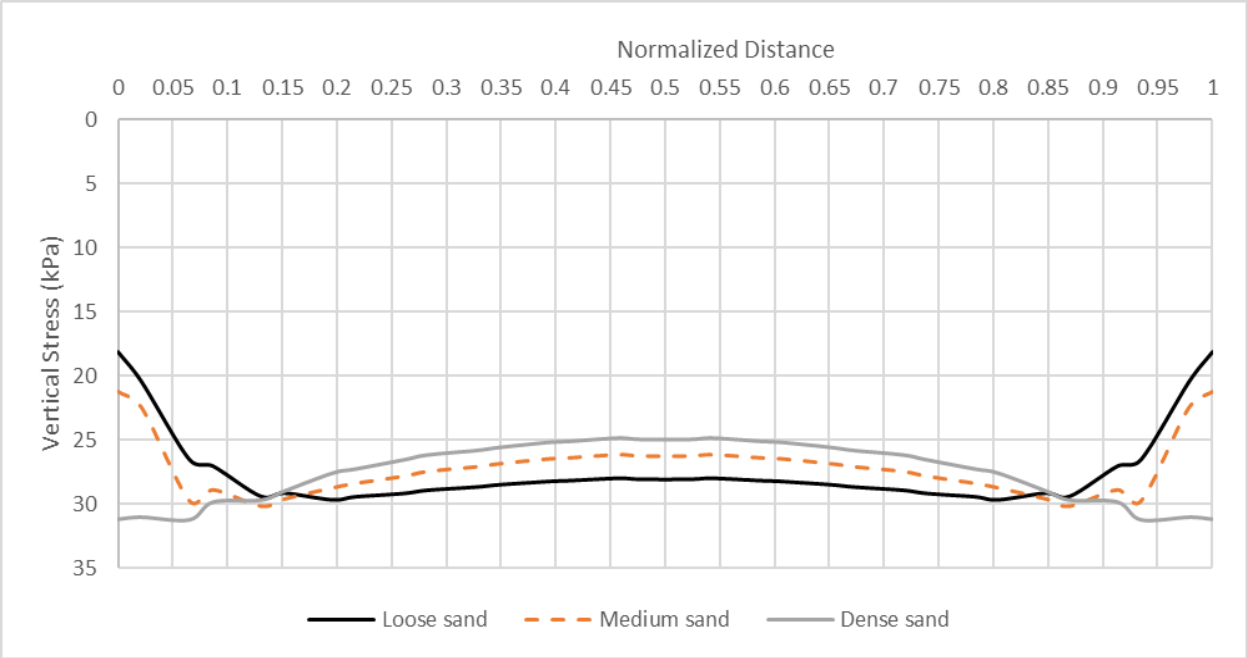

Figure 4.23 Stress distribution at D = 0 below the triangular shell footing with θ = 25 degrees

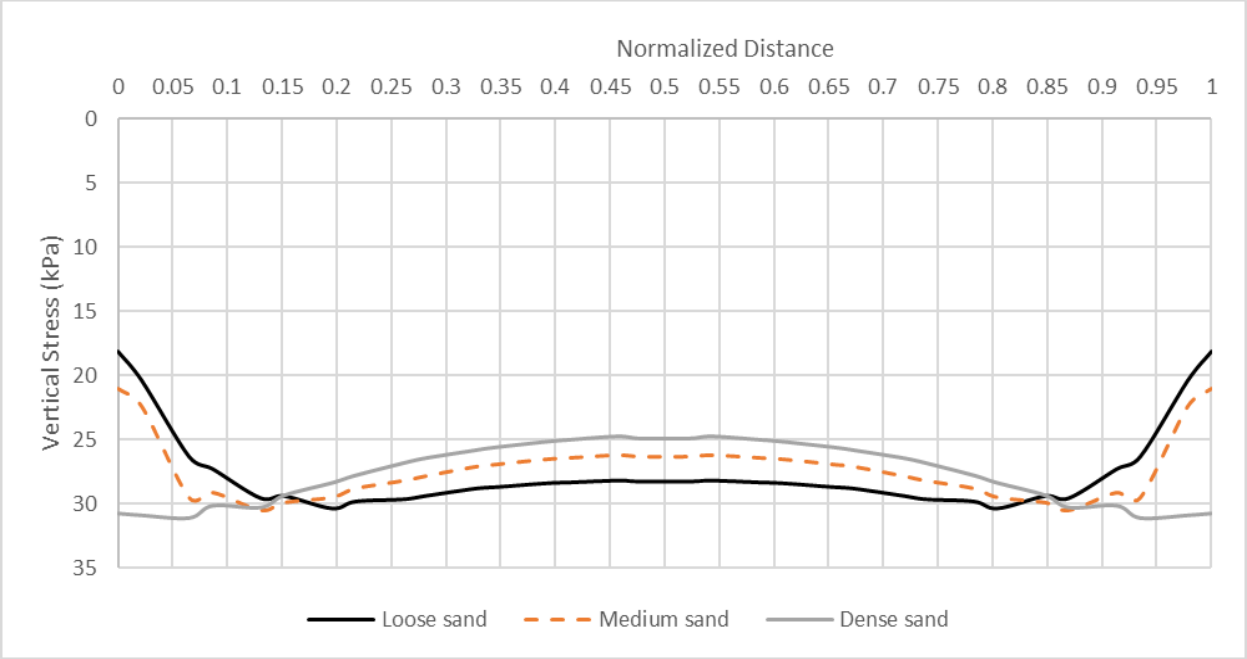

Figure 4.24 Stress distribution at D = 0 below the triangular shell footing with θ = 20 degrees

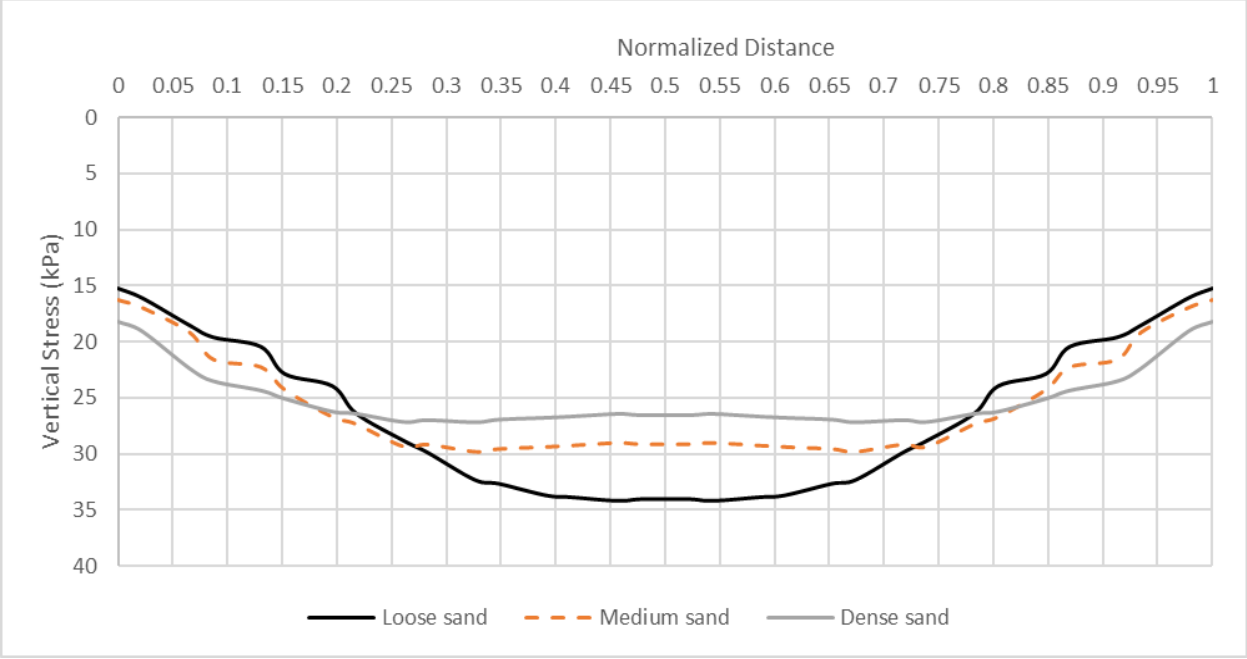

Figure 4.25 Stress distribution at D = 0.5B below the triangular shell footing with θ = 60 degrees

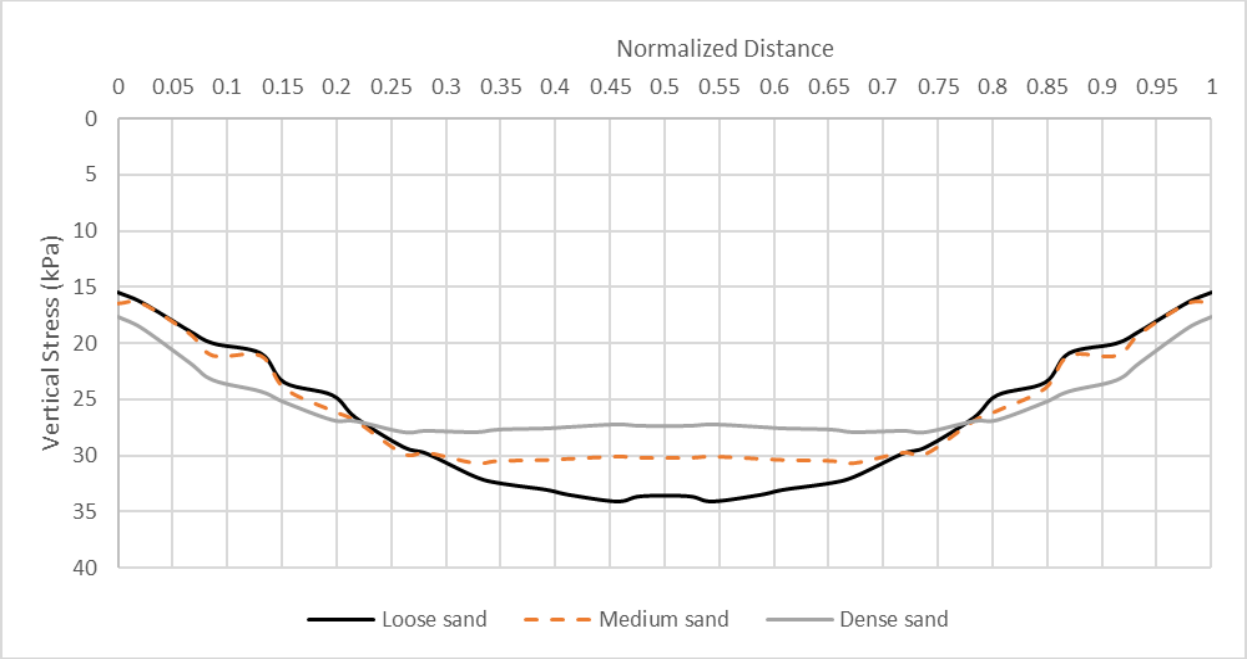

Figure 4.26 Stress distribution at D = 0.5B below the triangular shell footing with θ = 55 degrees

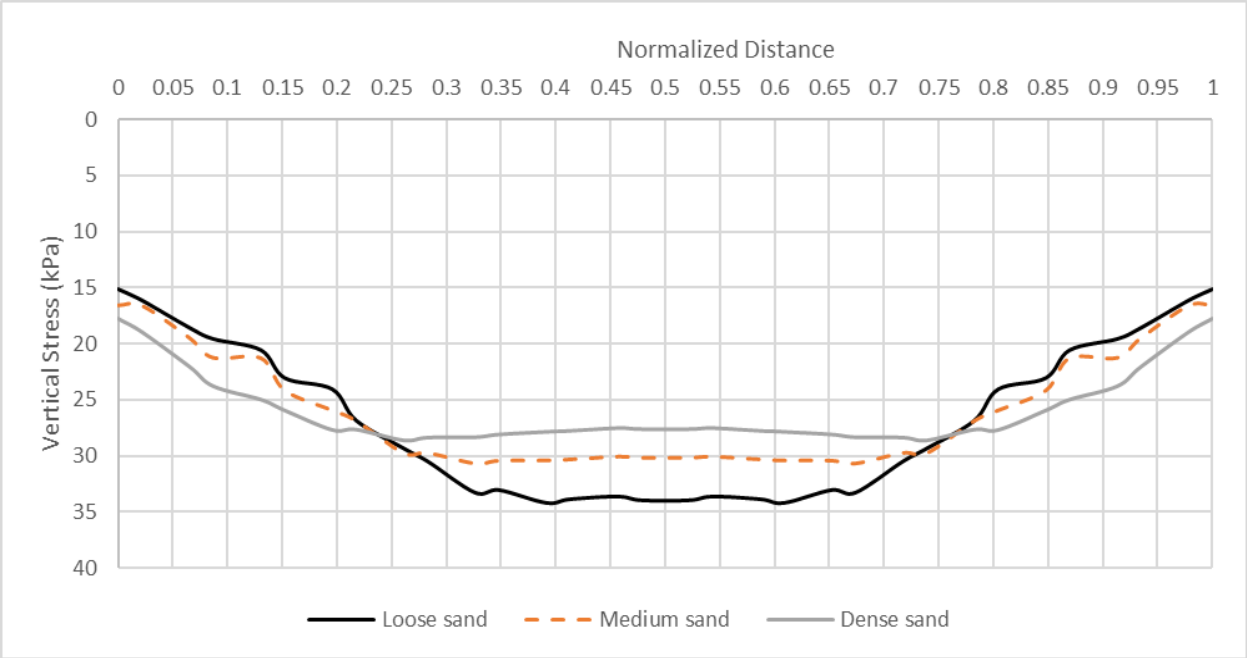

Figure 4.27 Stress distribution at D = 0.5B below the triangular shell footing with θ = 50 degrees

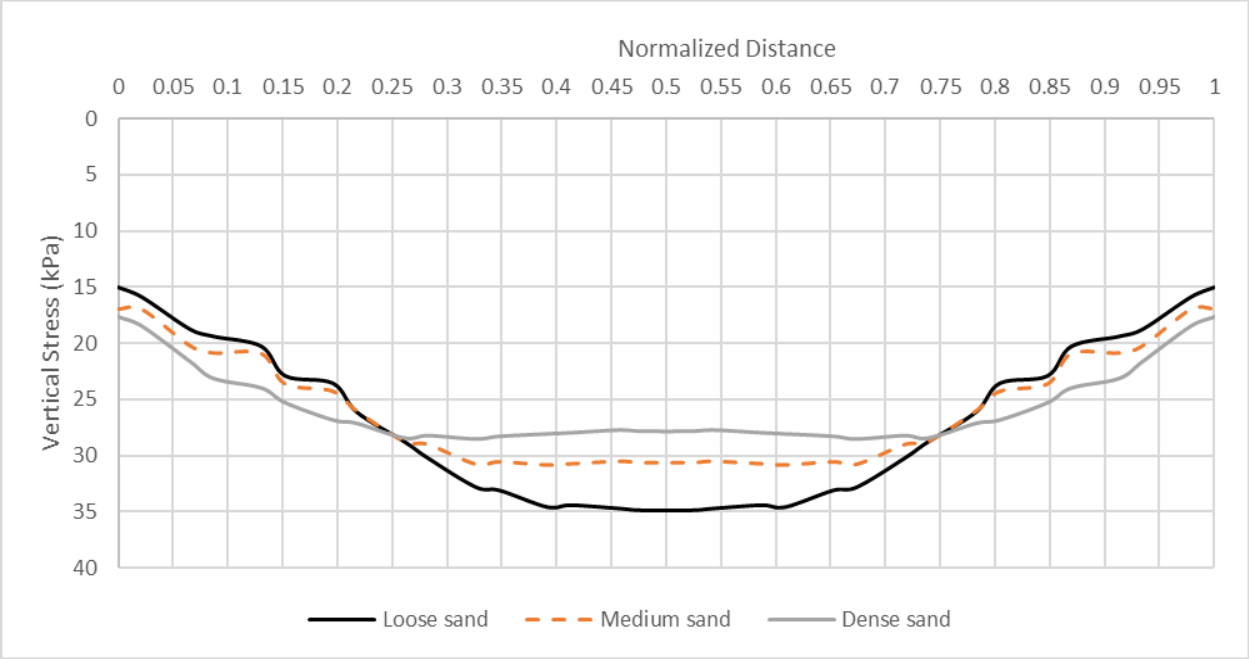

Figure 4.28 Stress distribution at D = 0.5B below the triangular shell footing with θ = 45 degrees

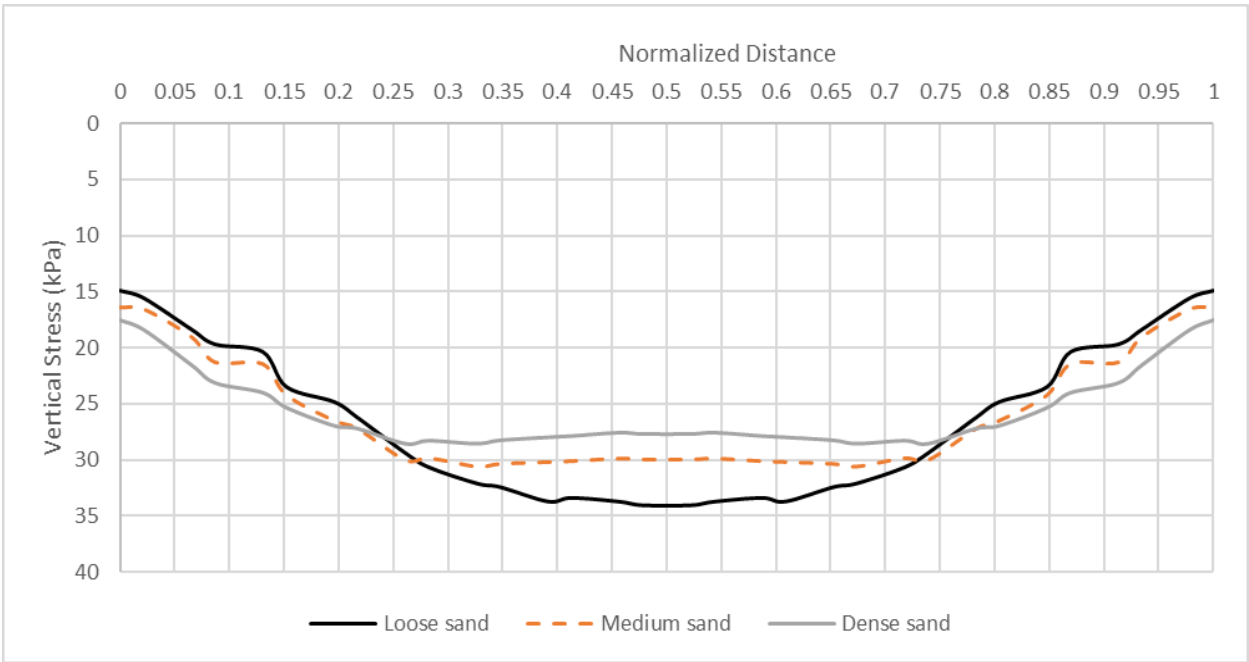

Figure 4.29 Stress distribution at D = 0.5B below the triangular shell footing with θ = 40 degrees

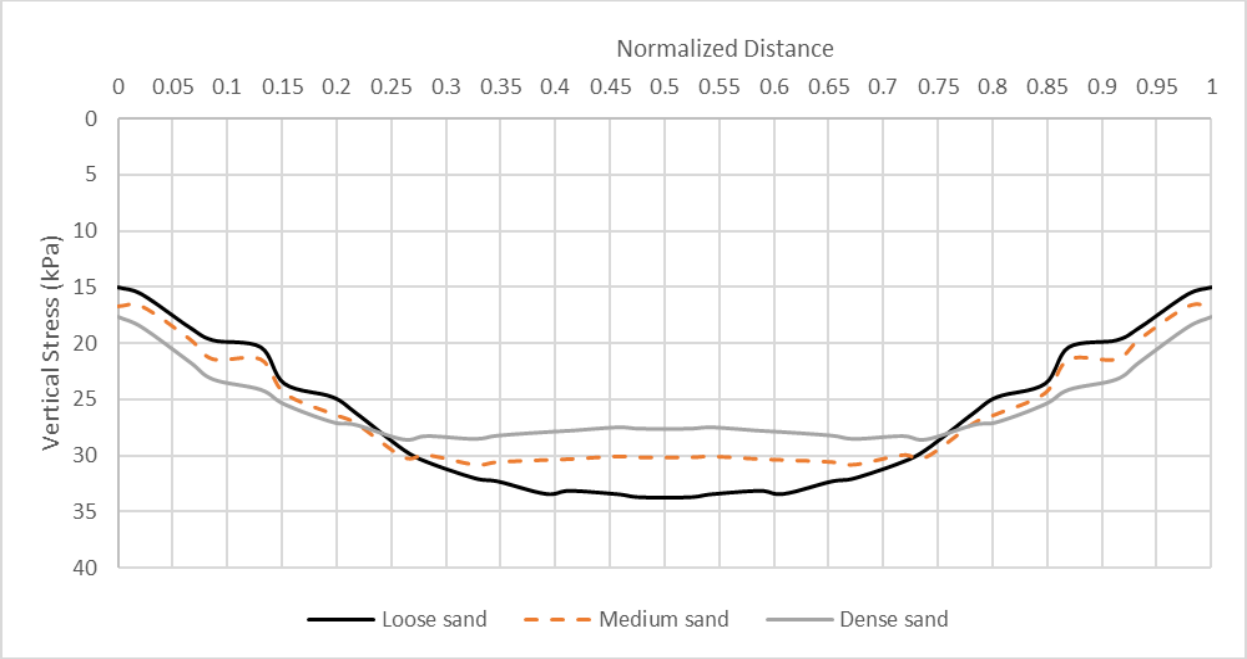

Figure 4.30 Stress distribution at D = 0.5B below the triangular shell footing with θ = 35 degrees

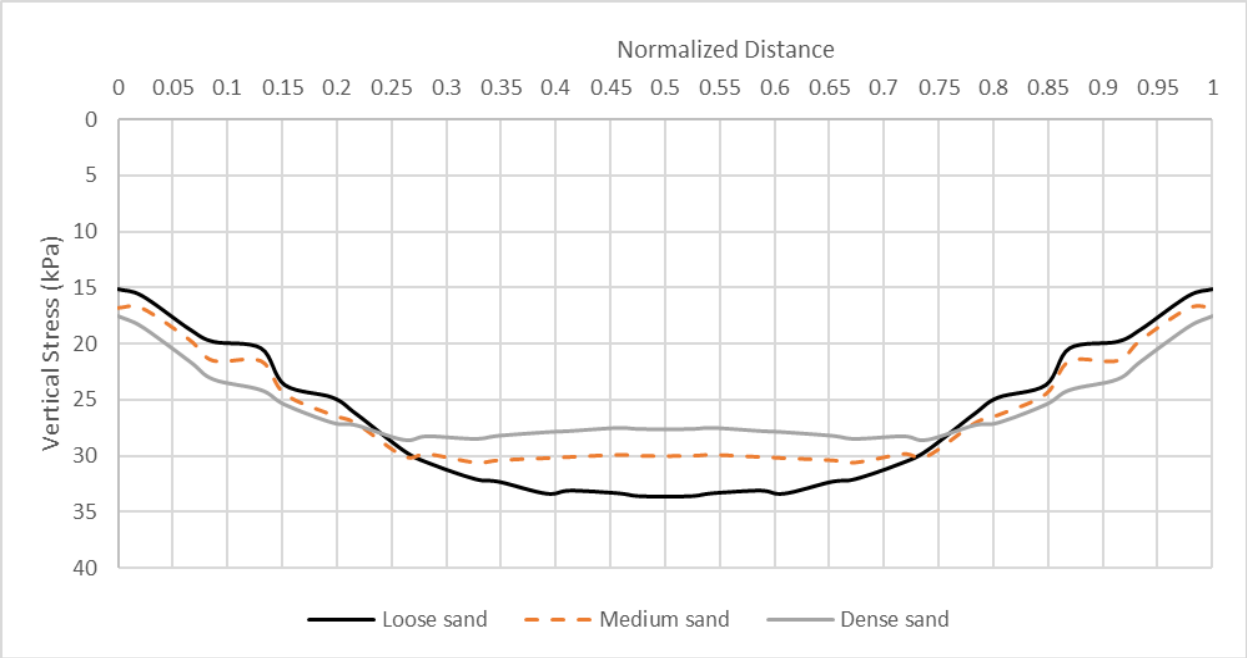

Figure 4.31 Stress distribution at D = 0.5B below the triangular shell footing with θ = 30 degrees

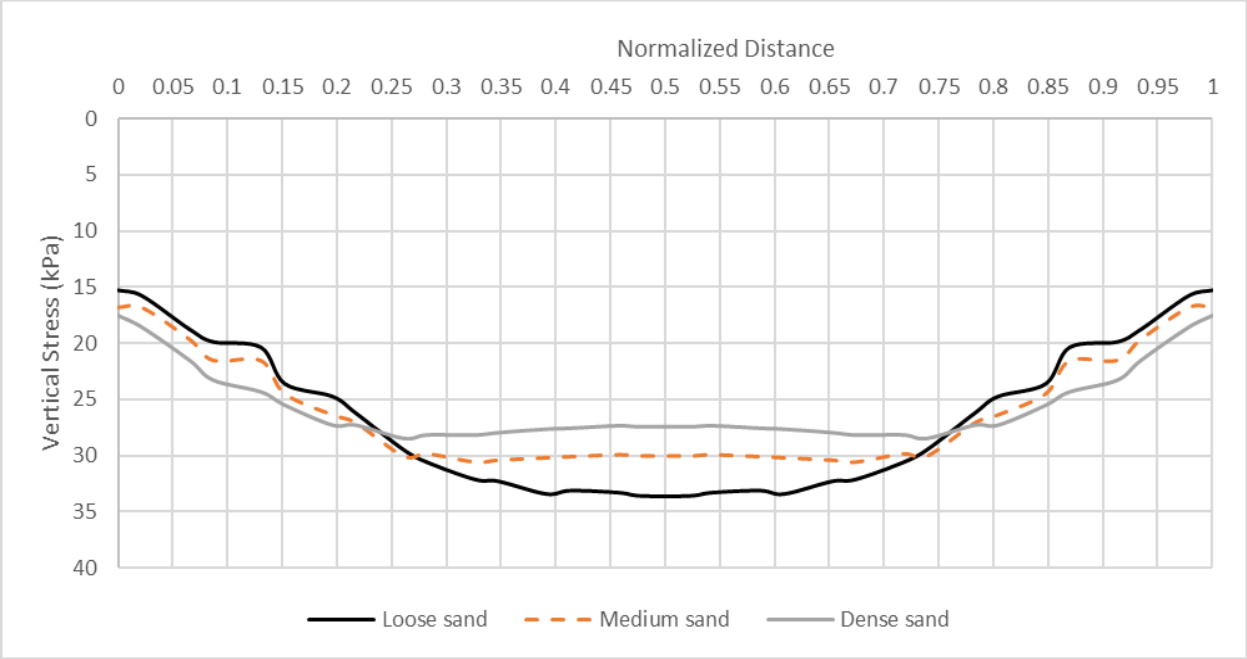

Figure 4.32 Stress distribution at D = 0.5B below the triangular shell footing with θ = 25 degrees

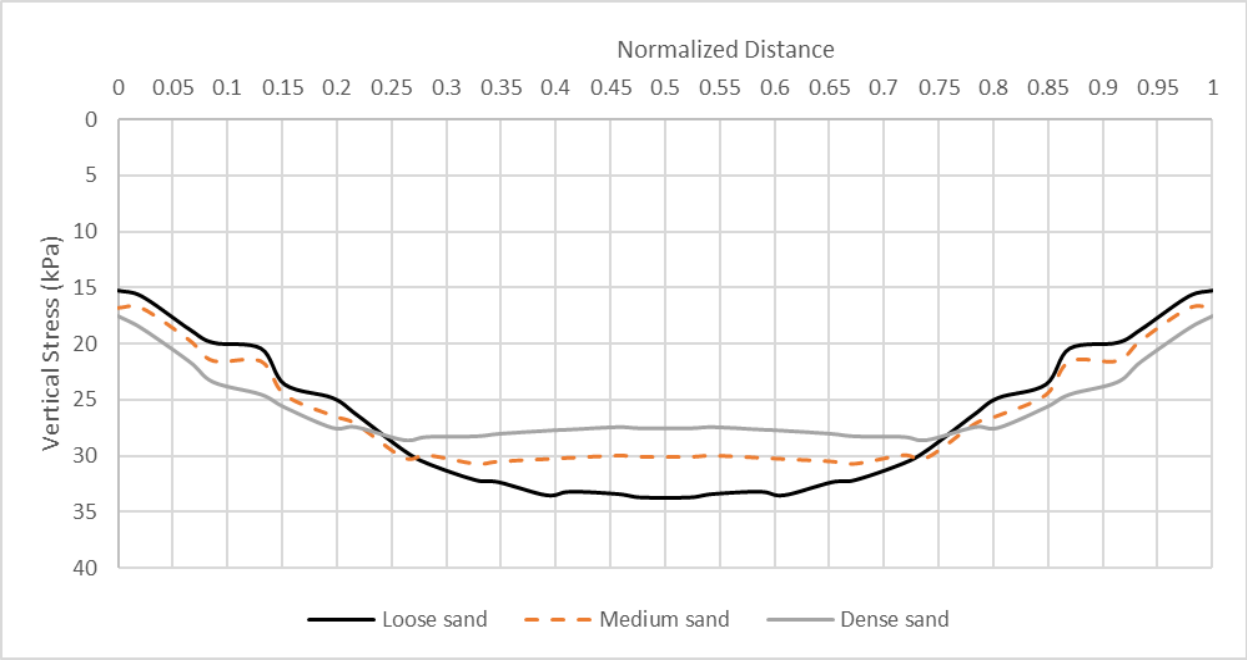

Figure 4.33 Stress distribution at D = 0.5B below the triangular shell footing with θ = 20 degrees

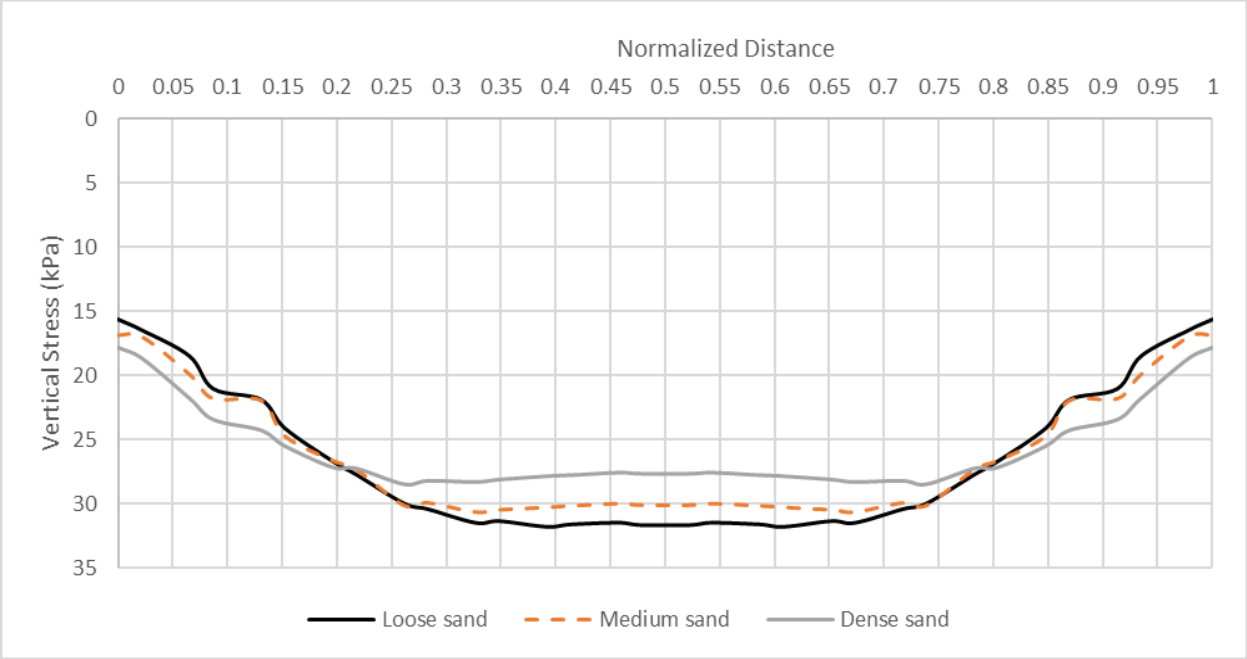

Figure 4.34 Stress distribution at D = 0.5B below the triangular shell footing with θ = 15 degrees

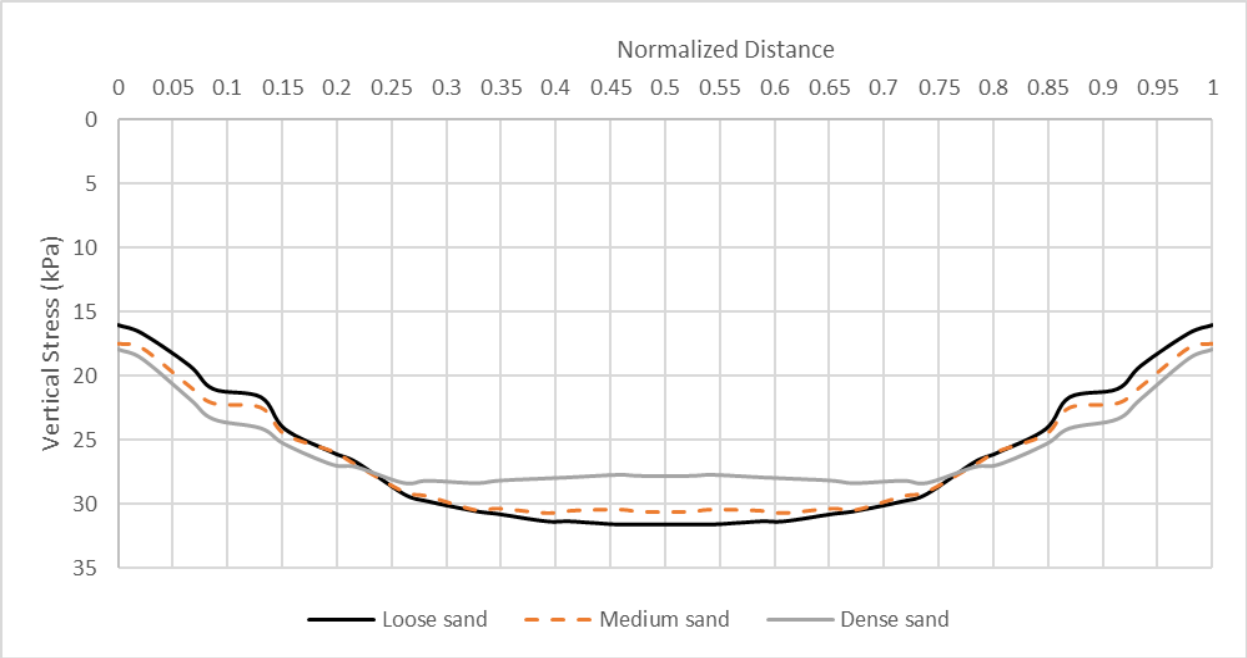

Figure 4.35 Stress distribution at D = 0.5B below the triangular shell footing with θ = 10 degrees

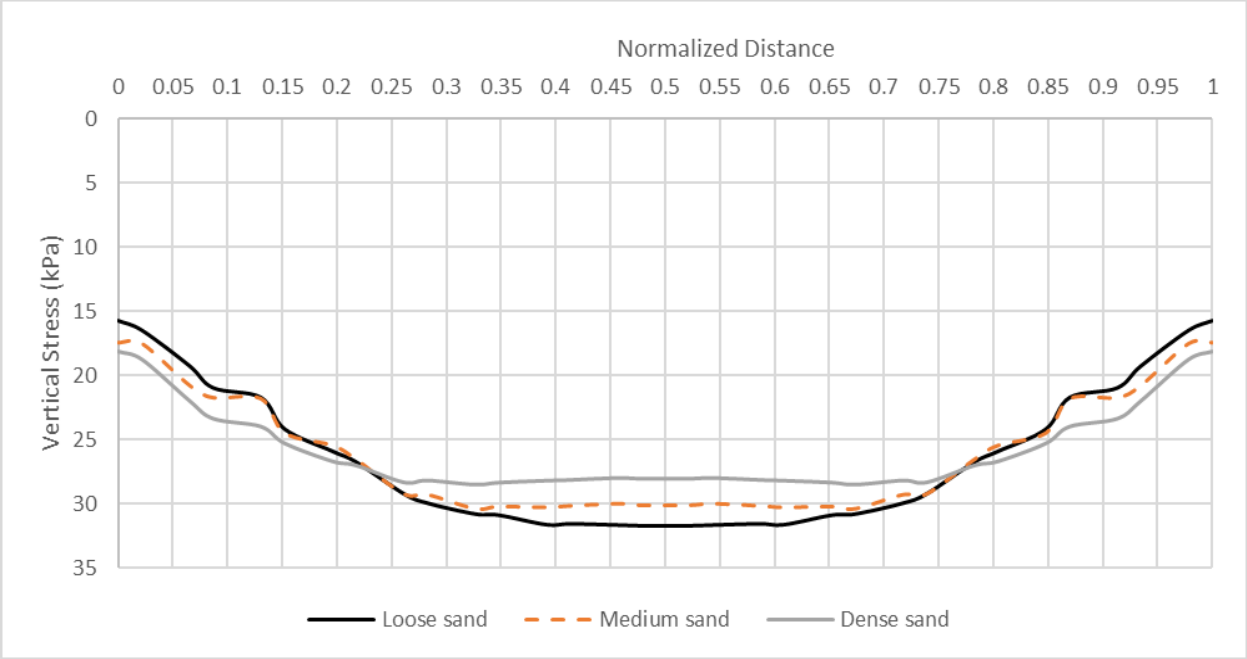

Figure 4.36 Stress distribution at D = 0.5B below the triangular shell footing with θ = 5 degrees

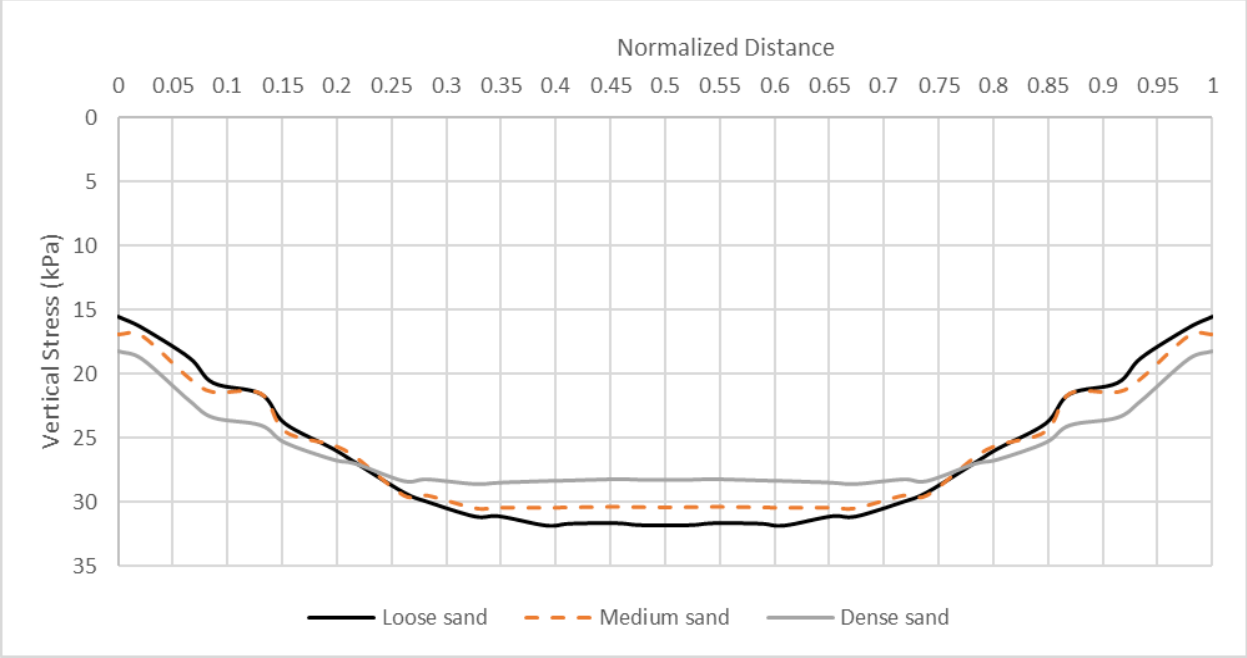

Figure 4.37 Stress distribution at D = 0.5B below the flat footings

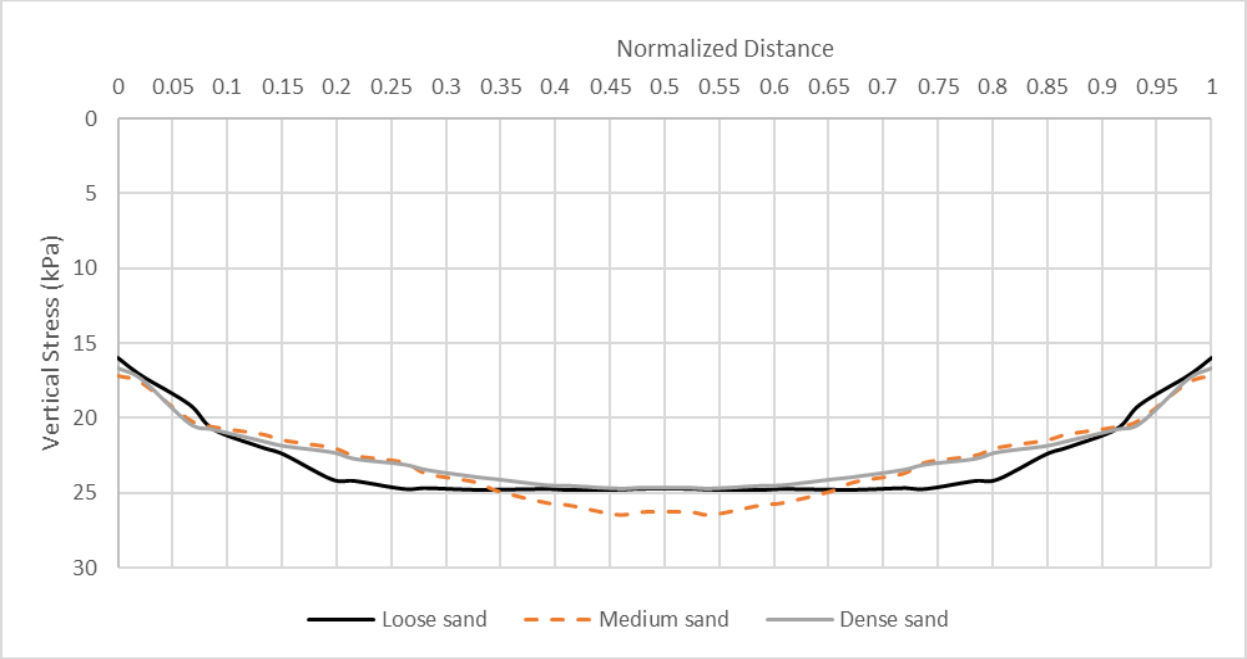

Figure 4.38 Stress distribution at D = B below the triangular shell footing with θ = 60 degrees

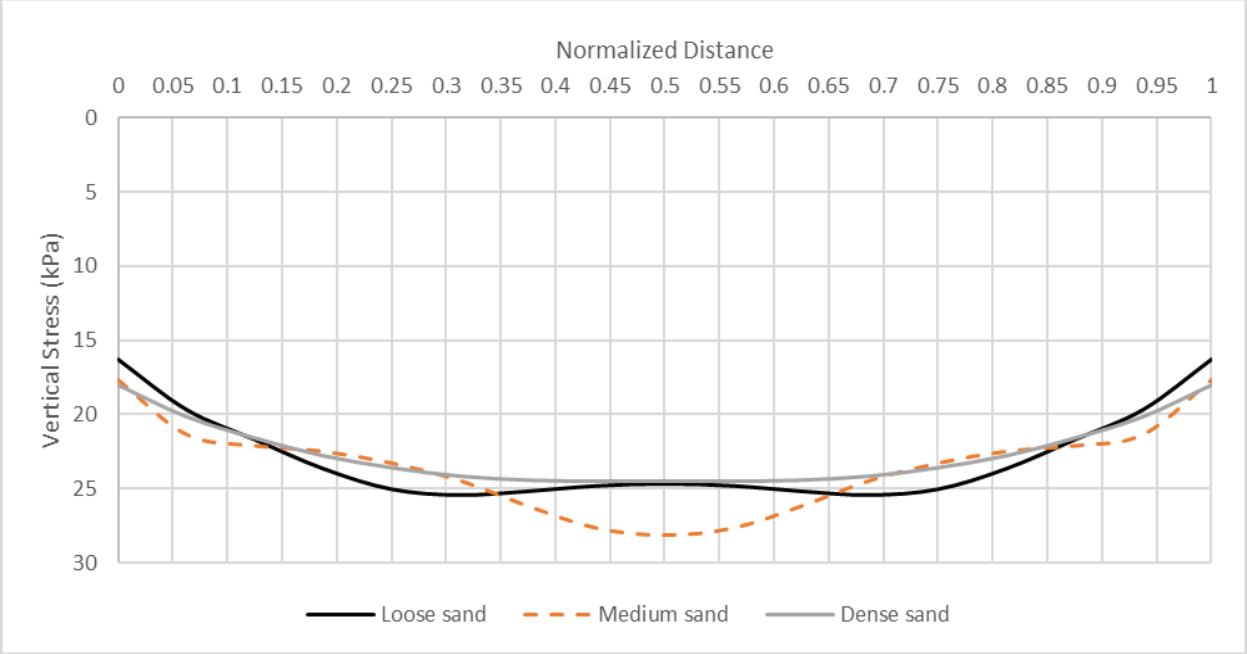

Figure 4.39 Stress distribution at D = B below the triangular shell footing with θ = 55 degrees

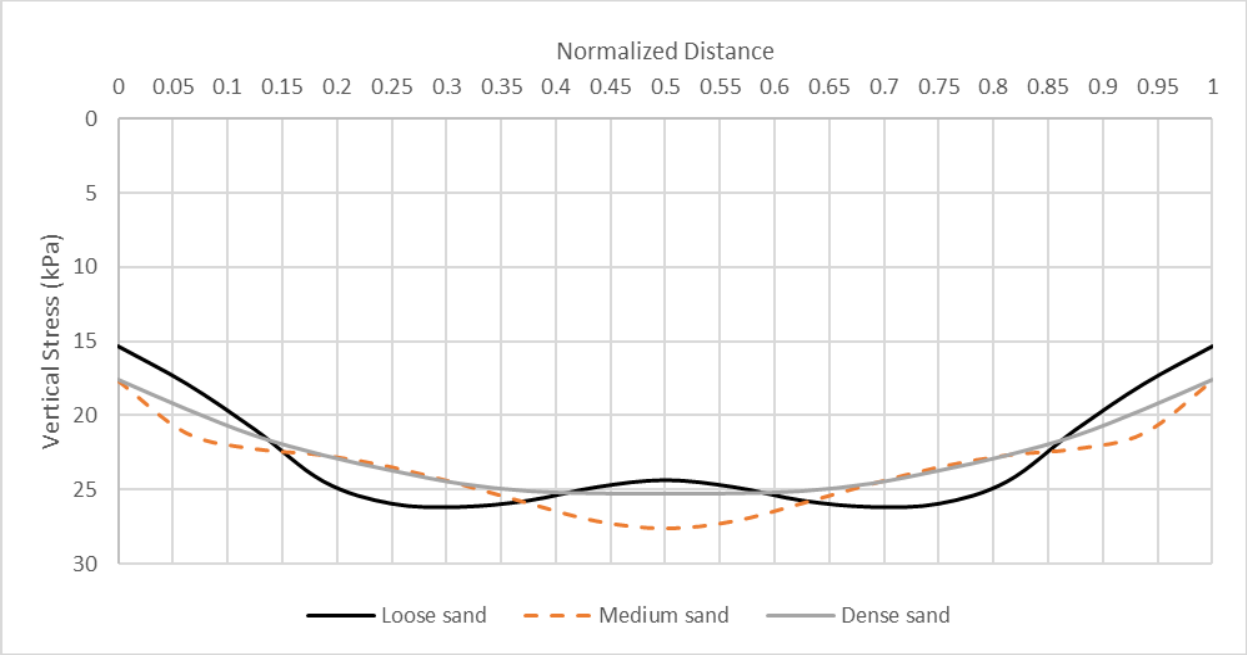

Figure 4.40 Stress distribution at D = B below the triangular shell footing with θ = 50 degrees

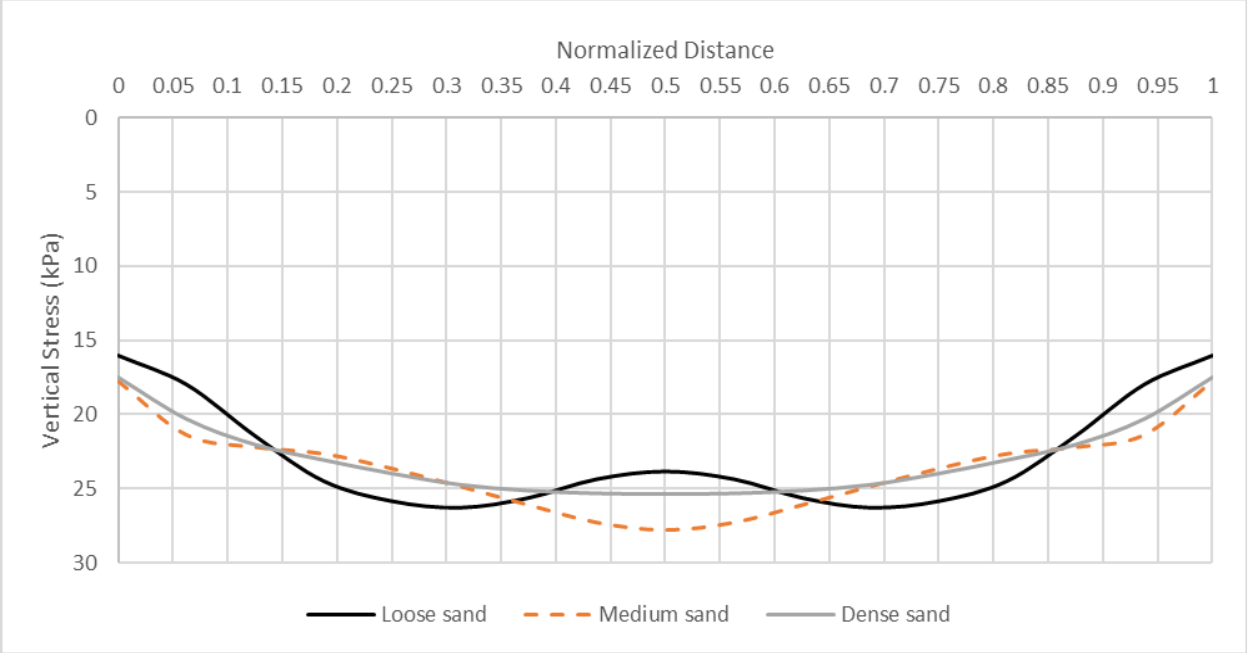

Figure 4.41 Stress distribution at D = B below the triangular shell footing with θ = 45 degrees

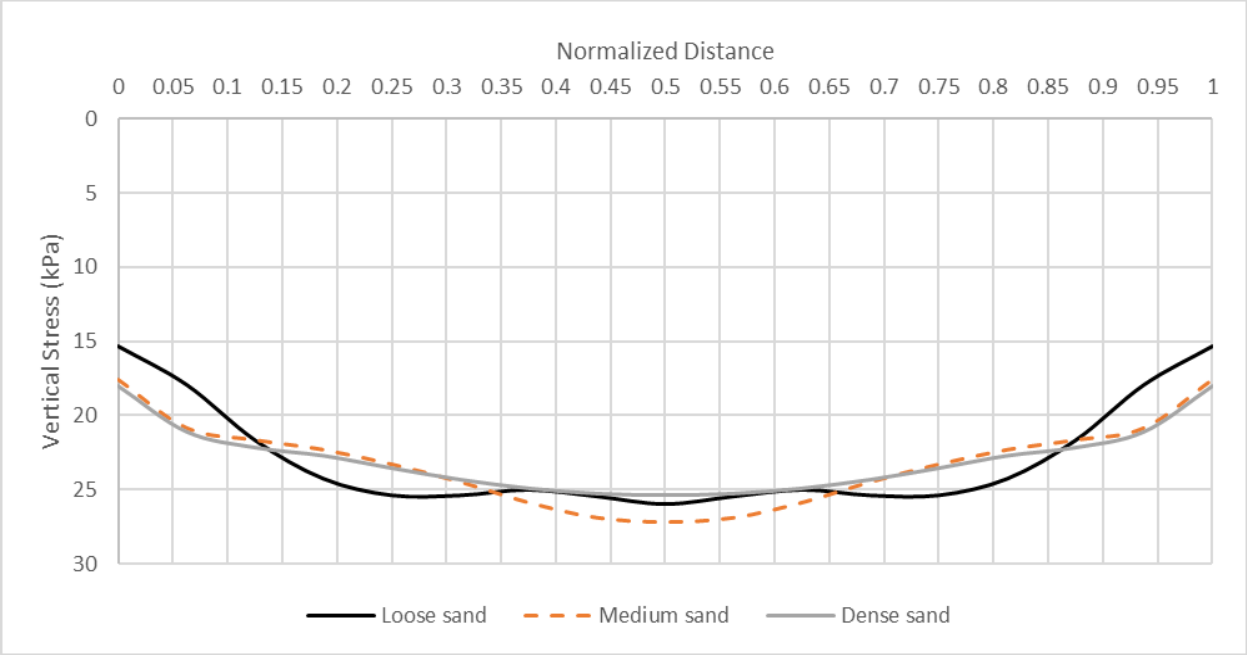

Figure 4.42 Stress distribution at D = B below the triangular shell footing with θ = 40 degrees

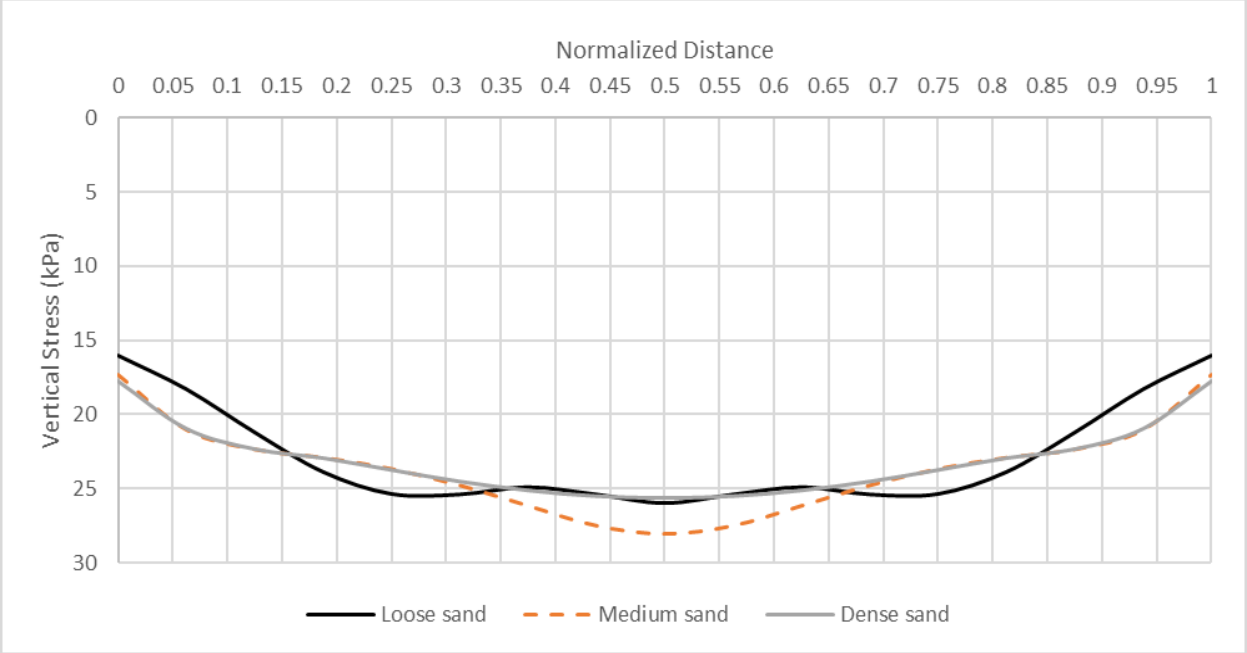

Figure 4.43 Stress distribution at D = B below the triangular shell footing with θ = 35 degrees

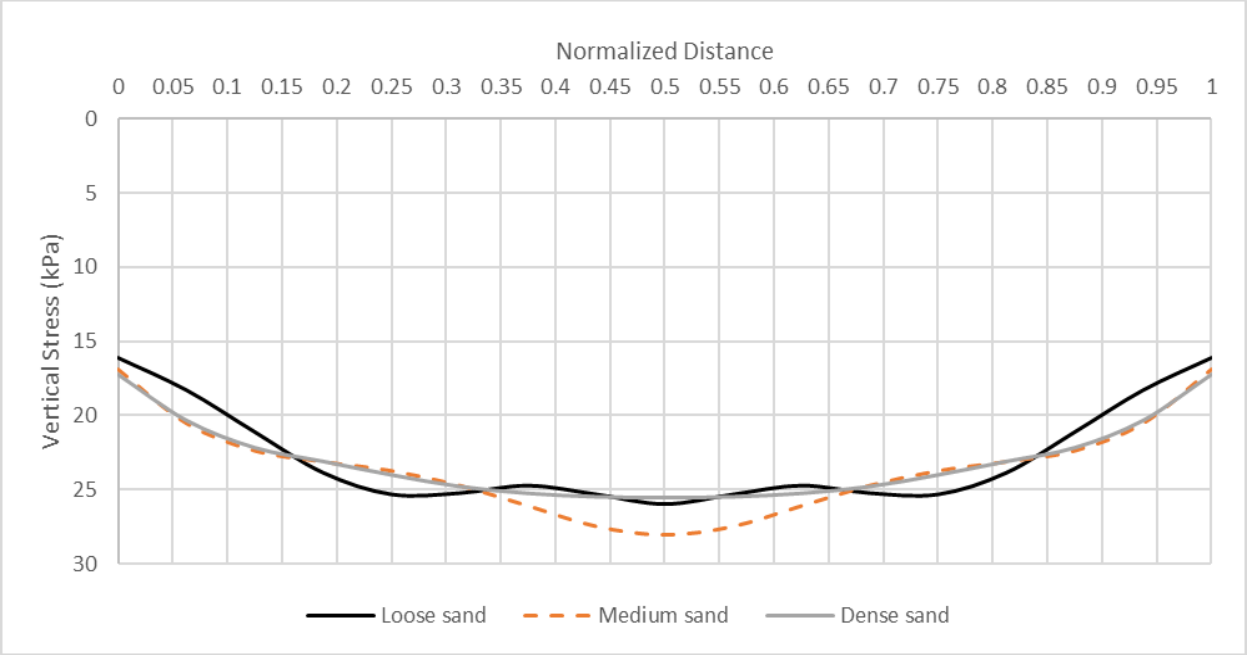

Figure 4.44 Stress distribution at D = B below the triangular shell footing with θ = 30 degrees

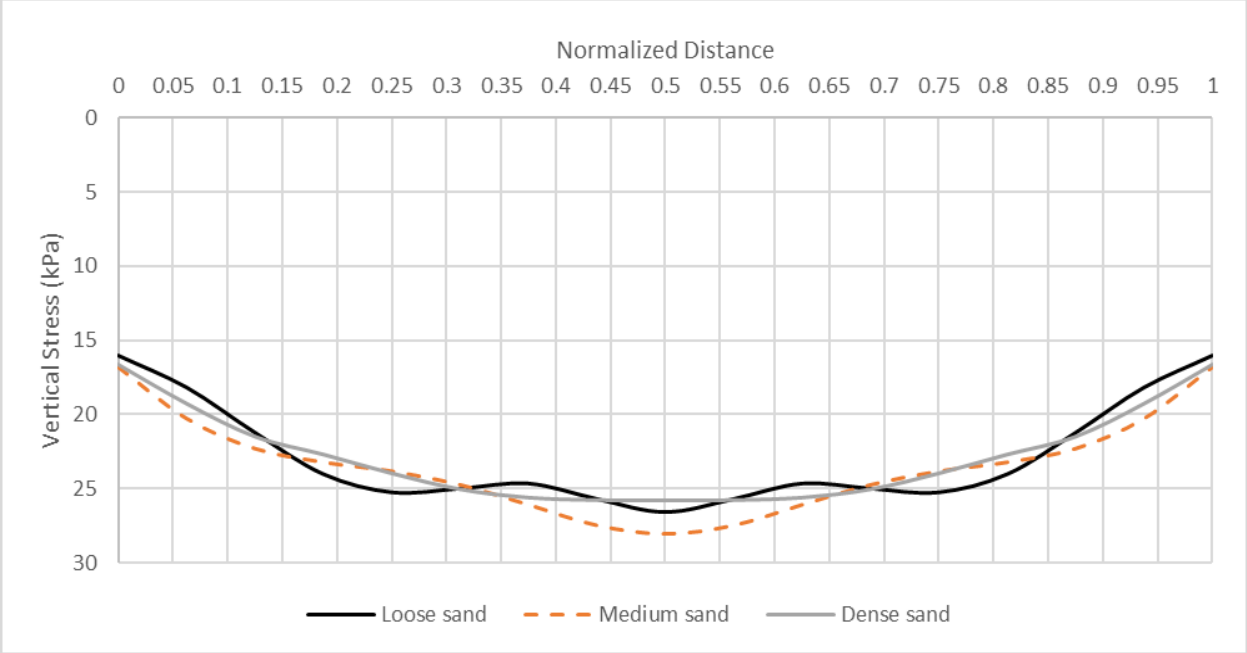

Figure 4.45 Stress distribution at D = B below the triangular shell footing with θ = 25 degrees

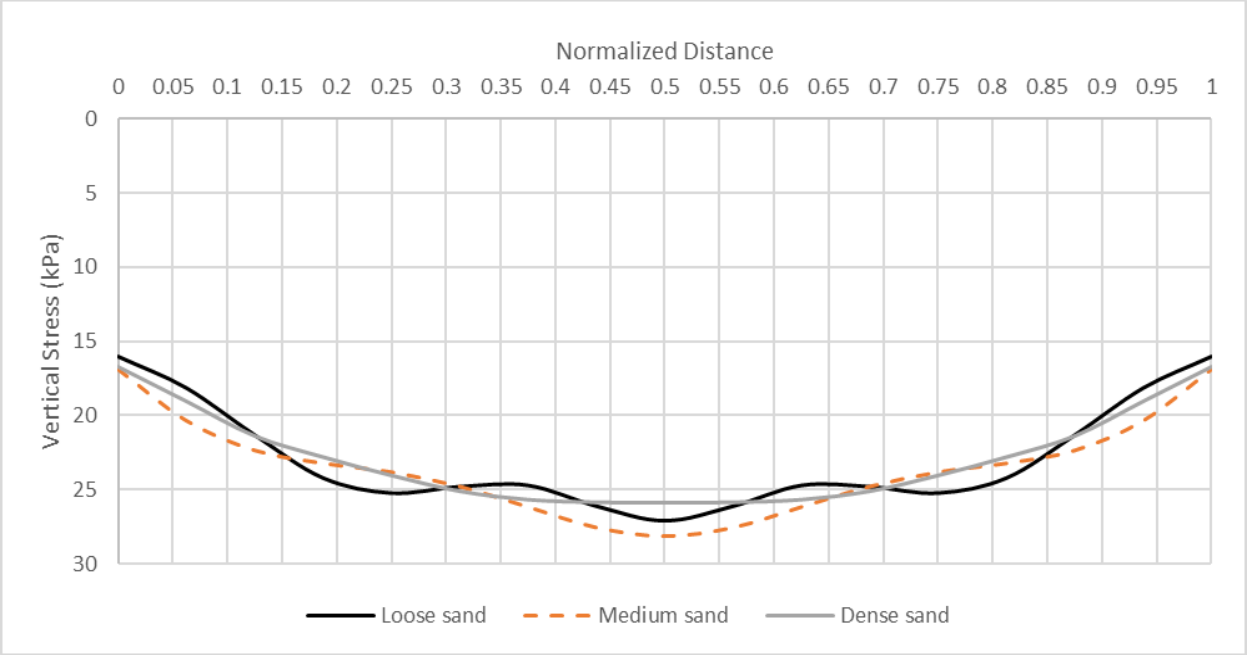

Figure 4.46 Stress distribution at D = B below the triangular shell footing with θ = 20 degrees

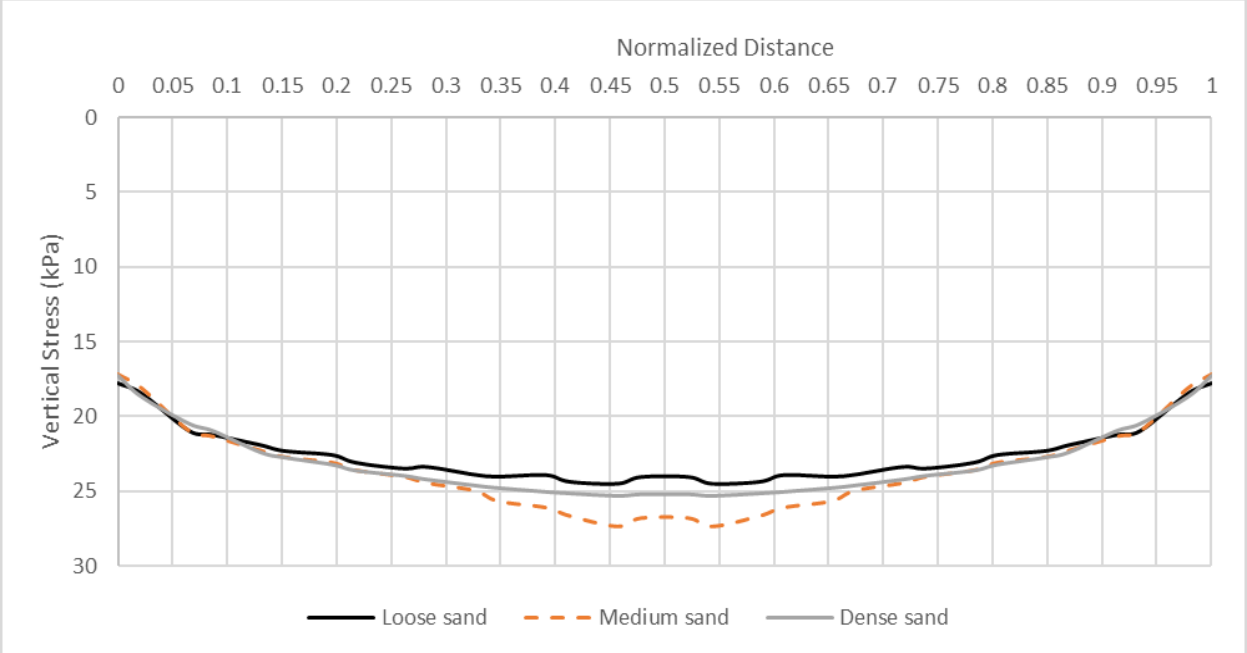

Figure 4.47 Stress distribution at D = B below the triangular shell footing with θ = 15 degrees

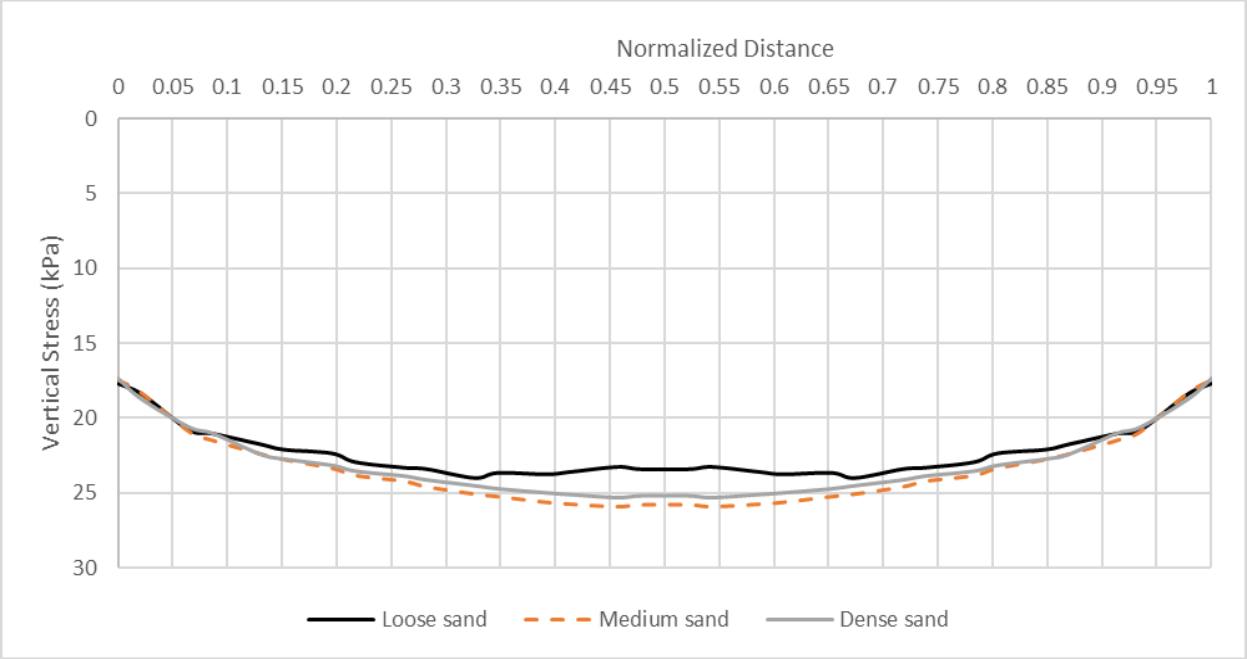

Figure 4.48 Stress distribution at D = B below the triangular shell footing with θ = 10 degrees

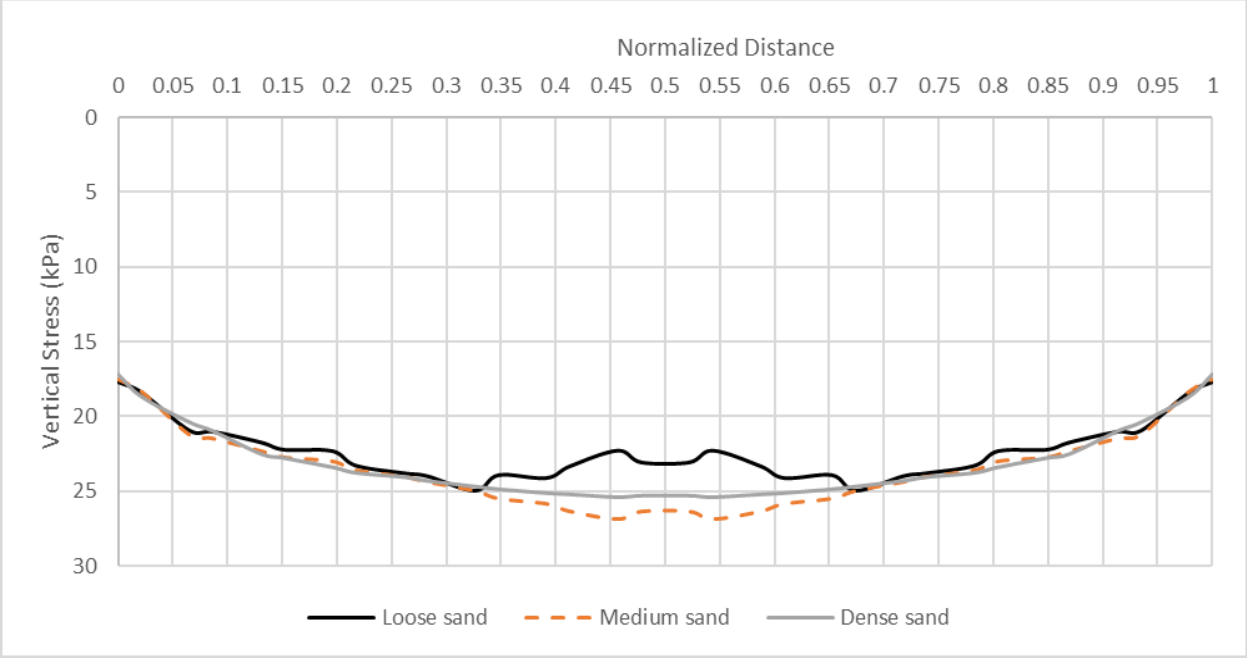

Figure 4.49 Stress distribution at D = B below the triangular shell footing with θ = 5 degrees

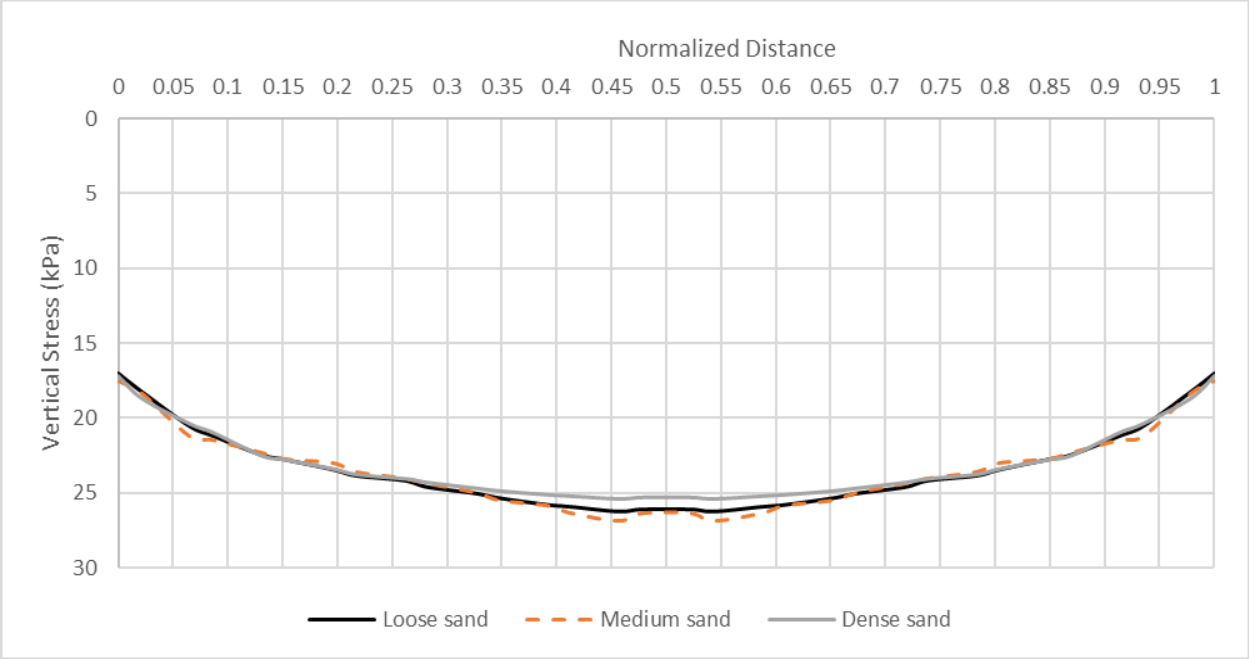

Figure 4.50 Stress distribution at D = B below the flat footings

4.3 Effects of edge angles on contact pressure

In figures 4.51 through 4.53, the value of the contact stress versus the edge angle of the shell foundations are plotted for loose, medium, and dense sand states, respectively. It is evident that the lowest amount of edge stress takes place at the peripheries of the shell with an edge angle of 60 degrees. Subsequently, the edge stresses increase by decreasing the edge angle to reach the maximum values at $\theta = 30$ to 25 degrees for all types of sands. Eventually, it decreases slightly by reducing the edge angle to the flat situation. The edge stress diagrams present similar variations in loose, medium, and dense sands. Nonetheless, the values of edge stresses become higher by densifying the sands.

The effects of edge angle on the central stresses at the soil-foundation interface are demonstrated in figures 4.54 to 4.56. Under a specified load, the graphs authenticate that a decrease in the edge angle from 60 to 40 degrees leads to decreasing in the central stresses in loose sand.

This edge angle range is from 60 to 45 degrees in the cases of medium and dense sands. Thereafter, the central stresses enhance progressively by decreasing the edge angle to the flat foundation.

In order to analyze and compare the load-carrying capacity, the averages of the stress by changing the edge angle are presented in figures 4.57 to 4.59. All figures verify that the averages of the stress magnitudes increase by diminishing the edge angle. In other words, shell foundations exercise lower stresses in the soil beneath relative to their flat counterparts, and they utilize the resistance capacity of the soil optimally. Conclusively, shell foundations can tolerate higher loads than flat footings with the same plain dimensions.

Figures 4.60 to 4.65 contribute to investigating the most uniform stress distributions and optimum geometry of triangular shell foundations. Stress ranges (the difference between maximum and the minimum stresses) are computed in each case and graphed versus the edge angle in figures 4.60 to 4.62. In loose and medium sands, the stress distributions are more confined below the shells with the edge angles from 55 to 20 degrees. In the case of dense sand, the lowest stress ranges belong to θ = 10 and 15 degrees, and the shell foundation with an angle of 55 degrees is slightly higher. The variance of data is assumed as a parameter to measure the uniformity of the contract pressure distributions. Variance is calculated as follows:

$$S^2 = \frac{\Sigma(x_i - \bar{x})^2}{n-1} \tag{4.1}$$

where:

$$S^2 = Variance$$

$$x_i = The\ value\ of\ each\ stress$$

$$\bar{x} = The\ mean\ of\ all\ data\ points\ i\ for\ each\ stress$$

$$n = The\ number\ of\ data\ points\ i\ for\ each\ stress$$

Figures 4.63 through 4.65 illustrate the efficacy of edge angle on the variance of the stress distributions in loose, medium, and dense sands. The lowest amounts of variance are in possession of the shells with edge angles of 55 and 25 degrees, leading to more uniformity. However, the

minimum values of variance and the most uniform contact pressure distribution occur at the edge angles 55 and 10 degrees.

Based on the average stresses, stress ranges, and the variance of the stress data, it can be concluded that the optimum shape of triangular shell foundations belongs to the shell footing with an edge angle of 55 degrees in all sand states. Although the graphs reveal uniform stress dispersion at 25 and 10 degrees, the higher average stress contributes to a lower bearing capacity than the shell with an edge angle of 55 degrees. The stress distributions below the triangular shell foundation with the edge angle of 55 degrees and the flat counterpart for all sands are presented in figures 4.66 to 4.69.

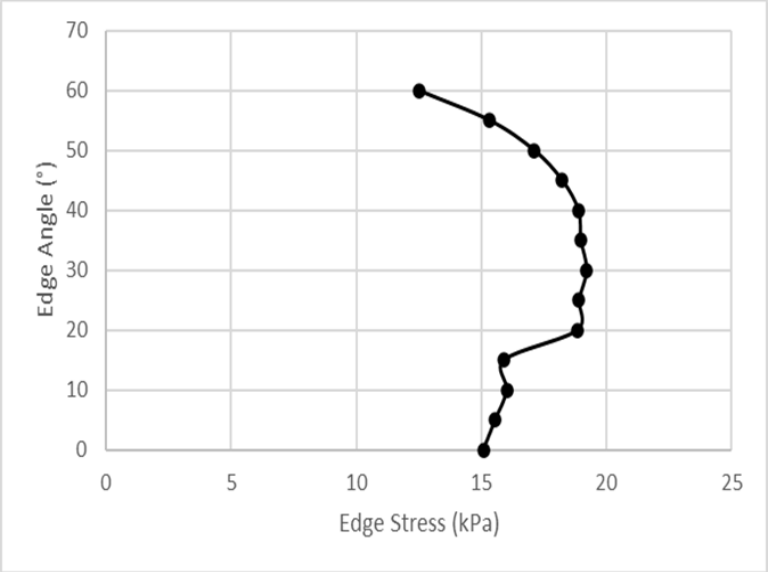

Figure 4.51 Edge stress versus edge angle at the soil-footings interface in loose sand

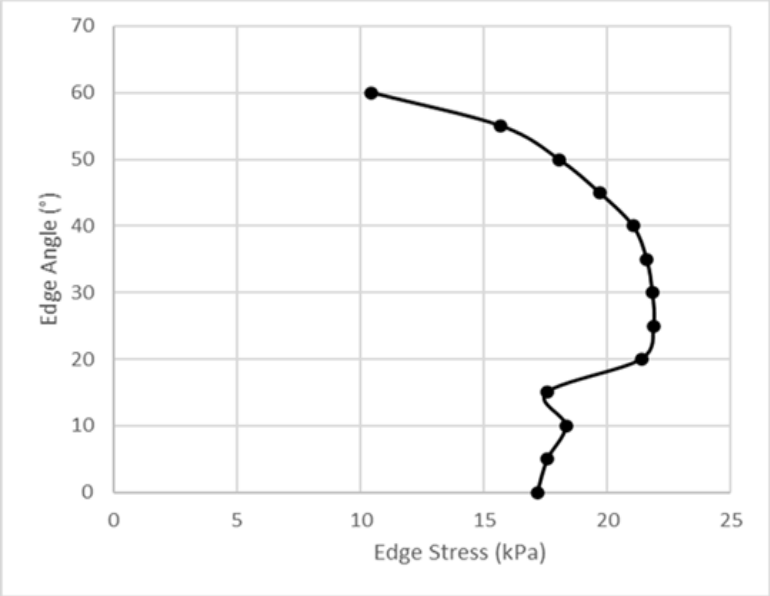

Figure 4.52 Edge stress versus edge angle at the soil-footings interface in medium sand

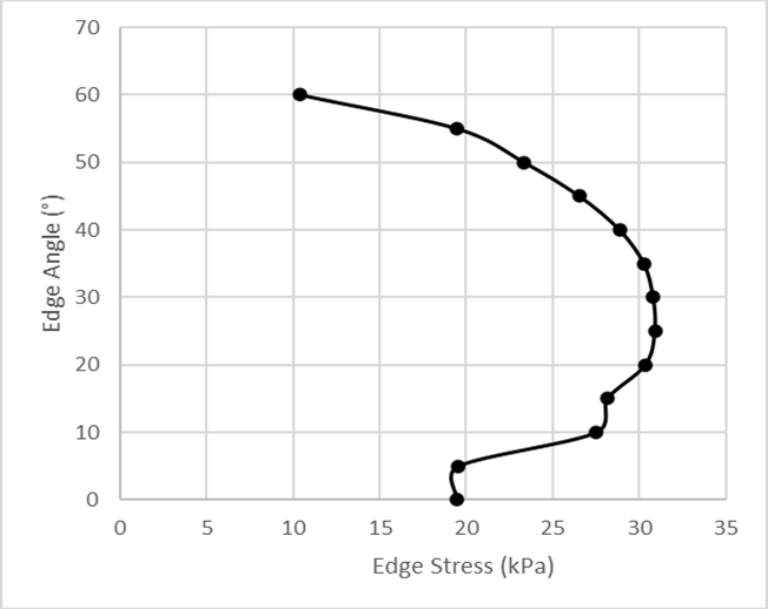

Figure 4.53 Edge stress versus edge angle at the soil-footings interface in dense sand

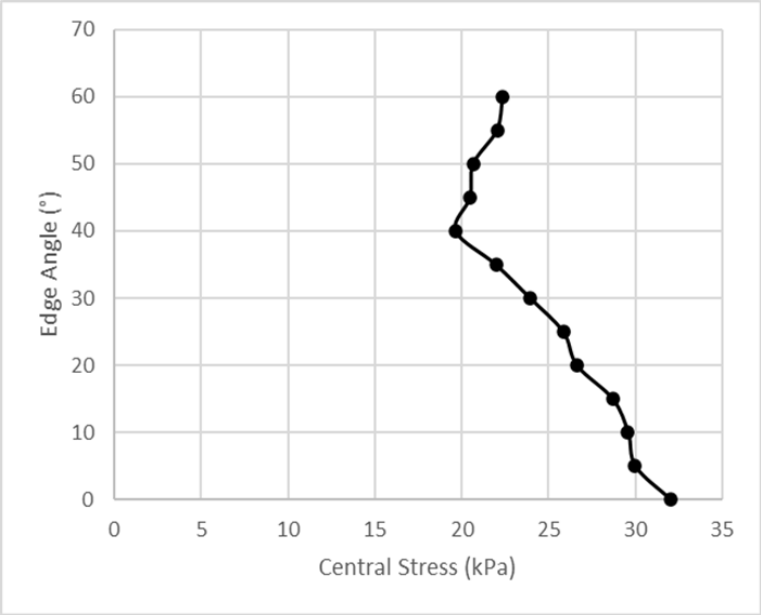

Figure 4.54 Central stress versus edge angle at the soil-footings interface in loose sand

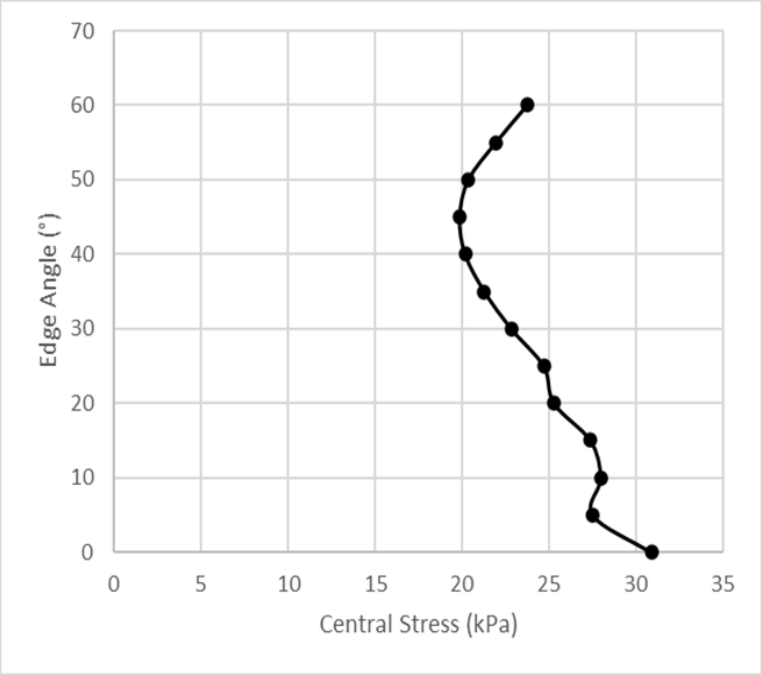

Figure 4.55 Central stress versus edge angle at the soil-footings interface in medium sand

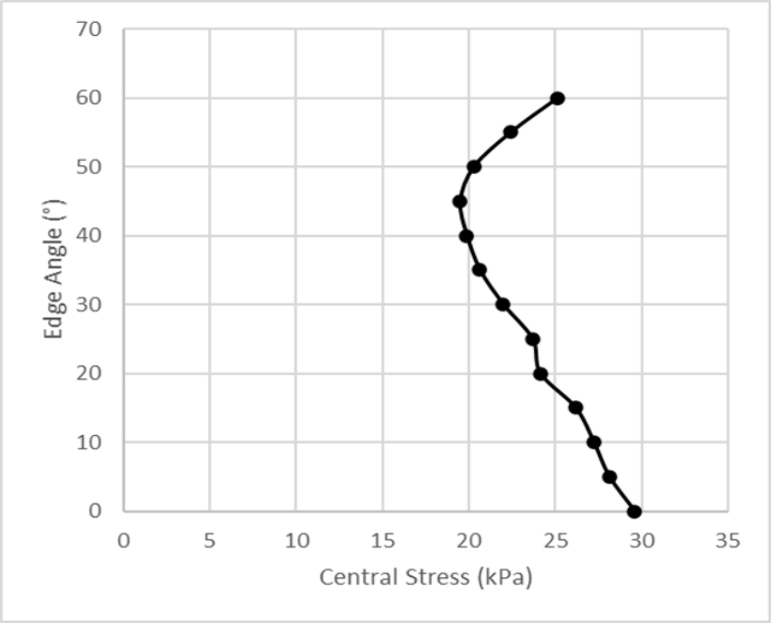

Figure 4.56 Central stress versus edge angle at the soil-footings interface in dense sand

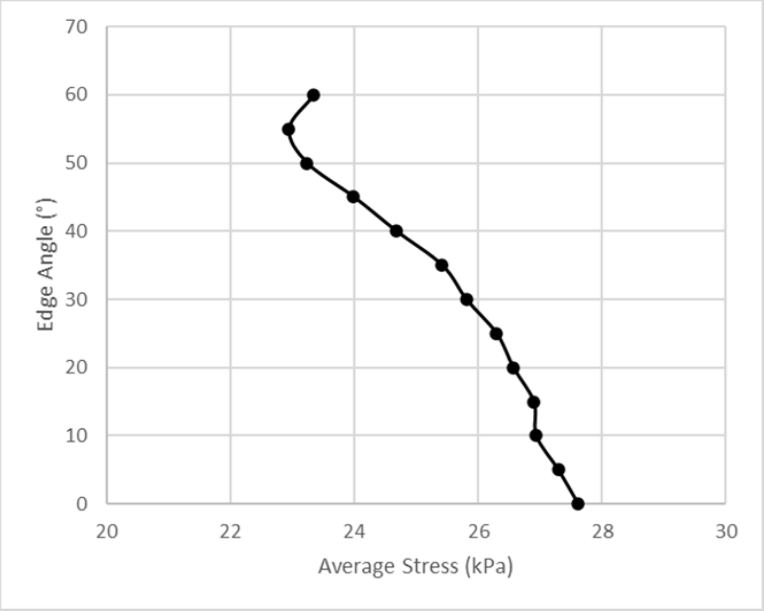

Figure 4.57 Average stress versus edge angle at the soil-footings interface in loose sand

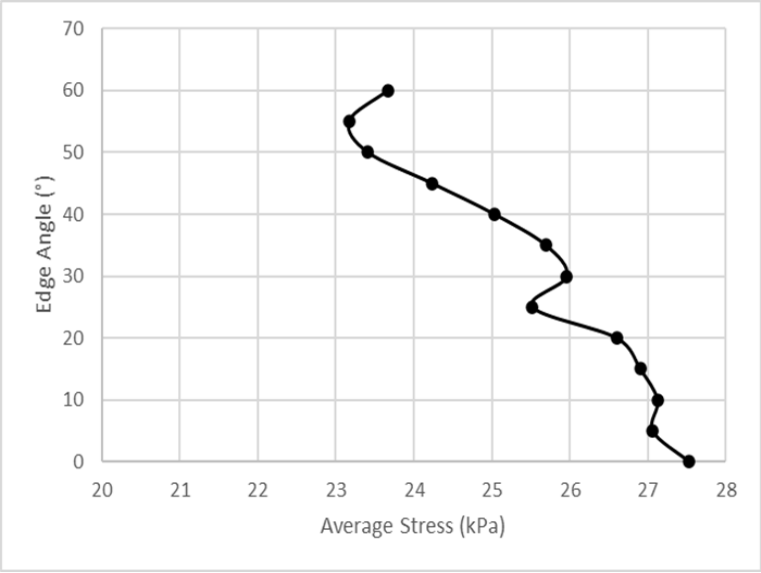

Figure 4.58 Average stress versus edge angle at the soil-footings interface in medium sand

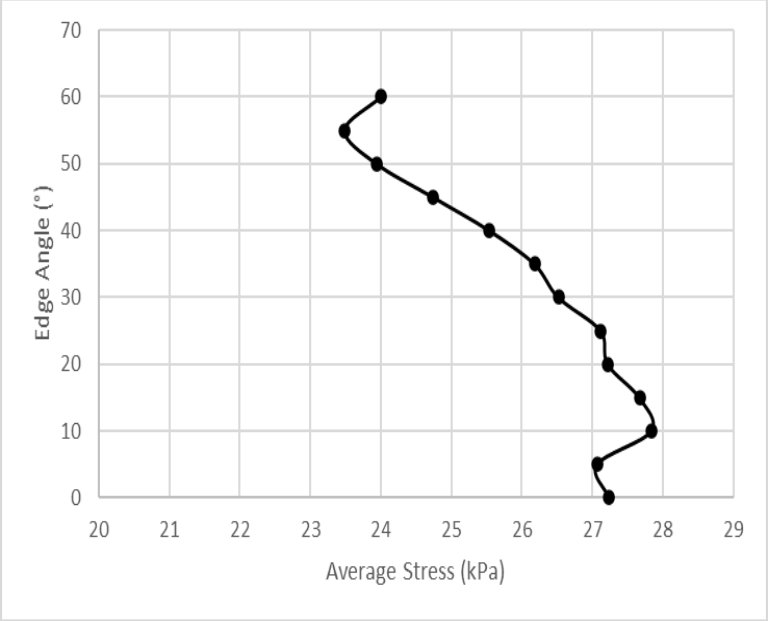

Figure 4.59 Average stress versus edge angle at the soil-footings interface in dense sand

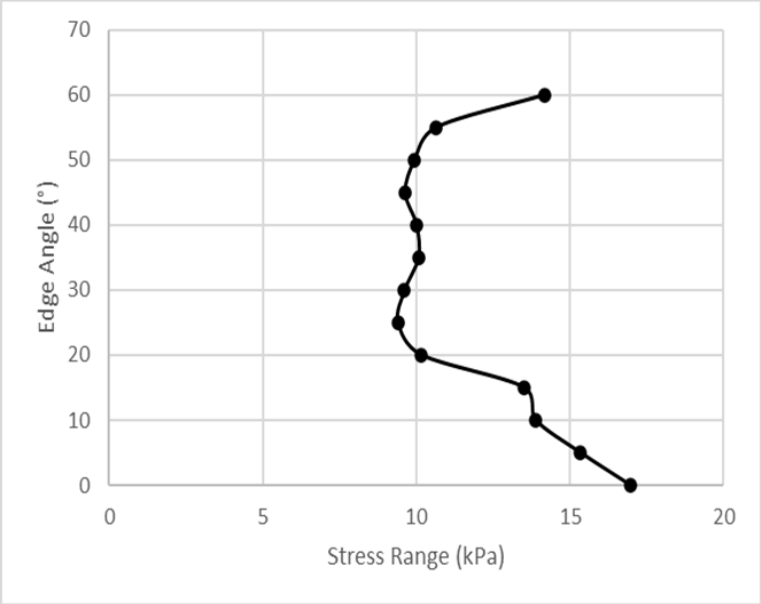

Figure 4.60 Stress range versus edge angle at the soil-footings interface in loose sand

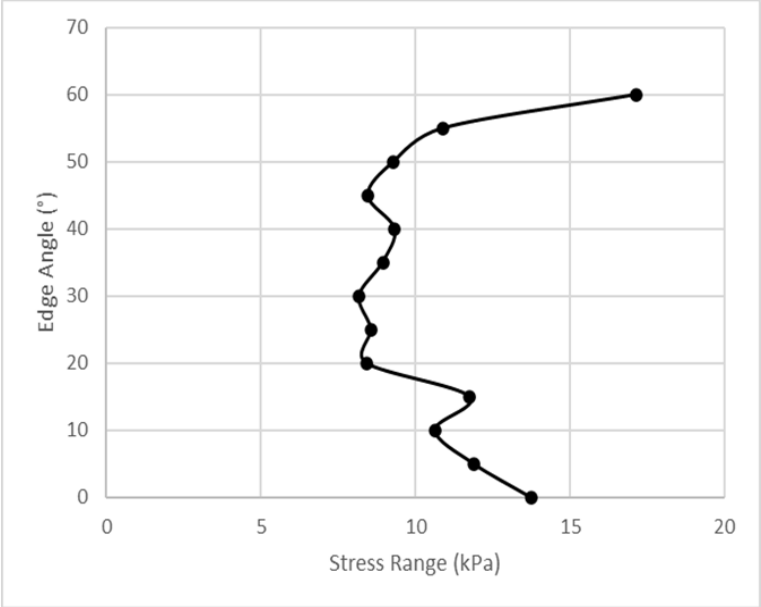

Figure 4.61 Stress range versus edge angle at the soil-footings interface in medium sand

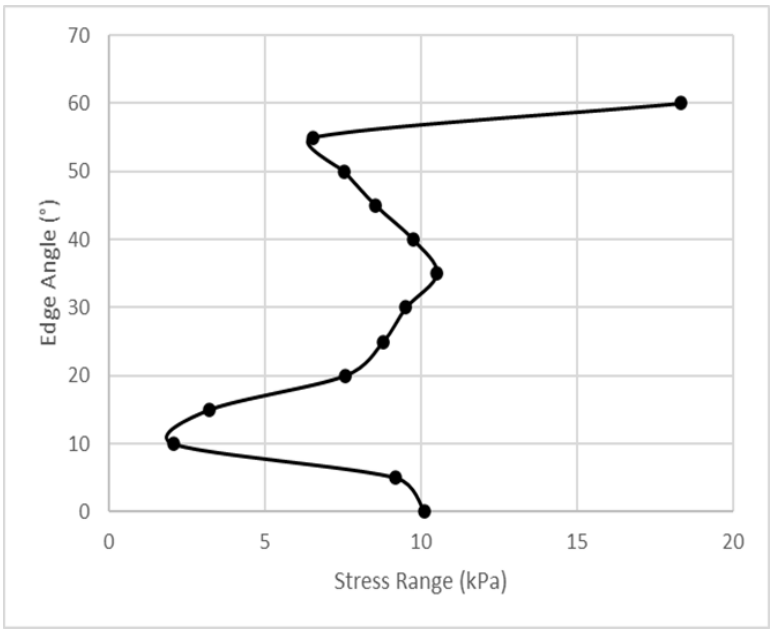

Figure 4.62 Stress range versus edge angle at the soil-footings interface in dense sand

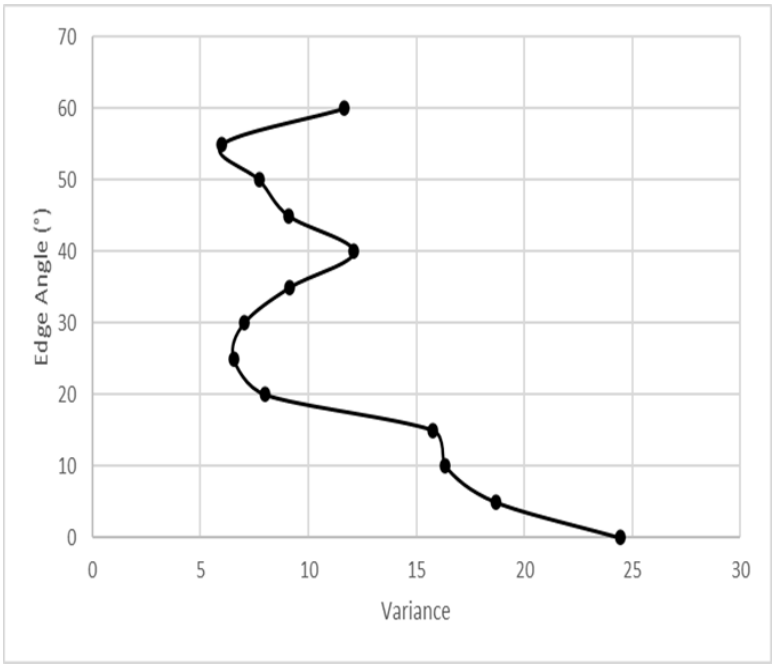

Figure 4.63 Variance versus edge angle at the soil-footings interface in loose sand

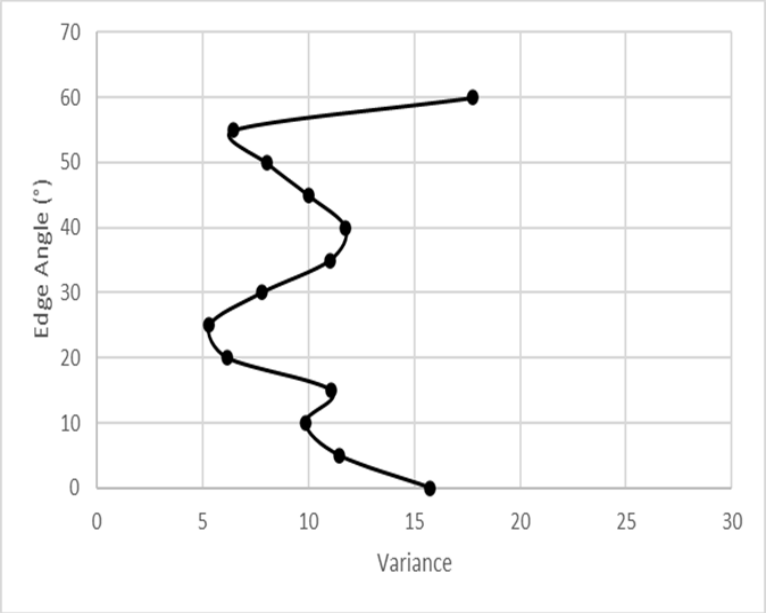

Figure 4.64 Variance versus edge angle at the soil-footings interface in medium sand

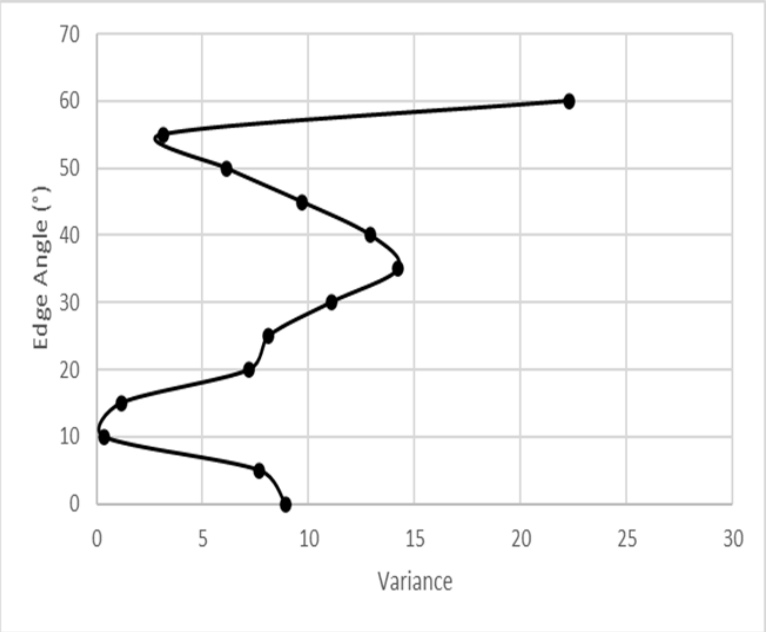

Figure 4.65 Variance versus edge angle at the soil-footings interface in dense sand

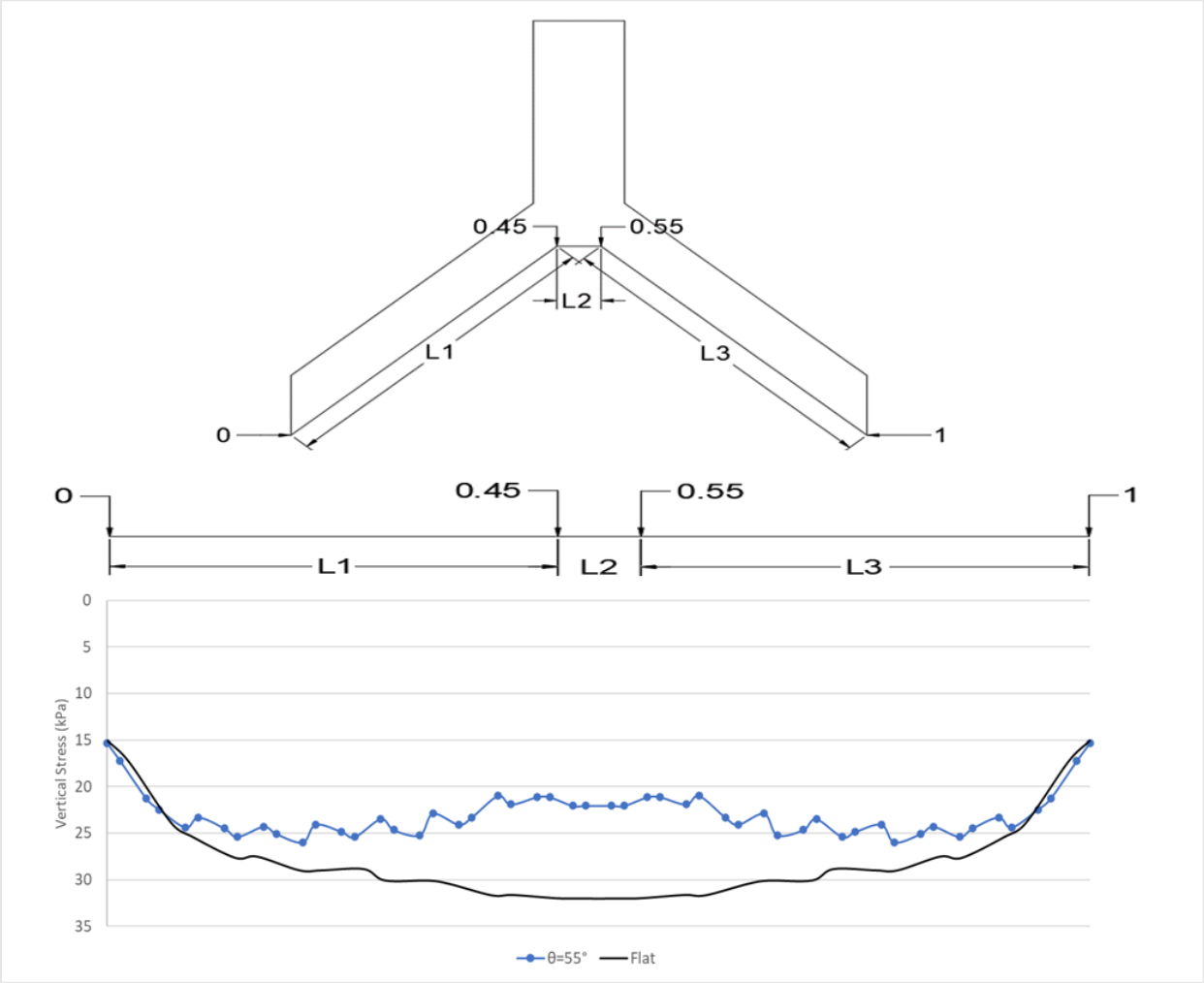

Figure 4.66 Contact pressure distribution below the optimum shell foundation and flat foundation in loose sand

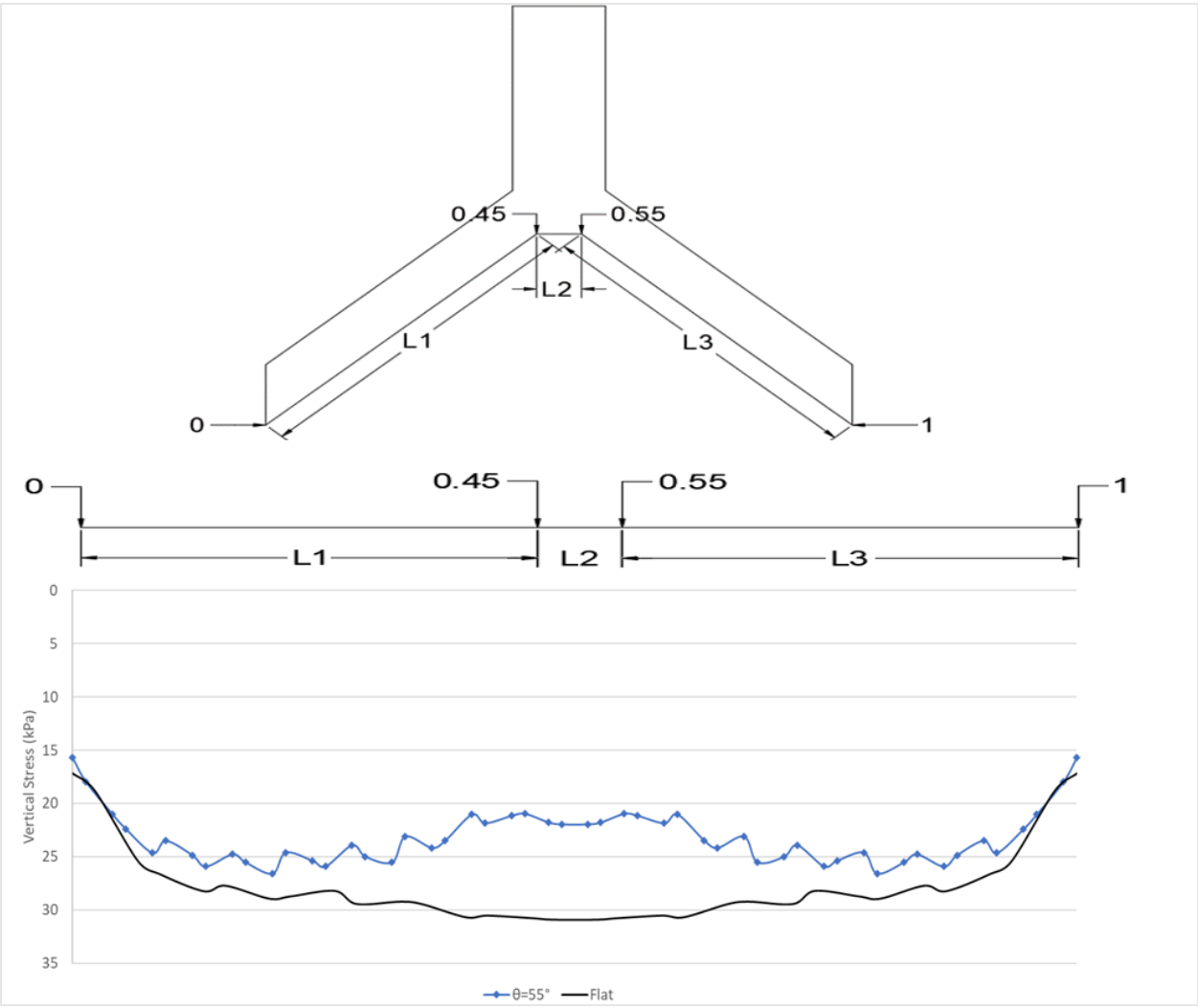

Figure 4.67 Contact pressure distribution below the optimum shell foundation and flat foundation in medium sand

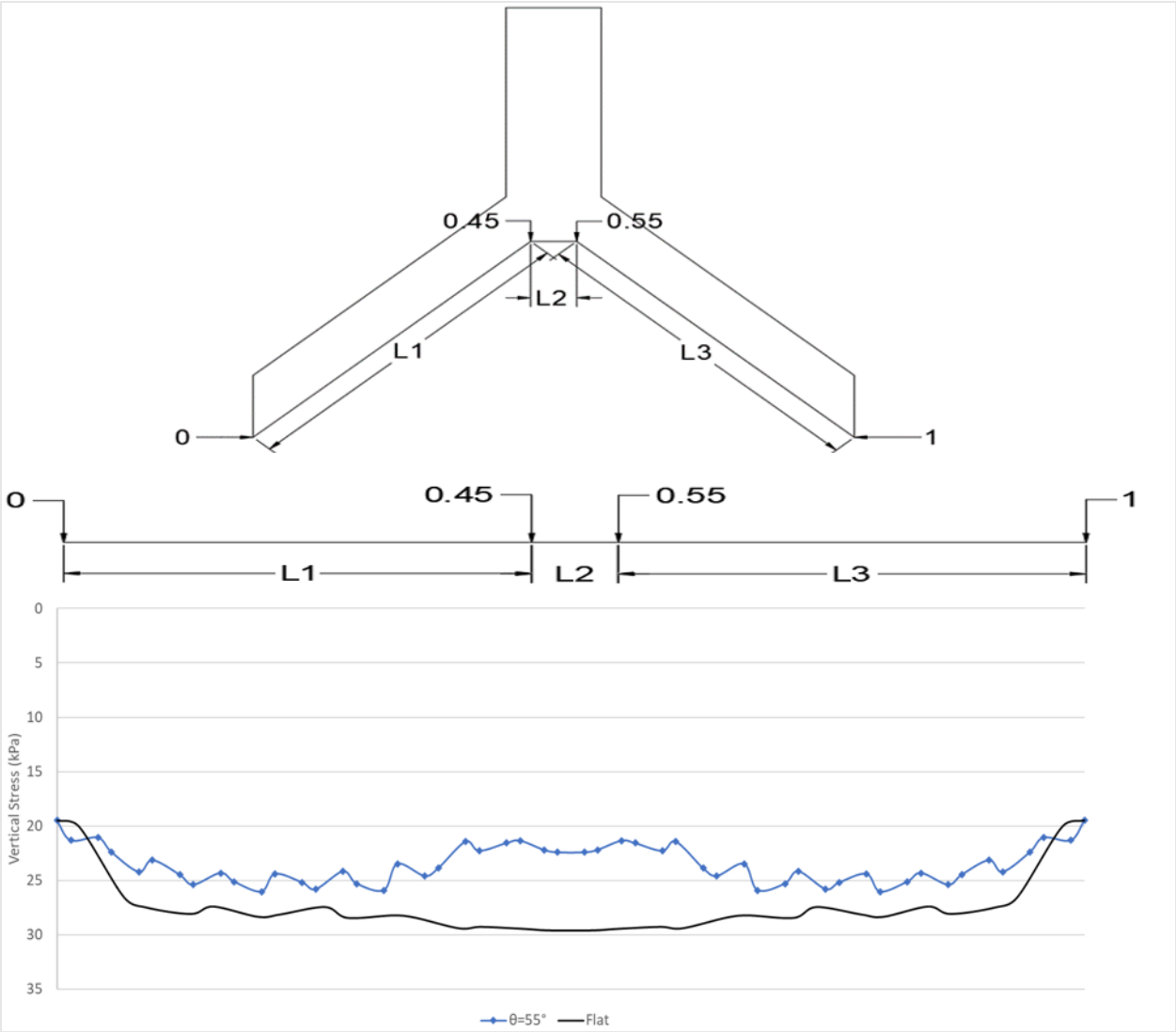

Figure 4.68 Contact pressure distribution below the optimum shell foundation and flat foundation in dense sand

4.4 Effects of edge angle on stresses at specified depths below the foundation base

The following figures investigate averages of stresses and central stresses below shell foundations with different edge angles at particular depths beneath the foundations. Figures 4.69 through 4.71 indicate a slight increase in stress averages by decreasing the edge angle at the base level (D = 0) in all sand types. In addition, the central stresses at this depth exhibit a reduction in the values from θ=60 degrees to 30 degrees, then they increase linearly by decreasing the edge angle approaching the flat configurations according to figures 4.72 to 4.74. Comparing the central stress magnitudes and soil densifications demonstrates higher values in loose sand relative to medium and dense sands.

Figures 4.75 to 4.86 study the effect of edge angle and the stresses at D = 0.5B and D = B below the founding level. It can be understood that the influence of the geometry of the foundations progressively disappears at lower elevations. At D = 0.5B, the vertical stress values in loose and medium sands are lower than dense sand. However, the effect of soil densifications at D = B below the base of the foundations does not show a significant difference in stress magnitudes.

In order to examine the variation of the stress magnitudes versus depth, figures 4.87 to 4.92 are reported. The central stresses increase from the contact surface to D = 0.5B below the founding level, then initiate to decrease in all sand states beneath the shell foundations. Although the averages of stresses achieve their maximum values at the base level of the shell foundation, they are lesser than the stress values at the same level below the flat foundations. As expected, the stresses below flat foundations decrease gradually at lower depths.

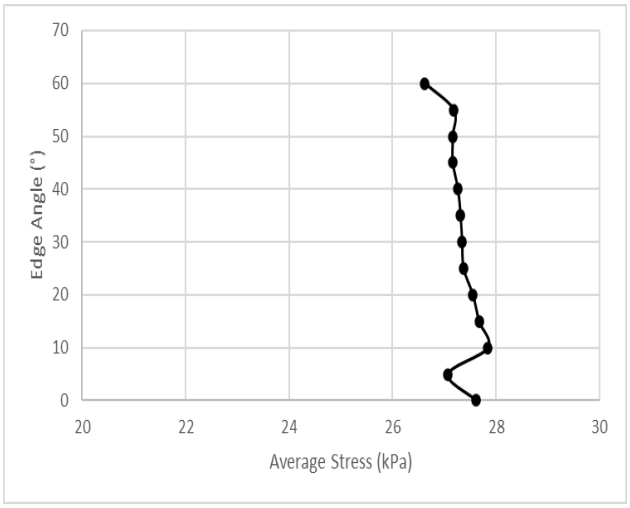

Figure 4.69 Average stress versus edge angle at D = 0 in loose sand

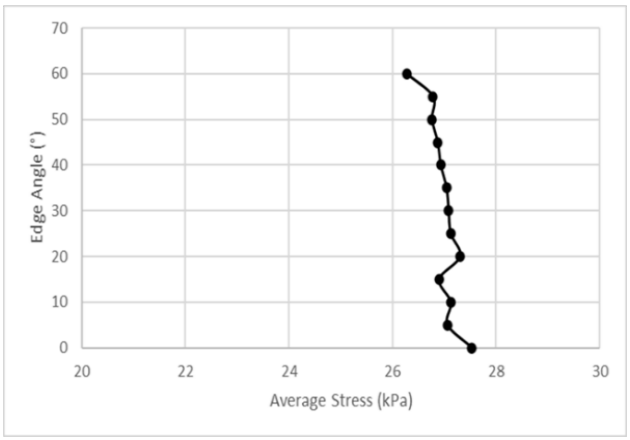

Figure 4.70 Average stress versus edge angle at D = 0 in medium sand

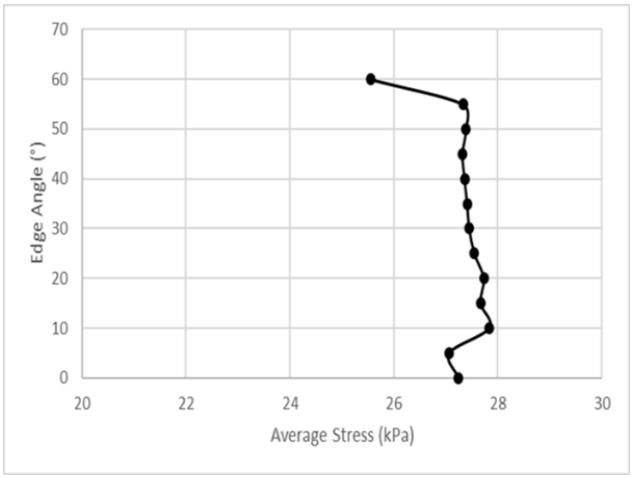

Figure 4.71 Average stress versus edge angle at D = 0 in dense sand

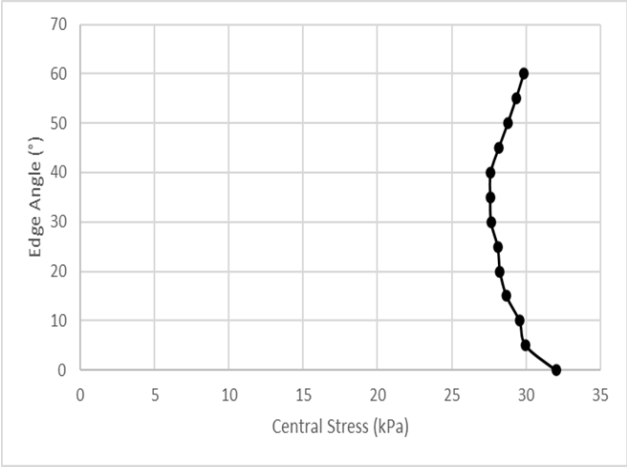

Figure 4.72 Central stress versus edge angle at D = 0 in loose sand

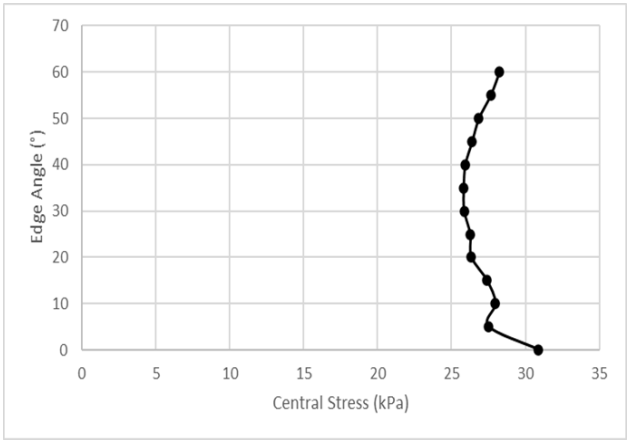

Figure 4.73 Central stress versus edge angle at D = 0 in medium sand

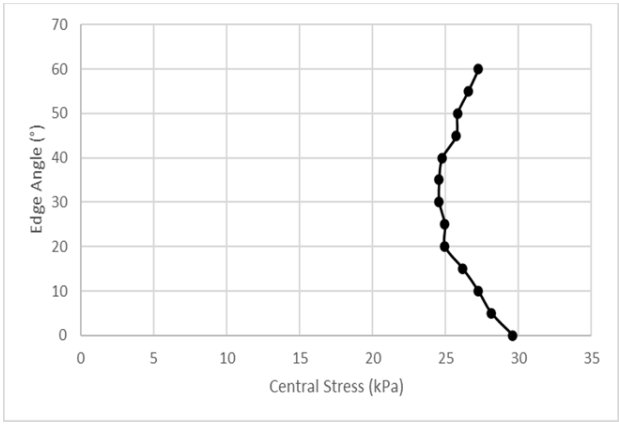

Figure 4.74 Central stress versus edge angle at D = 0 in dense sand

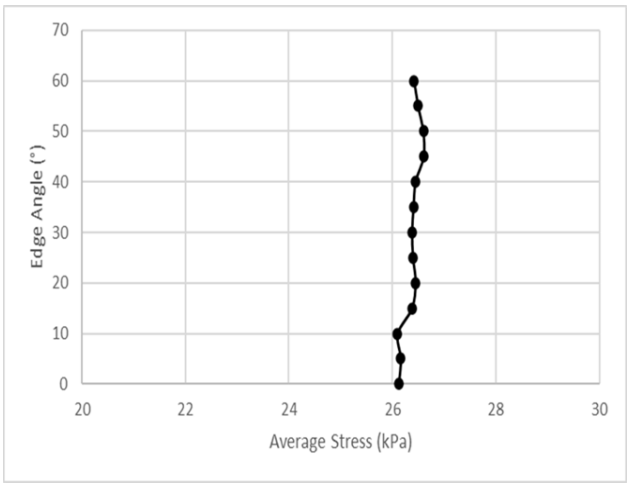

Figure 4.75 Average stress versus edge angle at D = 0.5B below the foundation base in loose sand

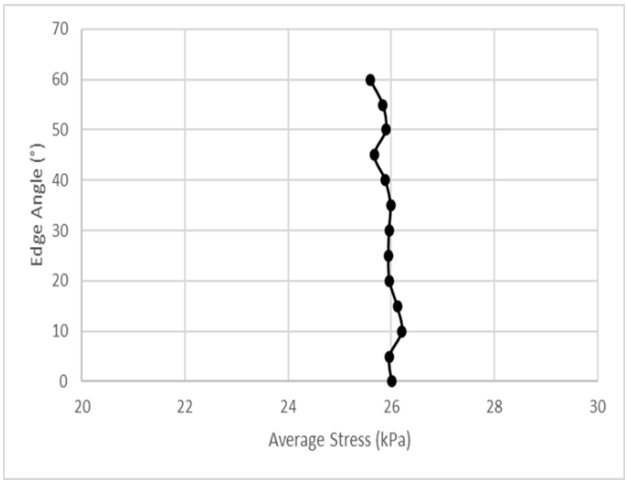

Figure 4.76 Average stress versus edge angle at D = 0.5B below the foundation base in medium sand

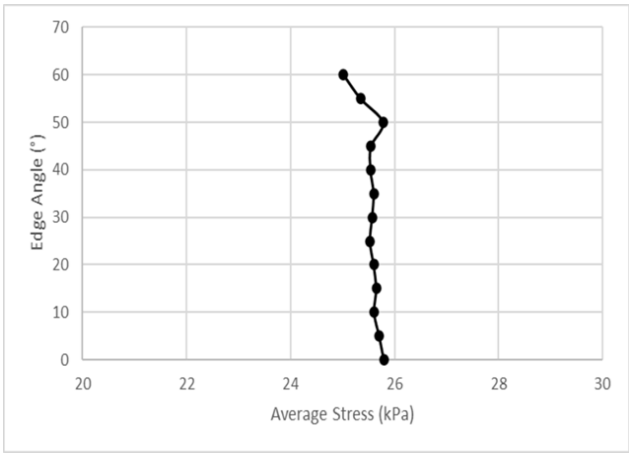

Figure 4.77 Average stress versus edge angle at D = 0.5B below the foundation base in dense sand

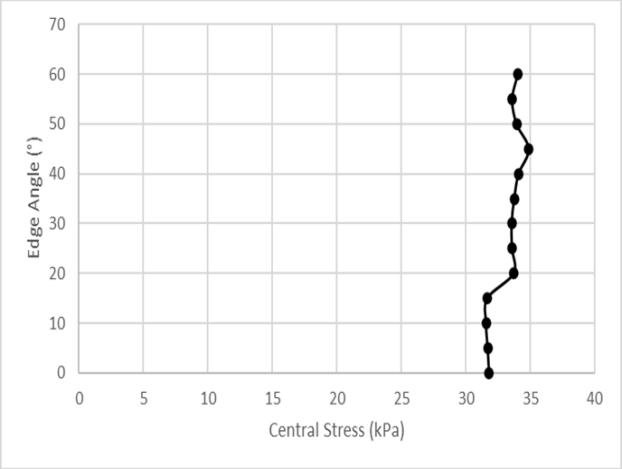

Figure 4.78 Central stress versus edge angle at D = 0.5B below the foundation base in loose sand

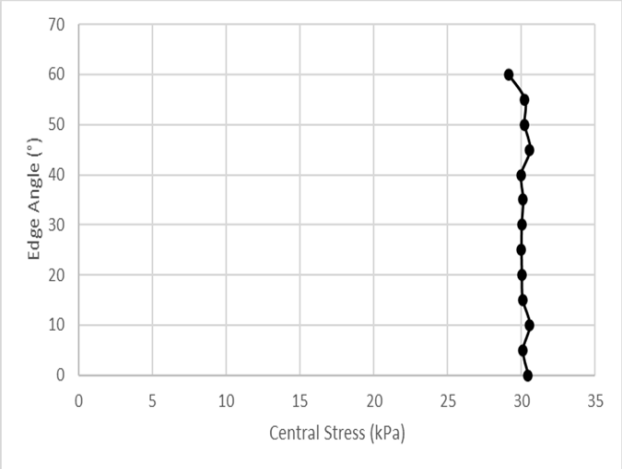

Figure 4.79 Central stress versus edge angle at D = 0.5B below the foundation base in medium sand

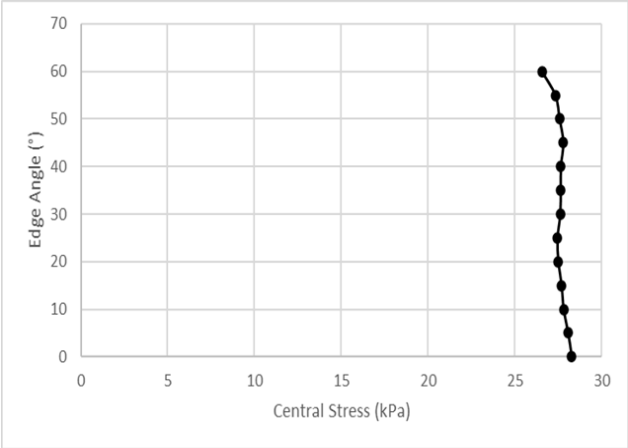

Figure 4.80 Central stress versus edge angle at D = 0.5B below the foundation base in dense sand

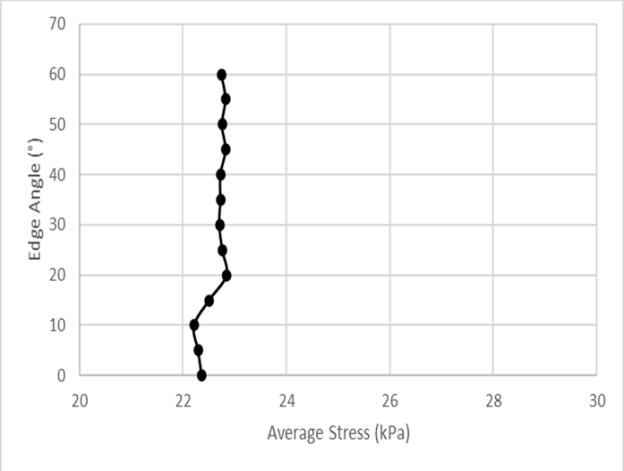

Figure 4.81 Average stress versus edge angle at D = B below the foundation base in loose sand

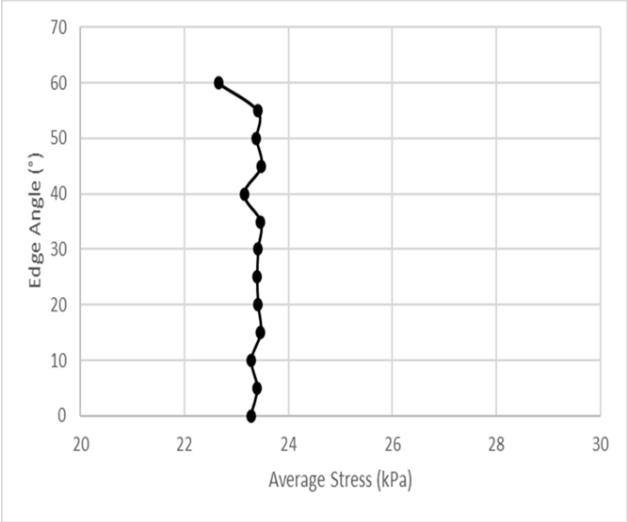

Figure 4.82 Average stress versus edge angle at D = B below the foundation base in medium sand

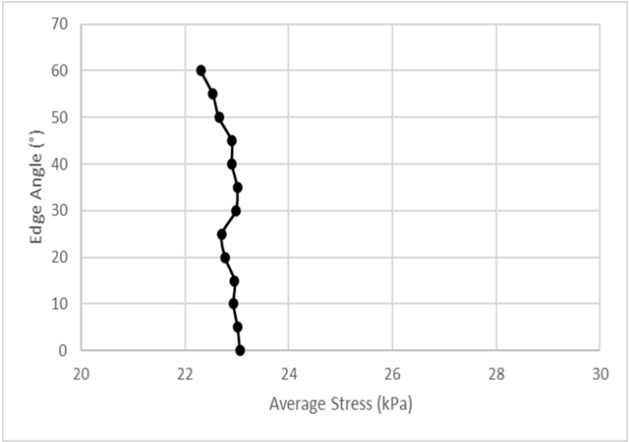

Figure 4.83 Average stress versus edge angle at D = B below the foundation base in dense sand

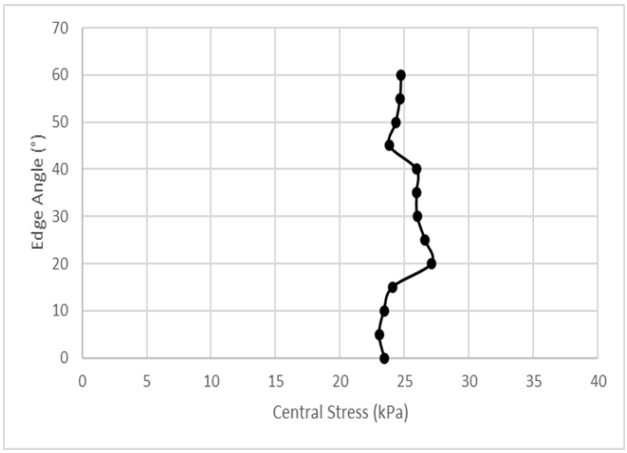

Figure 4.84 Central stress versus edge angle at D = B below the foundation base in loose sand

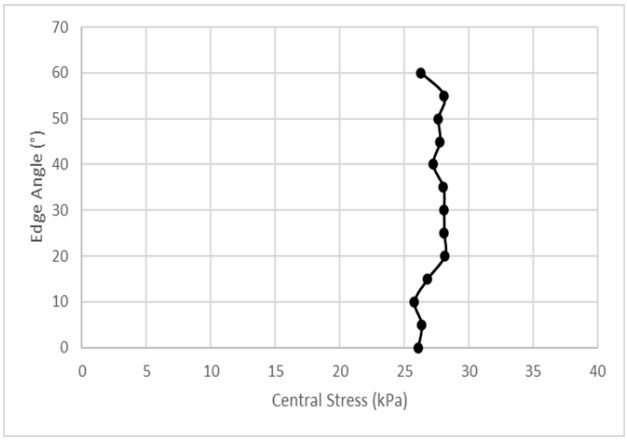

Figure 4.85 Central stress versus edge angle at D = B below the foundation base in medium sand

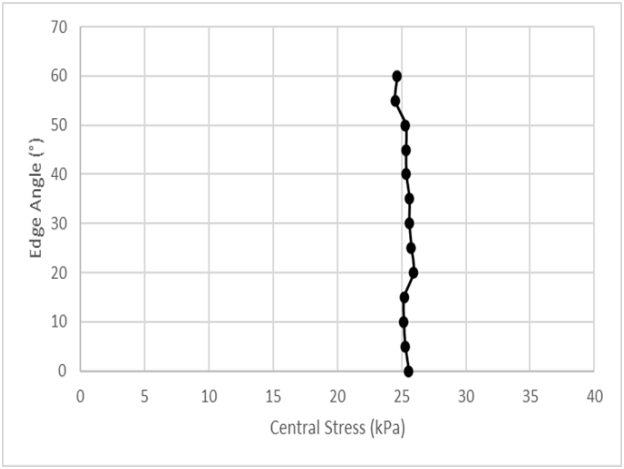

Figure 4.86 Central stress versus edge angle at D = B below the foundation base in dense sand

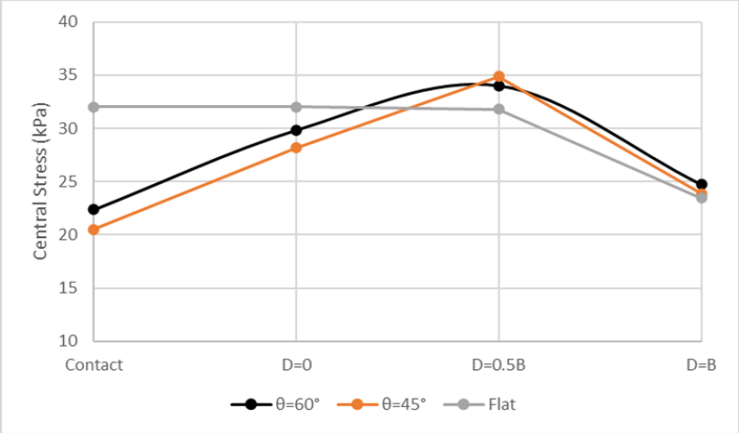

Figure 4.87 Central stress versus depth in loose sand

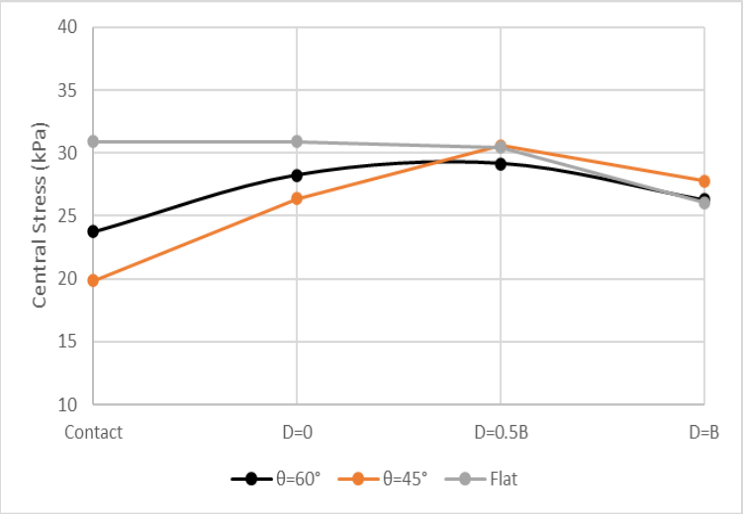

Figure 4.88 Central stress versus depth in medium sand

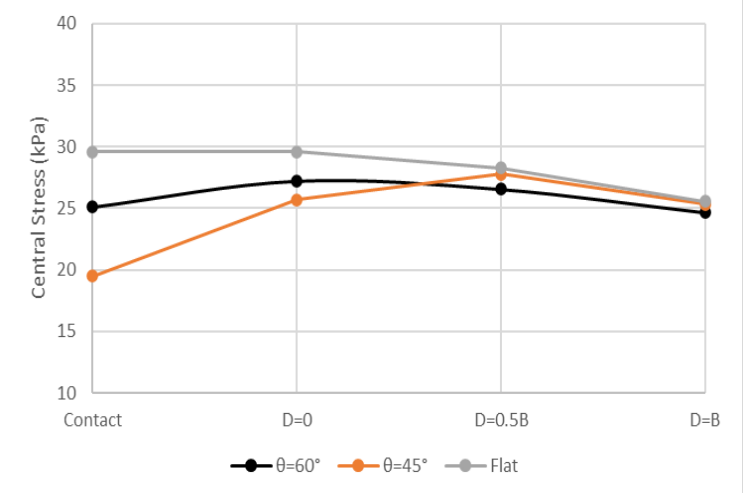

Figure 4.89 Central stress versus depth in dense sand

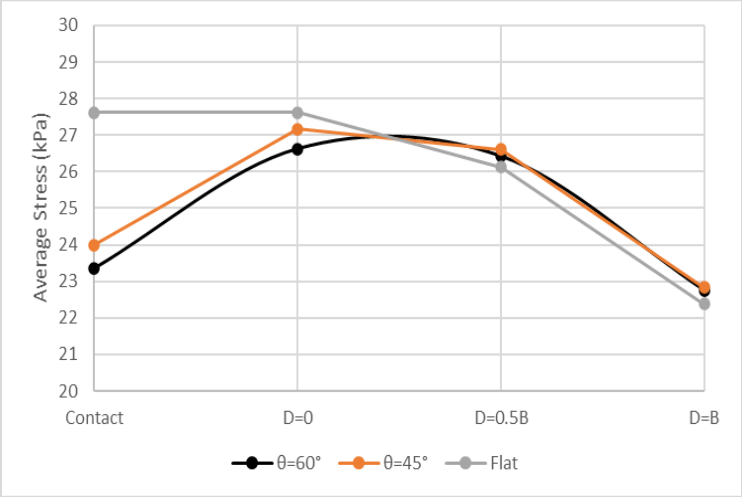

Figure 4.90 Average stress versus depth in loose sand

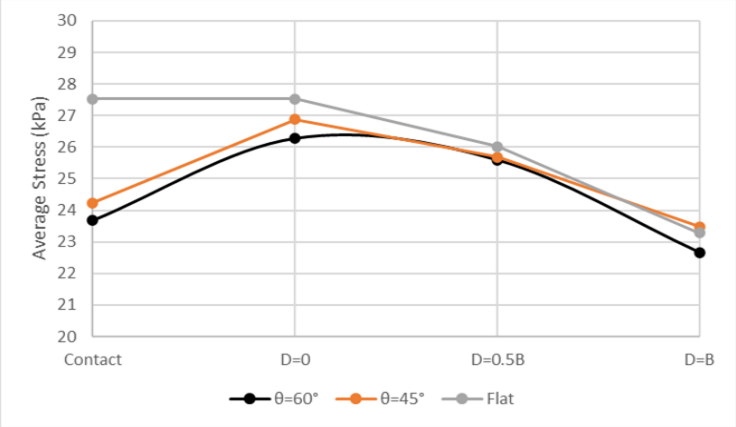

Figure 4.91 Average stress versus depth in medium sand

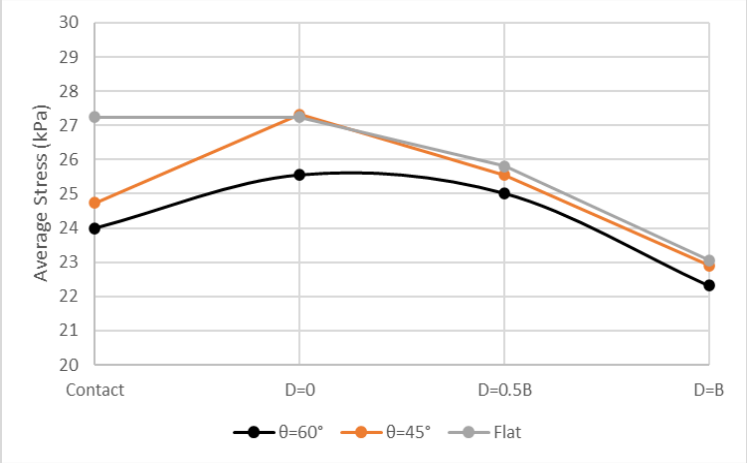

Figure 4.92 Average stress versus depth in dense sand

4.5 Bearing Capacity

In the following figures, load-settlement curves (vertical stress versus settlement) of the optimum shape of triangular shell foundations (edge angle = 55°) and the alternative flat footing are graphed in order to evaluate the bearing capacity on loose, medium, and dense sand states. Figures 4.93 through 4.95 indicate that the bearing capacity of the optimum shape of shell foundations is remarkably higher than flat foundations. The bearing capacity of the optimum shape of triangular shell foundations are 2.5 MPa, 4.3 MPa, and 6.9 MPa on loose, medium, and dense sands, respectively. However, the bearing capacities of the flat counterpart are found to be 1.9 MPa, 2.9 MPa, and 4.5 MPa on loose, medium, and dense sands. Based on the presented values, the bearing capacity of the optimum shape of the triangular shell foundations increases by 31%, 48%, and 53% compared with the flat counterpart on loose, medium, and dense sands.

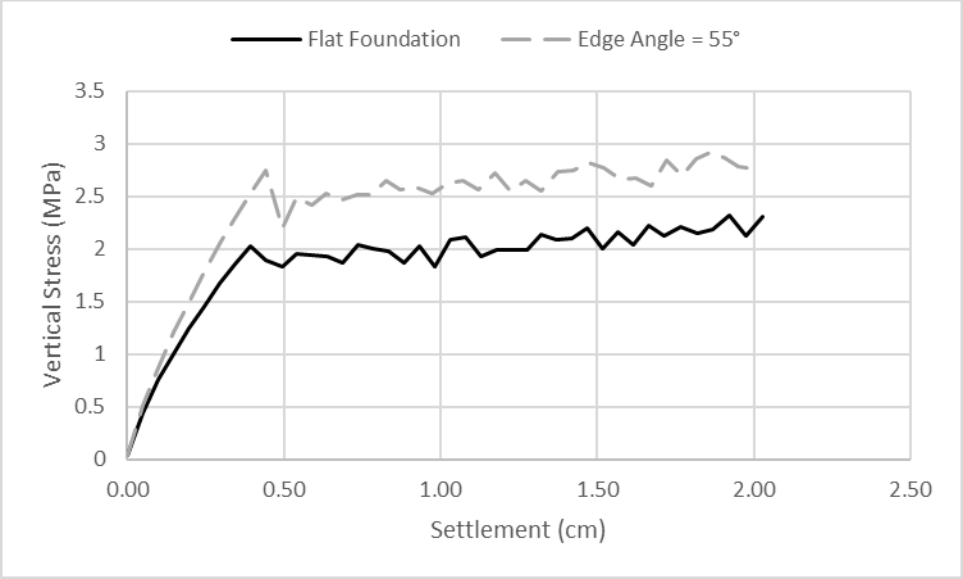

Figure 4.93 The load-settlement curve for loose sand

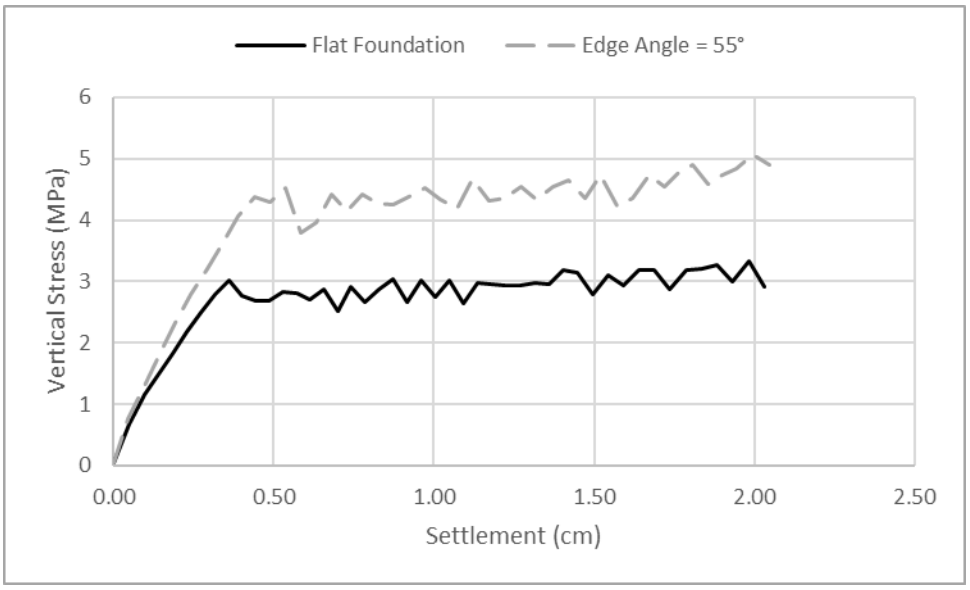

Figure 4.94 The load-settlement curve for medium sand

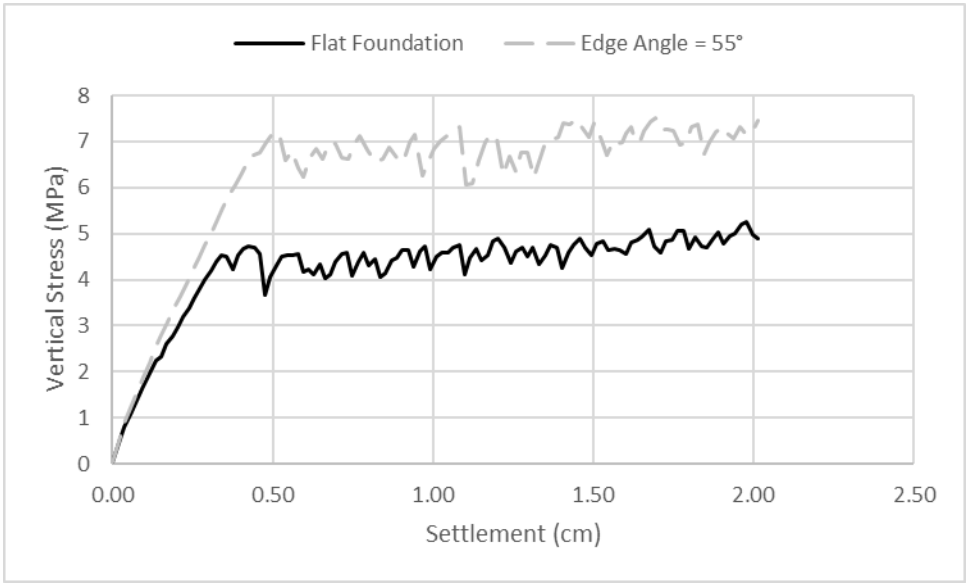

Figure 4.95 The load-settlement curve for medium sand

CHAPTER 5

CONCLUSIONS

5.1 General

The stress distributions beneath the soil below triangular shell foundations at different depths were examined numerically and compared with the conventional flat footings. Also, the optimum geometry of triangular shell footings was obtained, and the bearing capacity of the optimum shape was investigated and compared with the alternative flat one. Triangular shell foundations with edge angles ranging from 60 degrees to 0 (flat situation) with increments of 5 degrees were examined on loose, medium, and dense sand states. In order to determine the optimum geometry, all other configurations remained unchanged, such as the applied load, shell thickness, etc. The following conclusions were drawn:

1. At lower depths, the efficacy of the different shell geometries on stress distribution diagrams gradually diminishes for all types of sands. The proper path to investigate the effects of shell form on stress distributions stands at the soil-foundation interface.
2. Contact pressures below the shell foundations demonstrate a similar behavior in loose and medium sand soils. The minimum stresses occur around the edges; however, the location of the maximum pressures along the length of the sloped parts is variable within 0.1 – 0.3 of that length (L1 and L3) from the edges based on the edge angles.
3. In the case of dense sand, the minimum contact pressures appear at the center when the edge angle is from 10 to 50 degrees. At this range, the maximum stresses happen at the peripheries.
4. The bearing capacity of shell foundations is significantly higher than their flat counterparts. The bearing capacity of the optimum shape of the triangular shell foundations increases by up to 53% compared with the alternative flat one.
5. By decreasing the edge angle of shell footings, the averages of stresses increase in loose, medium, and dense sands. Conclusively, the bearing capacity of triangular shell foundations decreases by reducing the edge angle.
6. Considering the average stress magnitudes and the uniformity, the optimum geometry for triangular shell foundations is 55 degrees for loose, medium, and dense sand states.

7. At the founding level (D = 0), the averages of stresses indicate a slight increase by decreasing the edge angle in all sand types.
8. At lower elevations below the base of the footings (D = 0.5B and D = B), the stress distributions for all shell forms would not be affected by the shell angles. The maximum stresses are at the center, and the minimum stresses are at the edges.
9. At D = 0.5B, only the soil densification affects the stress distribution. The vertical stress values in loose and medium sands are lower than dense sand.
10. The average stresses below the shell foundations achieve the maximum value at the base level (D = 0), then initiate to decrease. However, the stresses decrease continuously by lower depths below the flat foundations.

5.2 Recommendations for Future Work

1. Develop numerical models and experimental tests to investigate the geotechnical behavior of shell foundations under lateral and eccentric loads to simulate wind and seismic loads.
2. Conduct field tests and three-dimensional numerical models to validate and compare the stress distributions with the presented study.
3. Study the contact pressure and stress distribution in soil beneath other geometries of shell foundations and explore the optimum shapes.
4. Consider the shell footings structure by examining the foundation material to determine the stresses in the footing structure under particular column loads.
5. Evaluate the influence of the combination of shell foundations and piles by developing numerical and laboratory tests.
6. Investigate the geotechnical behavior of shell foundations resting on collapsible and problematic soils. In addition, examine the stress distributions in the case of shell footings on cohesive soils.
7. Develop theoretical models to present analytical solutions for bearing capacity, stress, and strain below shell foundations.

8. Utilize neural networks to establish predicting models for contact pressure below shell foundations by examining various parameters.

REFERENCES

1. Smith, M. (2009). ABAQUS/Standard User's Manual, Version 6.9. Dassault Systems Simulia Corp.
2. Abdel-Rahman MM, Hanna A.M. (2003). “Contact pressure distribution under shell Foundations,” Proceedings of the 10th International Colloquium for Structural and Geotechnical Engineering, Faculty of Engineering, Ain Shams University, 22-25 April 2003, Cairo, Egypt, Paper No. F03GE22.
3. Abdel–Rahman M.M. (1996). “Geotechnical Behavior of Shell Foundations,” Ph.D. Thesis, Civil Engineering, Concordia University, Montreal, Quebec, Canada, pp. 126–137.
4. Abdel-Rahman M.M. (2020). “Lateral loading resistance for shell foundations,” HBRC Journal, 16:1, 227-241, DOI: 10.1080/16874048.2020.1802691
5. Al-Azzawi A. (2013). “A Study of the Behavior of Shell Footings using Finite Element Analysis,” 1st International Conference for Geotechnical Engineering and Transportation, Eng. & Tech. Journal, Vol. 31, Part (A), No.19, 2013.
6. Azzam W.R., Nasr A.M. (2015). “Bearing capacity of shell strip footing on reinforced sand,” Journal of Advanced Research, pp. 727–737.
7. Bolouri Bazaz j., Sajedi K., Oloomi H. (2018). “Numerical and Experimental Comparisons of Different Behavior Shapes of Folded Plate Shell Foundation on Sandy Soil,” Journal of Civil Engineering Sharif, DOI: 10.24200/J30.2018.1334.
8. Bowles JE. (1996). “Foundation analysis and design,” 5th edn. McGraw-Hill Book Company, New York
9. Bolton M.D. (1986). “The strength and dilatancy of sands,” Géotechnique, 36, No.65-78 DOI: 10.1680/geot.1986.36.1.65
10. Colmenares J.E., So-Ra Kang, Young-Jin Shin, Jong-Ho Shin (2013). “Ultimate Bearing Capacity of Conical Shell Foundation,” The 2013 world congress on Advances in Structural Engineering and Mechanics (ASEM13).

11. Ebrahimi K., Hamidi A., Homami P. (2013b). “Determination of the optimal form of shell foundations,” In: The first Iranian conference on geotechnical engineering, Ardabil, Iran (in Persian)
12. Ebrahimi K., Khazaei J. (2019). “Investigation of Bearing Capacity and Failure Pattern in Shell Foundations by FELA Method,” Geotech Geol. Eng., 37:3523–3534
13. El-kady M.S., Badrawi E.F. (2017). “Performance of isolated and folded footings,” Journal of Computational Design and Engineering, pp. 150-157.
14. Esmaili D., Hataf N. (2008). “Experimental and numerical investigation of ultimate load capacity of shell foundations on reinforced and unreinforced sand,” Iranian J. of Science & Technology. Transaction B. Engineering, 32(B5), 491-500.
15. Esmaili D., Hataf N. (2013). “Determination of ultimate load capacity of conical and pyramidal shell foundations using dimensional analysis,” Iranian J. of Science & Technology. Transaction B. Engineering, pp. 423-435.
16. Fattah M.Y., Waryosh W.A., Al-Hamdani M.A.E. (2015a). “Experimental and theoretical studies on bearing capacity of conical shell foundations composed of reactive powder concrete,” Acta Geodyn Geomater J 12(180):411–426.
17. Hadid W.H. (1983). “New-Foundation Models,” M.Eng. Thesis, Concordia University, Montreal, Quebec, Canada.
18. Hassan Sawsan A., Al-Soud Madhat S., Mohammed Shahad A. (2019). “Behavior of Pyramidal Shell Foundations on Reinforced Sandy Soil,” Geotech Geol. Eng. (2019) 37:2437–2452.
19. Hanna A.M., Abdel-Rahman, M.M. (1990). “Ultimate bearing capacity of triangular shell strip footings on sand,” J Geotech Eng., ASCE 116(12):1851–1863
20. Hanna A.M., Abdel–Rahman M.M. (1998). “Experimental Investigation of Shell Foundations on Dry Sand,” Canadian Geotechnical Journal, 35(5), pp. 847–857.
21. Hanna A.M., Hadid W.H. (1987). “New Models of Shallow Foundations,” International Journal of Mathematical Modeling, 4, pp. 799–811.
22. Huat B.B.K. Thamer, A.M. (2006). “Finite Element Study Using FE Code (PLAXIS) on the Geotechnical Behavior of Shell Footings,” Journal of Computer Science, 2(1), pp. 104–108.

23. Huat B.B.K., Mohammed T.A., Abang Ali A.A.A., Abdullah A.A. (2007). "Numerical And Field Study on Triangular Shell Footing for Low Rise Building," International Journal of Engineering and Technology, Vol. 4, No. 2, 2007, pp. 194-204.
24. Salencon J. (2001), "Handbook of Continuum Mechanics: General Concepts, Thermoelasticity," Springer Science & Business Media, ISBN 3-540-41443-6
25. Kurian N.P. (2006). "Shell Foundations: Geometry, Analysis, Design and Construction," Alpha Science International Ltd., Madras Chennai, India.
26. Kurian N.P., Jayakrishna Devaki V.M. (2005). "Analytical studies on the geotechnical performance of shell foundations," Canadian Geotechnical Journal, 42(2), pp. 562–573.
27. Meyerhof, G. G. (1951). "The Ultimate Bearing Capacity of Foundations", Geotechnique, Vol.2, pp 301-322.
28. Pronozin Y., Maltseva T., Poroshin O., Medvedeva A. (2019). "Thin-walled shell foundations," MATEC Web of Conferences 265, 05032, https://doi.org/10.1051/matecconf/201926505032
29. Naumkina J.V., Pronozin Y.A., Epifantseva L.R., (2016). "Load-bearing capacity of soil loaded with strip-shell foundations," Magazine of Civil Engineering, 66(06):23-34
30. NAVFAC documentation index: keywords out of context - KWOC. (1986). Alexandria, Va.: Naval Facilities Engineering Command.
31. Rinaldi, R. (2012). "Inverted Shell Foundation Performance in Soil," Ph.D. Thesis, Concordia University, Montreal, Quebec, Canada.
32. Sajedi K., Bolouri Bazaz J., Rezaee Pajand M. (2018). "Elastic-Plastic Analysis of Inverted Folded Shell Strip Foundation on Sandy Soil," Journal of Civil and Environmental Engineering, University of Tabriz, Iran. (In Persian)
33. Shoukath S., Rajesh A.K. (2017). "Seismic Performance of Hyperbolic Paraboloid and Inverted Spherical Shell Foundation," International Research Journal of Advanced Engineering and Science, ISSN: 2455-9024.
34. Sidqi R., Mahmood M. N. (2020). "Investigating the Nonlinear Performance of Reinforced Concrete Shell Foundations," 3rd International Conference on Recent Innovations in Engineering (ICRIE 2020), doi:10.1088/1757-899X/978/1/012050.
35. Terzaghi, K. (1943). "Theoretical Soil Mechanics," *John Wiley and Sons Inc.*, New York, London.

36. Thilakan S., Naik N. (2015). “Geotechnical Behaviour of Shell Foundations,” 50th Indian Geotechnical Conference, College of Engineering (Estd. 1854), Pune, India, https://www.researchgate.net/publication/295531931